Aus der Fachrichtung 2.4, Experimentelle und Klinische Pharmakologie und Toxikologie
der Medizinischen Fakultät
der Universität des Saarlandes, Homburg/Saar

STIM1, ORAI and TRPC5 proteins:
Key players in cellular Ca^{2+}-signaling

Dissertation zur Erlangung des Grades eines Doktors der Naturwissenschaften

der Medizinischen Fakultät

der UNIVERSITÄT DES SAARLANDES

2008

vorgelegt von: **Stefan Alfred Groß**

geb. am: **26.03.1980 in Püttlingen**

Homburg, Juni 2008

Table of contents

Table of abbreviations

2-APB	-	2-aminoethoxydiphenyl borate
AM	-	Acetoxymethylester
BAPTA	-	1,2-bis(2-aminophenoxy)ethane-N,N,N´,N´-teraacetic acid
CaM	-	Calmodulin
CBII	-	Calmodulin binding site II
CCH	-	Carbachol
CIRB	-	Calmodulin-IP$_3$ receptor binding site
CRAC	-	Calcium release-activated calcium (current or channel)
CRACM	-	CRAC modulator
Cyt D	-	Cytochalasin D
DAG	-	Diacylglycerol
DMSO	-	Dimethylsulfoxide
EGF	-	Epidermal growth factor
EGTA	-	Ethyleneglycol bis- N,N,N´,N´-teraacetic acid
ER	-	Endoplasmatic reticulum
G1/2	-	Gamma1/2 (Gamma subunit of voltage-gated calcium channel)
HBSS	-	Hank´s Buffered Salt Solution
HEDTA	-	N-hydroxyethyl-ethylenediamine-triacetic acid
HEK	-	Human embryonic kidney (cells)
I$_{CRAC}$	-	Calcium release-activated calcium current
IP$_3$	-	Inositol-1,4,5-triphosphate
LB	-	Lysogeny broth (medium)
NAADP	-	Nicotinic acid adenine dinucleotide phosphate
ORAI2L	-	ORAI2 long
ORAI2S	-	ORAI2 short
PKC	-	Protein kinase C
RBL	-	Rat basophilic leukaemia (cells)
RiVIT	-	Rapid vesicular insertion of TRP (channels)
ROCE	-	Receptor-operated calcium entry
SCID	-	Severe combined immuno deficiency
S.E.M.	-	Standard error of the mean
SOCE	-	Store-operated calcium entry

SR	-	Sarcoplasmic reticulum
STIM	-	Stromal interaction molecule
TG	-	Thapsigargin
TRP	-	Transient receptor potential (channel protein)
VGCC	-	Voltage-gated calcium channel

1 Summary

STIM, ORAI and some TRP proteins are believed to participate in store-operated Ca^{2+} entry (SOCE). The calcium-release activated calcium (CRAC) channels represent the best characterized SOCE pathway in non-excitable cells. First described in immune cells, CRAC channels were shown to play an important role in the Ca^{2+} signalling pathway for T cell activation and differentiation but the molecular components of the CRAC channels remained enigmatic for a long time. Recently, crucial experiments attracted the attention to the stromal-interacting molecule 1 (STIM1) and ORAI (CRACM) proteins as central components of CRAC channels. Furthermore, the non-selective TRPC5 ion channels were reported to play a role in SOCE and they were also discussed as receptor-activated ion channels. Despite intensive research with recombinant TRPC5 ion channels, however, little is known about their possible functional role and their activation mechanism is still discussed controversially.

In this thesis, I explore the following issues:

1. Murine STIM1 and ORAI proteins: Role in the formation and activation of CRAC channels.

2. TRPC5 ion channels: Activation mechanisms and coupling to Ca^{2+}-selective ion channels.

Four different murine ORAI variants were cloned and functionally studied in electrophysiological experiments. Here, it is shown that murine ORAI1, ORAI2L, ORAI2S and ORAI2S (N130Y) form functional CRAC channels which are activated via STIM1 translocation to the plasma membrane in response to store-depletion. Murine ORAI proteins seem to form multimeric complexes to establish functional Ca^{2+}-selective ion channels both as homo- and heteromultimeric assemblies. Since ORAI variants differing in N-terminus length generate distinct current densities, the N-terminus of ORAI proteins apparently plays a critical role in ion channel gating. In HEK 293 cells, for instance, STIM1 plus the long variant of ORAI2 generate larger current densities than STIM1 plus the short variant of ORAI2. According to the

reported SCID mutation in human ORAI1, a single point mutation was introduced at the N-terminus of the murine ORAI variants. This mutation prevented CRAC current activation in response to Ca^{2+}-store depletion, demonstrating the importance of the N-terminal amino acid sequence for proper CRAC channel function. In summary, this thesis demonstrates that murine ORAI variants form functional CRAC channels by a multimeric assembly of ORAI proteins. In the presence of STIM1, these channels activate in response to store-depletion, showing inward-rectifying, Ca^{2+}-selective currents as originally described for CRAC currents.

Using transient transfections and a cell line stably expressing TRPC5, the activation mechanisms of TRPC5 ion channels were systematically studied. Here, it is shown that TRPC5 channels are not typically store-operated but, independently from the Ca^{2+}-source, they activate upon a local rise of internal Ca^{2+}. In addition, TRPC5 channels do not appear to directly interact with the STIM1/ORAI1 complex, which is responsible for SOCE. The local Ca^{2+} influx through CRAC channels was observed to activate TRPC5 currents and, moreover, additional experiments with L-type Ca^{2+} channels revealed a functional coupling of TRPC5 and Ca^{2+}-selective ion channels. Upon Ca^{2+}-entry through CRAC channels, the non-selective TRPC5 channels activate and the cell membrane depolarizes. Further experiments provided evidence that TRPC5 channels are dose-dependently activated by a local rise of cytosolic Ca^{2+}. Thus, Ca^{2+} alone activates TRPC5 channels in a dose-dependent manner, indicating that TRPC5 channels might function as Ca^{2+}-activated non-selective ion channels. Based on these experiments, a novel model is proposed in which Ca^{2+}-activated TRPC5 channels may modulate Ca^{2+} signals by regulating the membrane potential and, consequently, the Ca^{2+} driving force.

Zusammenfassung

STIM-, ORAI- und einigen TRP-Proteinen wird in der Literatur eine wichtige Funktion für die Speicher-aktivierten Kalzium-Ströme (SOCE) eingeräumt. Die am besten beschriebene Untergruppe sind die so genannten CRAC- („calcium-release activated calcium") Ströme. Ursprünglich wurden die CRAC-Ströme in Immunzellen entdeckt und es wurde gezeigt, dass sie eine wichtige Rolle bei der T-Zell-Aktivierung und -Differenzierung spielen. Die molekularen Bausteine, die für CRAC-Kanäle verantwortlich sind, konnten über einen langen Zeitraum nicht identifiziert werden. In den letzten Jahren jedoch wurde durch aufschlussreiche Forschungsergebnisse die Aufmerksamkeit auf die STIM1- (Stromal-interacting molecule 1) und ORAI-Proteine (CRACM-Proteine) gelenkt. Darüber hinaus wurden die nicht-selektiven TRPC5-Ionenkanäle sowohl als SOCE-Ionenkanäle als auch als Rezeptor-aktivierte Ionenkanäle beschrieben. Obwohl die Ionenkanaleigenschaften in TRPC5-Überexpressionssystemen ausgiebig erforscht wurden, besteht kein fundiertes Wissen über die Funktion von TRPC5-Ionenkanälen und die Mechanismen zur Kanalaktivierung werden kontrovers diskutiert.

Von daher wurden in der vorliegenden Arbeit folgende Schwerpunkte untersucht:

1. STIM1- und ORAI-Proteine aus der Maus: Erforschung der Funktion für die Aktivierung und die Bildung der CRAC-Ionenkanäle.

2. TRPC5-Ionenkanäle: Untersuchung des Aktivierungsmechanismus und ihre funktionelle Interaktion mit Ca^{2+}-selektiven Ionenkanälen.

Für die vorliegende Arbeit wurden ORAI-Proteine aus der Maus kloniert und in elektrophysiologischen Experimenten untersucht. Es wird hier gezeigt, dass die murinen ORAI1-, ORAI2L-, ORAI2S- und ORAI2S-(N130Y) Varianten funktionelle Ca^{2+}-selektive Ionenkanäle bilden, die durch die Translokation der STIM1-Proteine, hervorgerufen durch die Entleerung der Ca^{2+}-Speicher, aktiviert werden. Die funktionellen ORAI-Proteinkomplexe bestehen wahrscheinlich aus vier ORAI-Untereinheiten, wobei sowohl homo- als auch heteromultimere Proteinkomplexe selektive Ca^{2+}-Ströme leiten. Die Größe der Stromdichte ist von den Ionenkanal-bildenden ORAI-Varianten abhängig, da der N-Terminus eine wichtige Rolle

bezüglich der Ionenkanalaktivität spielt. Die N-terminal längere Variante des ORAI2-Proteins erzeugt größere Stromdichten als die verkürzte ORAI2-Variante. Der Einfluss des N-Terminus wird in immundefizienten SCID-Patienten deutlich, denen, durch einen einzelnen Aminosäureaustausch am N-Terminus des ORAI1-Proteins, der Ca^{2+}-Einstrom durch den CRAC-Ionenkanal fehlt. Gemäß dieser humanen ORAI-Mutationen wurden die murinen ORAI-Scid-Proteine generiert und funktionell untersucht. Zusammenfassend beschreibt die vorliegende Arbeit die murinen ORAI-Varianten als die molekularen Bausteine der CRAC-Ionenkanäle, die aus mehreren ORAI-Proteinen gebildet werden. In der Anwesenheit von STIM1 werden diese Kanäle durch die Entleerung der Kalziumspeicher aktiviert und weisen die typischen Charakteristika von CRAC-Strömen auf.

Außerdem wird der Aktivierungsmechanismen von TRPC5-Kanälen in dieser Arbeit systematisch untersucht. Es wird gezeigt, dass diese Ionenkanäle keine typischen Speicher-aktivierten Kanäle sind, jedoch allein durch einen lokalen Kalziumanstieg aktiviert werden. Ebenso wird untersucht, ob TRPC5 mit STIM1- und ORAI-Proteinen interagiert, die für den Speicher-aktivierten Ca^{2+}-Einstrom verantwortlich sind. Eine direkte Interaktion wurde nicht festgestellt, jedoch aktivieren TRPC5-Ströme, sobald Ca^{2+} durch CRAC-Kanäle in die Zelle einströmt. Ca^{2+}-Einstrom durch L-Typ-Ca^{2+}-Kanäle führt ebenfalls zur Aktivierung der TRPC5-Ionenkanäle. Es besteht somit eine funktionelle Interaktion zwischen TRPC5- und Ca^{2+}-selektiven Ionenkanälen. Durch den Ca^{2+}-Einstrom werden die nicht-selektiven TRPC5-Ionenkanäle aktiviert, was zur Depolarisation der Zellmembran führt und den CRAC- oder spannungsabhängigen Ca^{2+}-Kanal-abhängigen Ca^{2+}-Einstrom hemmt. Weitere Experimente zeigen, dass TRPC5-Ionenkanäle durch erhöhte intrazelluläre Ca^{2+}-Konzentrationen dosis-abhängig aktiviert werden. Somit wird postuliert, dass die nicht-selektiven Ca^{2+}-aktivierten TRPC5-Ionenkanäle den Ca^{2+}-Einstrom durch CRAC-Kanäle oder L-Typ-Ca^{2+}-Kanäle modulieren, da durch die Aktivierung der TRPC5-Ionenkanäle das Membranpotential steigt und davon abhängig auch der elektrochemische Gradient für Ca^{2+} sinkt.

2 Introduction

Calcium (Ca^{2+}) signalling controls a vast array of cellular functions in the anatomy, physiology and biochemistry of an organism. These functions range from short-term responses, such as muscle contraction and neurotransmitter secretion, to long-term regulation of cell growth and proliferation. At the cellular level, Ca^{2+} is derived from two sources – the extracellular space and intracellular Ca^{2+} stores such as the endoplasmatic or sarcoplasmatic reticulum[1]. For precise Ca^{2+} signalling, the intracellular Ca^{2+} concentration must be accurately controlled with respect to space[2], time[3] and amplitude[4]. In excitable cells, the major pathway for Ca^{2+} influx is via Ca^{2+}-selective voltage-gated Ca^{2+} channels (VGCC) whereas, in non-excitable cells, Ca^{2+} influx is mediated via SOCE (store-operated Ca^{2+} entry) channels or triggered by receptor stimulation, named as receptor-operated Ca^{2+} entry (ROCE). The best characterized SOCE is the Ca^{2+} release-activated Ca^{2+} current hereafter referred to as CRAC current or I_{CRAC}[5]. Firstly described in 1992, the molecular components of I_{CRAC} remained elusive until the Ca^{2+}-sensor STIM1[6, 7] (stromal interaction molecule) and ORAI1 / CRACM1[8-10] proteins were reported to reconstitute the CRAC current[11, 12]. Additionally, it has also been suggested that, in overexpression systems, transient receptor potential ion channels (TRPCs) might form SOCE ion channels[13-15].

Here I report that the murine ORAI1, ORAI2L and ORAI2S form functional CRAC channels in HEK 293 or RBL 2H3 cells. In addition, I show that TRPC ion channels are activated in response to local Ca^{2+} influx carried by CRAC currents and Ca^{2+} influx through voltage-gated Ca^{2+} channels (VGCC) in HEK 293 cells overexpressing STIM1 and ORAI1 or VGCC subunits. Furthermore, I have investigated the involvement of intracellular Ca^{2+} in the activation for TRPC5 in detail. My results point to a central role of TRPC channels in intracellular Ca^{2+} signalling.

2.1 Store-operated Calcium entry (SOCE)

The cytosolic Ca^{2+} is a key signalling messenger that regulates a plethora of cellular functions from gene transcription to apoptosis. Ca^{2+} levels can be altered by Ca^{2+} influx from the extracellular space into the cell or by calcium release from intracellular stores such as the endoplasmic reticulum (ER). Store depletion is triggered by a

relatively small number of second messengers. Besides Ca^{2+} itself, inositol 1,4,5-triphosphate (IP_3), cyclic ADP ribose and nicotinic acid adenine dinucleotide phosphate (NAADP) have been reported to trigger Ca^{2+} release from intracellular stores[16]. The Ca^{2+} release from stores is transient in most cases. However, many cellular processes and store refilling require sustained elevated intracellular Ca^{2+} levels and this is achieved by Ca^{2+} entry across the cell membrane. The ~10000-fold concentration gradient for Ca^{2+} across the plasma membrane coupled with a resting membrane potential at about -70 mV creates a huge electrochemical driving force for Ca^{2+}. Consequently, modest changes in membrane permeability to Ca^{2+} by opening Ca^{2+} permeable ion channels result in a large Ca^{2+} influx. A wide variety of Ca^{2+}-selective ion channels are responsible for this Ca^{2+} influx. In excitable cells, such as neurons and muscle cells, voltage-gated Ca^{2+} channels (VGCC) represent the major entry pathway for Ca^{2+}. In contrast, in non-excitable cells, store replenishment is carried out by store-operated Ca^{2+} entry (SOCE) channels. By definition store-operated channels activate in response to store depletion even when cytosolic Ca^{2+} levels are buffered to low levels[17]. Replenishment of the primary cellular Ca^{2+} store, the ER, is an essential process to maintain the functional integrity of this compartment. Therefore, after store depletion, store-operated channels are activated and Ca^{2+} influx occurs refilling the stores. The maintenance of the ER Ca^{2+} levels is important for proper cellular functioning and it has been implicated in diseases such as severe combined immunodeficiency[18], acute pancreatitis[19] and Alzheimer`s disease[20] when SOCE is aberrant. The best characterized type of SOCE is the so called Ca^{2+} release-activated Ca^{2+} current (I_{CRAC}) initially reported in mast cells[5].

2.1.1 Calcium release-activated calcium (CRAC) currents

Over the past 15 years, CRAC currents have been extensively studied in different cell types without knowledge of the molecular components. In mast cells, these tiny, highly Ca^{2+}-selective currents are activated when ER Ca^{2+} levels drop independent of whether Ca^{2+} stores are actively depleted via intracellular infusion of IP_3 or extracellular application of ionomycin or whether Ca^{2+} store depletion occurs passively in response to intracellular perfusion with ethylene glycol bis-N,N,N´,N´-tetraacetic acid (EGTA) or 1,2-bis(2-aminophenoxy)ethane- N,N,N´,N´-tetraacetic

acid (BAPTA)[21]. As already mentioned, I_{CRAC} was measured in several cell types including mast cells, Jurkat leukemic T cells[22] and rat basophilic leukaemia cells (RBL)[23] showing specific biophysical and pharmacological characteristics. CRAC currents reveal a single-channel conductance of around ~15 femtosiemens (fS). In whole-cell patch clamp experiments, I_{CRAC} displays an inward rectifying I-V-characteristic with a reversal potential of approximately +50 mV and an amplitude highly dependent on the extracellular Ca^{2+} concentration. CRAC currents activate in immediate response (4 – 14 s) to store-depleting reagents such as IP_3, thapsigargin (TG) or ionomycin whereas current development is delayed when stores are passively depleted by intracellular perfusion of EGTA or BAPTA. Notably, CRAC currents show a Ca^{2+}-dependent current decay of 30 – 64 % depending on the intracellular Ca^{2+} buffer. I_{CRAC} is inhibited by 2-aminoethoxydiphenyl borate (2-APB) and trivalente cations, La^{3+} and Gd^{3+}, potently block CRAC currents too[21, 24, 25]. Additionally, a CRAC current hallmark characteristic for CRAC currents is the permeability for monovalente cations. Similar to VGCC, Na^+ inward currents are only conducted in a divalent-free extracellular environment resulting in a strong inwardly-rectifying current and a modest shift in reversal potential to less positive potentials[21] when compared to I_{CRAC} carried by Ca^{2+} ions. These CRAC characteristics were used to identify CRAC currents in several cell types and to elucidate the molecular components in the past 15 years.

2.1.2 Stromal-interaction molecule (STIM) 1

In 2005, Roos et al.[26] found an essential component for CRAC currents. The formerly described stromal-interaction molecule 1 (STIM1)[27] was discovered to maintain a required and conserved role in SOCE. Using an RNA interference (RNA_i)-based screen, 170 genes were tested for involvement in CRAC currents. *Drosophila* S2 cells incubated with double stranded RNA (dsRNA) corresponding to a 500 bp fragment of CG9126 (*Drosophila Stim*) demonstrated a clearly reduced (>90 %) thapsigargin-induced Ca^{2+} entry. Additionally, the level of STIM mRNA was reduced by >50 % compared to the controls.

Drosophila STIM protein has two mammalian homologs named STIM1 and STIM2 which also control CRAC channel activation[26, 28-30]. STIM1, a 1-transmembrane-

spanning protein, is localized in the ER membrane functions as a Ca^{2+} sensor with its carboxy-terminus-located EF hand motif reaching into the ER lumen. Interestingly, store depletion causes STIM1 to redistribute from a diffuse ER localization into so-called punctae that are localize in the cell periphery without insertion into the plasma membrane. This translocation occurs several seconds before CRAC channels open indicating that it is an essential step in CRAC current activation[31] (Fig. 1).
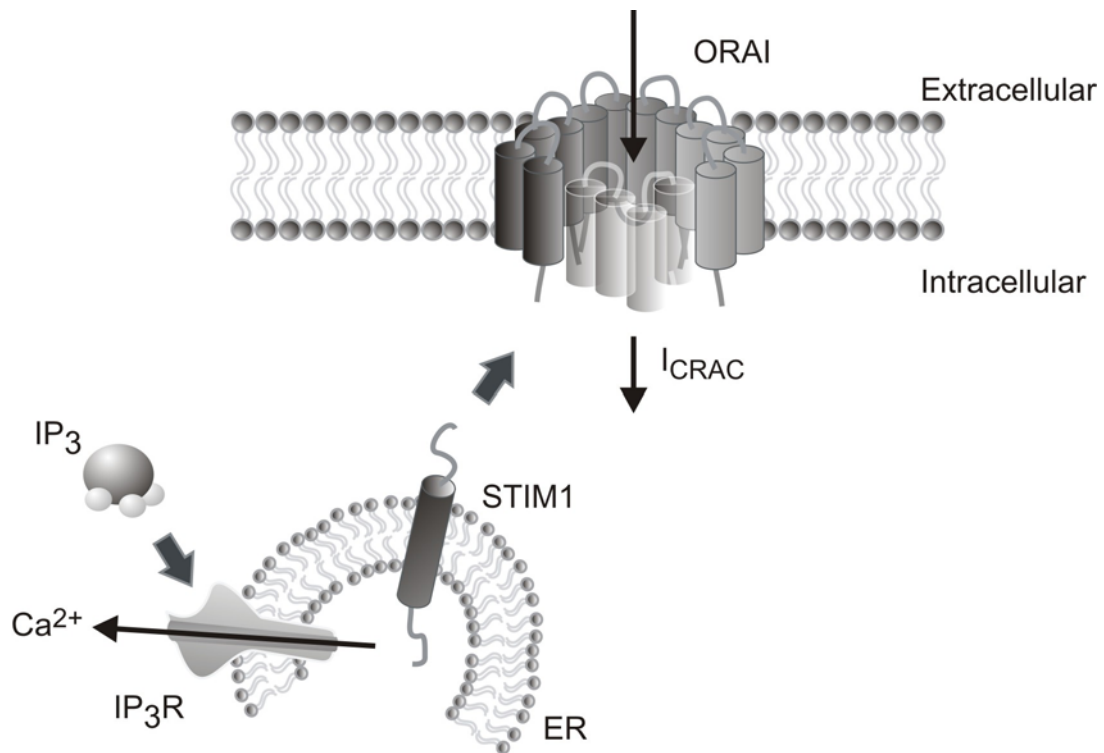
Figure 1: Illustration of CRAC current activation via Ca^{2+} store (endoplasmatic reticulum; ER) depletion by inositol–1, 4, 5–triphosphate (IP_3). IP_3 binds to the IP_3 receptor (IP_3R) localized in the ER membrane. Ca^{2+} is released from the ER and STIM1 redistributes into punctae close to the plasma membrane activating the CRAC currents (I_{CRAC}) through ORAI. In this process, the cytosolic STIM1 C-terminus associates with ORAI C-terminus.

2.1.3 The ORAI (CRACM) protein family

In early 2006, three groups individually reported a novel protein designated as ORAI1 or CRACM1 that represents another essential component for store-operated Ca^{2+} entry. An RNAi screen confirmed that *Drosophila* olf186-F is an important regulator of Ca^{2+} entry and it was hypothesized that ORAI1 by itself forms the responsible CRAC channel, a subunit of the channel or at least a component of the CRAC signalling pathway [8, 9, 32]. Additionally, T cells derived from two SCID (severe combined immuno-deficiency) patients were studied showing decreased Ca^{2+} entry due to a missense mutation in exon 1 of human ORAI1.

A single cytosine to thymin (C -> T) nucleotide substitution in position 271 of the coding sequence of ORAI1 leads to an arginine to tryptophan mutation at position 91 (R91W) of the amino acid sequence and disrupts the Ca^{2+} signal for NFAT translocation[8].

ORAI proteins are located in the plasma membrane and reveal four transmembrane segments in hydropathy plots with the N- and C-terminus facing the cytosol[9, 32]. Moreover, it was suggested that ORAI proteins form the CRAC channel pore because a change in the ion selectivity profile was observed due to the replacement of conserved charged amino acid residues in position 106 and 190 with uncharged amino acids[33]. Nevertheless, overexpression of ORAI family members (human ORAI1, ORAI2 or ORAI3) alone did not alter endogenous CRAC currents in several cell types[9] but Jurkat cells injected with ORAI1 or ORAI2 siRNA show suppression of SOCE[9]. In addition, the overexpression of human ORAI1 in T cells derived from SCID patients reconstituted Ca^{2+} entry in response to thapsigargin[8].

A breakthrough observation simplified the following characterization of ORAI proteins. Cells overexpressing STIM1 plus ORAI1 showed a clearly detectable CRAC current developing in immediate response to intracellular IP_3 perfusion[11]. These currents had all the CRAC current hallmark features such as Ca^{2+} selectivity, monovalente conductance upon removing all divalent ions in the extracellular solution, and an inhibition by 2-APB[11]. In combination with STIM1, the human ORAI1 homologs ORAI2 (CRACM2) and ORAI3 (CRACM3) showed I_{CRAC} potentiation as well[34]. All three ORAI variants exhibit distinct properties in terms of selectivity and

pharmacological effects in response to 2-APB and a potential heteromerization among ORAI proteins was proposed to provide flexible Ca^{2+} signalling[34].

Related project

As previously mentioned, human STIM1 and human ORAI proteins appear to be the molecular components for the store-operated CRAC current. In my study, I focused on the functional properties of murine ORAI proteins. The genomic organization of the ORAI genes was described by U. Wissenbach from our group[35].

The single copy ORAI1 and ORAI3 genes are localized on the murine chromosomes 5G1 and 7F2 – 7F3, respectively. Additionally, two gene loci exist for ORAI2, one on chromosome 5G2 and a second one on chromosome 16C1. Interestingly, locus 5G2 is composed of 5 predicted exons which give rise to the splice variants ORAI2Long (ORAI2L) and ORAI2Short (ORAI2S) (Fig. 2).

Alternative splicing involves the exons 2 and 3 and since the start methionine for ORAI2L is located in exon 3, the ORAI2S N-terminus is truncated by 14 amino acids (Fig. 2). The expression of orai2 on chromosome 16 might lead to a single amino acid substitution at position 130 (N130Y; hereafter referred to as ORAI2S (N130Y)) whereas ORAI2 proteins are believed to be transcripted exclusively from chromosome 5[35, 36].

In our group, we further investigated the expression of ORAI and STIM proteins in murine tissues and cell lines that were used for overexpression experiments. Detailed information about the expression pattern is reported in Gross et al., 2007 and Wissenbach et al., 2007[35, 36] in addition to the cloning of murine ORAI proteins and STIM1. U. Wissenbach cloned murine STIM1 and murine ORAI1, ORAI2L and ORAI2S and additionally murine ORAI2S (N130Y) into expression vector plasmids (see Materials and Methods) for investigation in transiently transfected HEK 293 and RBL 2H3 cells which provide different genomic backgrounds in endogenous ORAI and STIM expression, perfectly suited for the analysis of recombinant CRAC channels.

The aim of this study is to determine the functional properties of murine ORAI1, ORAI2L and ORAI2S. In co-expression experiments with STIM1, I recorded clearly

detectable currents showing CRAC current hallmarks and, furthermore, functional interactions between ORAI1 and ORAI2 variants were detectable. Here it is shown that the N-terminus of ORAI plays a crucial role in channel activity as it is impressively shown in the non-functional ORAI Scid variants.

Since L-type Ca^{2+} channel Gamma subunits show similar structural properties to ORAI proteins, I further investigated whether STIM1 and GAMMA1 (G1) or GAMMA2 (G2) reconstitute CRAC currents or whether G1 or G2 interfere with endogenous CRAC current development. Finally, I examined CRAC currents in cortical neurons, a cell type showing STIM1 and ORAI expression.
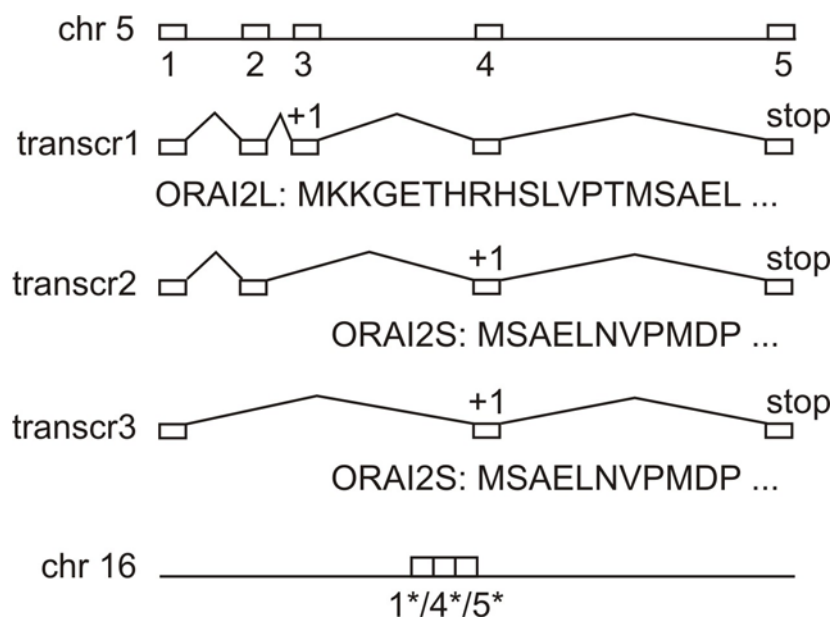

Figure 2: Two different orai2 loci have been identified in the mouse genome. The locus on chromosome 5 (chr 5) consists of 5 exons (1 – 5). Transcripts 1, 2 and 3 (transcr 1 – 3) are generated by alternative splicing. Start methionines (+1) and stop codons (stop) are shown. The N-termini of the encoded amino acid sequences are given below each transcript. Transcript 1 encodes a protein (ORAI2L) that is 14 amino acids longer than the protein ORAI2S encoded by transcript 2 and 3. The orai2 locus on chromosome 16 contains 3 intron-less exons (1[*], 4[*], 5[*]) that are highly homologous to exons 1, 4 and 5Modified from U. Wissenbach et al.[36].

2.2 TRP ion channels

The mammalian TRP (transient receptor potential) ion channel superfamily consists of 28 members divided into six subfamilies named TRPC (canonical), TRPV (vaniloid), TRPM (melastatine), TRPA (ankyrin), TRPML (mucolipid) and TRPP (polycystins)[37]. Within a subfamily, sequence homology approaches up to more than

90 %, but the corresponding similarity is hard to detect among members of different subfamilies. TRP proteins play critical roles in processes ranging from sensory physiology to vasorelaxation and male fertility. Originally, the TRP protein was identified as a *Drosophila* gene product required for visual transduction[38]. The name derived from the phenomenon that flies carrying a mutation in the *trp* locus showed rather a transient than a sustained response to light[39]. Although the crystal structures for TRP proteins are not available yet, it is believed that all TRP proteins comprise 6 transmembrane segments (TM 1 - 6) with a pore forming region between TM 5 and TM 6 (Fig. 3). As for voltage-gated K^+ channels, it is assumed that TRP channel proteins form homo- and heterotetrameric ion channels[40]. TRP proteins are located in the plasma membrane and function as cation permeable ion channels activated by a diverse variety of stimuli[37, 41]. To mention a few, TRPV1 for instance appears to be activated by vanilloid compounds such as the active ingredient in hot chilli peppers (capsaicin) and anandamide as well as by temperatures exceeding $42°C$[42]. In contrast, TRPM8 is activated by temperatures below $26°C$ and cooling agents such as menthol and icilin[43]. Furthermore, TRP channel modulation results from phosphorylation/dephosphorylation or other cellular signalling mechanisms such as regulation by Ca^{2+}/calmodulin[41]. Genetic approaches in worms, flies and mice demonstrate a role for many TRP proteins in sensory processes like thermosensation[44] and osmosensation[45], taste[46] and mechanosensation[47], just to mention a few. Additionally, mutations in TRPs have been linked to human diseases such as Mucolipidosis type IV or polycystic kidney disease. Down- and upregulation in cancer tissue[48, 49] is reported for some TRP proteins as well. Apart from this plethora of physiological functions, many TRP studies were designed around the SOCE hypothesis suggesting TRP channels as a critical component for Ca^{2+} entry. TRP proteins were reported to contribute to changes in intracellular Ca^{2+} levels by providing a Ca^{2+} entry pathway, by modulating the driving force for the Ca^{2+} entry or providing intracellular pathways for Ca^{2+} release from cellular organelles[50]. Anyhow, so far no mammalian TRP has fulfilled all the criteria set forth for SOCE.
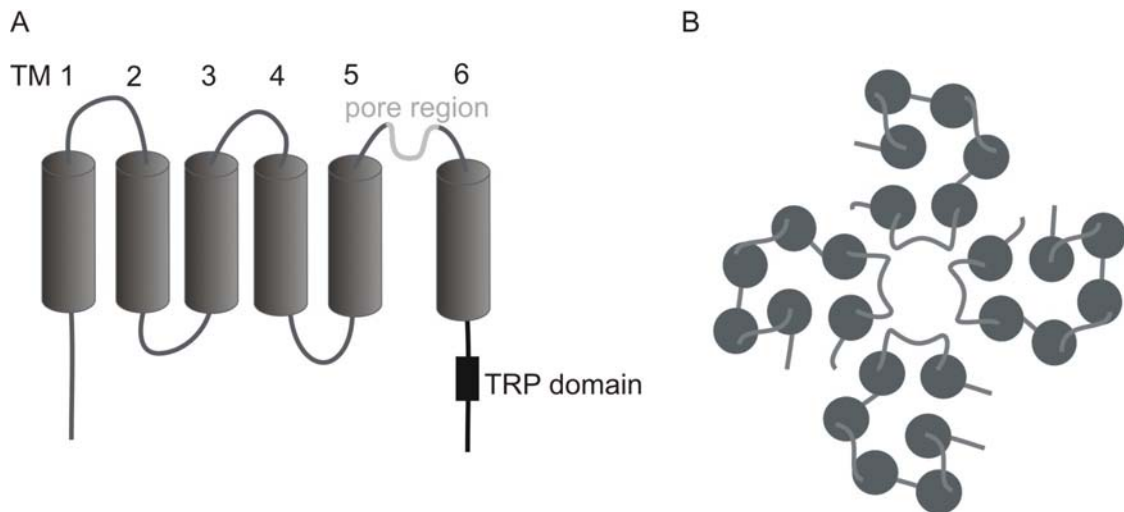
Figure 3: (A) A model TRP protein containing six transmembrane domains (TM 1 – 6) with a pore loop (pore region) between TM 5 and TM 6 and the TRP domain located at the C-terminus (B) Four TRP proteins are assumed to form homo- or hetero-oligomeric channels. Modified from Montell, Birnbaumer and Flockerzi, 2002[37].

2.2.1 Transient receptor potential channel 5 (TRPC5)

TRPC5 is a member of the TRPC subfamily and is closely related to TRPC4 (64 % homology) and was first cloned from rabbit and mouse brain by Philipp et al., 1998[13]. The protein is reported to be expressed in neurons, sperm head, smooth muscle cells and mast cells[51-54]. In homo-multimeric or hetero-multimeric assembly with TRPC1, the activation occurs via G-protein ($G_{q/11}$-type)-coupled receptor stimulation. Accordingly, intracellular GTP-γ-S (a stable analogue of guanosine triphosphate) is sufficient to stimulate TRPC5[55]. Channel activation by muscarinic agonists or epidermal growth factor (EGF) is surpressed by the phospholipase C (PLC) inhibitor U73122 suggesting that PLC activity plays an elementary role in channel activation[56]. IP_3 or its receptor are discussed to be involved in TRPC5 activation whereas diacylglycerol (DAG) appears to inhibit TRPC5 rather than activate[56]. Moreover, a striking feature of TRPC5 is its strong activation by extracellular lanthanides such as lanthanum or gadolinium[57]. All the other TRP channels show inhibition in the presence of extracellular lanthanides.

The importance of intracellular Ca^{2+} levels is widely discussed among several laboratories. It has been shown that TRPC5 is activated in response to ionomycin[58], a store-depleting ionophore, as well as in response to thapsigargin (TG)[13]. Furthermore, the buffering of intracellular Ca^{2+} levels to sub-physiological concentrations suppresses the activation of TRPC5 by other stimuli[59].

Channel activation and also rapid translocation from intracellular vesicles to the plasma membrane occurs in response to epidermal growth factor (EGF). These vesicles are located in close proximity to the plasma membrane and TRPC5 channels relocate to the plasma membrane providing a greater surface expression of the channel protein[60]. An important binding partner of TRPC5 is the Ca^{2+}-binding protein calmodulin (CaM) which plays a role in mediating Ca^{2+} signals. Two binding CaM domains were identified (Fig. 4): A so called CIRB site (CaM-IP$_3$ receptor binding) and a second binding site named CBII (CaM binding site II)[61, 62] located at the C-terminus. CaM binding site mutants differ in current activation by receptor stimulation. Cells overexpressing TRPC5ΔCBII mutants show a reduced histamine-induced Ca^{2+} entry in comparison to WT TRPC5 transfected HEK 293 cells. TRPC5 with CIRB site mutations did not show any current development in response to histamine perfusion[62].

TRPC5 inhibition is mediated by 2-aminoethoxydiphenyl borate (2-APB) occurring exclusively at the external face of the channel[63]. Moreover, chlorpromazine[64], calmidazolium and SKF-96365[65] block receptor-activated TRPC5 currents and hallmark activators lanthanum and gadolinium inhibit current development in high extracellular concentrations (>100 µM)[57].

Related Project

TRPC5 ion channels appear to be activated by a multiplicity of signals and, thus, there has been a lively discussion about whether TRPC5 is store-operated or activated by PLC signalling cascade. Recent reports define SOCE channels as ion channels activated by STIM1 and they show that STIM1 is obligatory for TRPC5 channel activation by agonists[66]. Another TRPC5 channel modulator is diacylglycerol (DAG) and protein kinase C (PKC) activation leads to a current fade out over time[59]. As seen in Fig. 4, the TRPC5 activation pathway depends on several crucial steps, whereas the direct activator has not been identified so far.
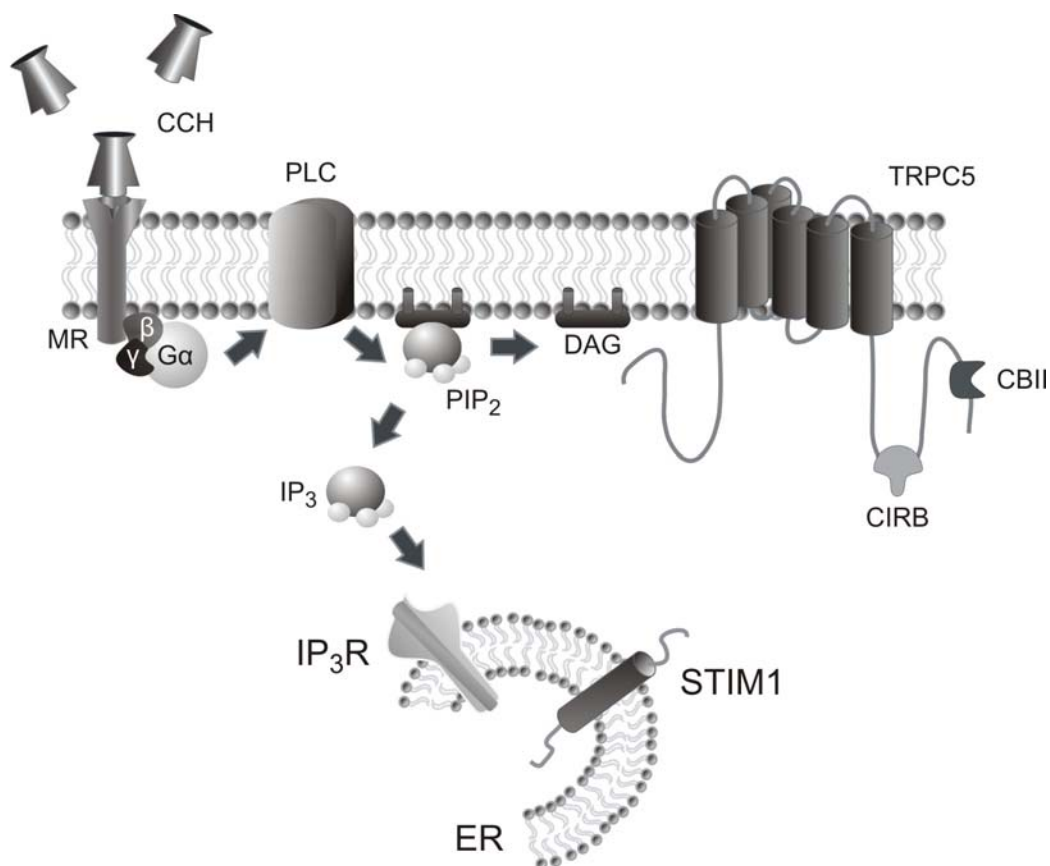
Figure 4: Schematic summary of TRPC5 activation by muscarinic agonists (CCH: carbachol; MR: muscarinic receptor). GTP bound G-protein (Gα, β and γ) activates the phospholipase C (PLC) resulting in the cleaving of phosphatidylinositol bisphosphate (PIP$_2$) into inositol triphosphate (IP$_3$) and diacylglycerol (DAG). IP$_3$ binds to the endoplasmatic reticulum (ER) membrane located IP$_3$ receptor (IP$_3$R) resulting in store depletion. DAG remains on the cell membrane activating protein kinase C (PKC; not shown here). Two calmodulin binding sites are located at the C-terminus of TRPC5 (CIRB and CBII). The ultimate step in activation of TRPC5 channels is not known.

The aim of this study is to determine the final mediator for TRPC5 activation. TRPC5 channels were originally described as SOCE channels and initial investigations have left room for interpretations to functional interactions between TRPC5, STIM1 and ORAI1. Here, it is shown that the least common denominator for TRPC5 activation is the rise in the intracellular Ca^{2+} concentration ($[Ca^{2+}]_i$) leading to a dose-dependent Ca^{2+}-activation mechanism. Furthermore, CRAC currents mediated by STIM1/ORAI1 and Ca^{2+} influx through L-type Ca^{2+} channels act as a physiological Ca^{2+} donor. Thus, activation of these `donor´ channels have resulted in a rise of local Ca^{2+} levels inducing to TRPC5 current development. These observations make a good case for novel regulatory mechanisms in Ca^{2+} signalling and a new physiological relevance for TRPC5 ion channels.

3 Materials and Methods

3.1 Cell culture and transfection

3.1.1 STIM1 and ORAI experiments

Human embryonic kidney cells (HEK 293) and rat basophilic leukaemia cells expressing the human muscarinic receptor M1 (RBL 2H3 referred to as RBL) were cultured as previously described[67]. Plasmids containing the cDNAs of the murine STIM1, ORAI1, ORAI2L, ORAI2S, GAMMA1, GAMMA2, TRPC3 and TRPC5 were transfected into these cells either individually or in combination using the PolyFect transfection reagent (Qiagen, Hilden, Germany). For individual transfections, 3 µg of each plasmid was used per cell dish. For co-transfections, the STIM1 plasmid was mixed with one of the plasmids containing ORAI1, ORAI2L, ORAI2S, GAMMA1 or GAMMA2 at a ratio of 1:2 or a TRPC plasmid was mixed with one of the plasmids containing STIM1, ORAI1 or ORAI2S. The total amount of plasmid mix was 3 µg per cell dish. For triple co-transfections, plasmids containing STIM1, ORAI1 and either ORAI2L, ORAI2S, TRPC3 or TRPC5 were mixed at a ratio of 1:2:1. Accordingly, the total amount of plasmid mix was 4 µg per cell dish. The bicistronic expression vector pdi contained the cDNA of the enhanced green fluorescence protein (GFP) as expression marker. Patch clamp experiments were performed on GFP expressing cells 2-3 days after transfection.

3.1.2 TRPC5 experiments

HEK 293 cells were cultured as described. TRPC5 plus M_2R (muscarinic receptor 2) stably transfected HEK 293[68] (a gift from Mike Zhu, Ohio, USA) hereafter referred to as TRPC5-stably transfected HEK 293 cells were cultured in DMEM 41966 medium (Gibco, Karlsruhe, Germany) containing 10 % heat-inactivated fetal calf serum, penicillin-streptomycin (100 µg/ml; Gibco), hygromycin B (100 µg/ml; PAA) and G418 (400 µg/ml; Gibco). Individual transfections of STIM1, ORAI1, ORAI2S, ORAI1 Scid, ORAI2S Scid, TRPC3, TRPC5, TRPC5 CIRB mutant 1 in pIRESneo (J1305[62]),

TRPC5 DelCBII in pIRESneo (J1307[62]), were performed using the AMAXA Nucleofector® electroporation system (AMAXA biosystems, Cologne, Germany) according to the general protocol for nucleofection of adherent cell lines provided by AMAXA. J1305 and J1307 plasmids were kindly provided by Mike Zhu[62]. For co-transfections, plasmids containing STIM1 were mixed with ORAI1 and ORAI1 Scid in the ratio 1:1. For triple transfections, the alpha-subunit and the beta-subunit of L-type Ca^{2+}-containing expression vectors were mixed with a GFP-containing pCAGGS vector plasmid in the ratio 2:2:1. The total amount of plasmid per transfection was 5 µg. Experiments were performed on GFP expressing cells 1 - 3 days after transfection or in non-transfected TRPC5 stable cells or HEK 293 control cells 1 - 2 days after plating.

If not mentioned otherwise, all cDNAs were subcloned downstream of the chicken actin promotor into the pCAGGSM2 vector containing an IRES GFP site as described elsewhere[36, 69].

3.1.3 Isolation of cortical neurons

Single neurons for PCR analysis were prepared similar as described in Neumann et al., 1995[70]. Cells were maintained in culture for 1 – 2 days before use.

3.2 Treatment with cytochalasin D, U73122 and EGF

3.2.1 The mycotoxin cytochalsin D

Cytochalasin D, *Zygosporium mansonii* (Calbiochem) is a fungal metabolite that has the ability to bind actin filaments and block actin polymerization and, thus, the cellular morphology undergoes changes and cellular processes such as cell division and vesicular translocation are inhibited[71-73]. In the present experiments, cells were incubated in medium containing 10 µM cytochalasin D for 10 min at 37°C. Afterwards cells were washed with external solution used in the patch clamp experiments. The stock solution contained 1 mM cytochalsin D which was prepared using dimethyl sulfoxide (DMSO).

3.2.2 The PLC inhibitor U73122

U73122 (Calbiochem) inhibits agonist-induced phospholipase C (PLC) activation[74]. In indicated experiments, cells were incubated in 2 μM U73122 containing culture medium for 5 min at 37°C and washed with external solution prior to patch clamp recordings. Stock solution contained 2 mM U73122 in DMSO.

3.2.3 Epidermal growth factor (EGF)

Epidermal growth factor (EGF) from mouse submaxillary glands (Sigma-Aldrich) is a growth factor that plays an important role in the regulation of cell growth, proliferation and differentiation. Further roles include neuromodulation of the central nervous system[75] and also modulation of TRPC ion channels[60, 76]. In the present experiments, cells were incubated for 4 min at 37°C in external solution containing 100 ng/ml EGF and 0.5 % bovine serum albumin (BSA; Sigma-Aldrich). Cells were washed with basic external solution before experiments. The stock solution contained 10 μg/ml EGF diluted in H_2O.

3.3 Scid mutations in murine ORAI1 and murine ORAI2S proteins

Based on mORAI1 and mORAI2S containing pcDNA3 vector plasmids (Invitrogen) cloned by U. Wissenbach[36], murine ORAI1 Scid and murine ORAI2S Scid mutations were generated. The non-functional human ORAI1 Scid mutation was described as an C to T transition at position 271 of the coding sequence of ORAI1 resulting in an arginine to tryptophan substitution at position 91 in the ORAI1 amino acid sequence (R91W)[8]. According to Feske et al.[8], I designed the following primer pairs for ORAI1 and ORAI2S to introduce a single nucleotide exchange (C to T) at position 277 of the coding sequence of mORAI1 and at position 235 of mORAI2, respectively resulting in R91W in murine ORAI1 and R78W in murine ORAI2:

mOrai1:   5´-GCTCAAAGCTTCCAGCTGGACCTCGGC-3´ (SG1)

               5´-GCCGAGGTCCAGCTGGAAGCTTTGAGG-3´ (SG2)

mOrai2S: 5´-GCCTCCAGCTGGACCTCAGCCCTCC-3´ (SG3)

               5´-GGAGGGCTGAGGTCCAGCTGGAGGC-3´ (SG4)

               (Operon, Cologne, Germany)

For mutagenesis, the Quick Change® Site-Directed Mutagenesis Kit (Stratagene, California, USA) was used according to the provided protocol and mutated plasmids were transformed into competent XL1-blue *Escherichia coli* bacteria (Stratagene). Single colonies were picked and incubated in 50 µg/ml ampicillin containing LB-medium (lysogeny broth). DNA isolation was performed by using the QIAprep Spin-Miniprep Kit (Qiagen, Hilden, Germany) according to the provided protocol and the ABI Prism® sequencer 310 Genetic Analyzer (Applied Biosystems, California, USA) was used for DNA sequencing. This technique is based on the dye-terminator sequencing principle, a common alternative among the chain-termination methods of DNA sequencing. Chain termination sequencing was developed by Sanger and the key principle is the use of dideoxynucleotides triphosphates (ddNTPs) as DNA chain terminators. I used the Big Dye® terminator v.1.1 cycle sequencing kit providing a fluorescence-labelled ddNTPs containing dNTP mix as follows:

0.5 µg DNA template

1.5 µl Big Dye terminator v1.1 ready reaction mix

1 µl primer (10 pmol/µl)

ad 12 µl H_2O deionized.

PCR temperature cycle:

95°C 3 min

95°C 10 s

58°C 2 min 30 s   } 30 x

 4°C oo

After PCR, 12 µl probes were purified by sepharose spinning and denatured by adding 8 µl HiDye® (Applied Biosystems). Purified and denatured probes were sequenced using Prism® sequencer 310 Genetic Analyzer. Provided data collection

software and sequencing analysis software was used to record and analyse the resulting sequences.

Table 1: (A) Primer pairs to confirm the nucleotide exchange C to T in mORAI1 and mORAI2S containing pcDNA3 vector plasmids after mutagenesis. (B) Primer pair to check directed insertion into pCAGGSM2/IRES GFP vector plasmid after ligation. All primers were synthesized by Operon, Cologne, Germany.

	Sequencing	Primer name	Sequence 5´ to 3´
A	ORAI1/2S Scid pcDNA3	pRCforUW	CTAGAGAACCCACTGCTTAC
	ORAI2S Scid pcDNA3	UW615	GCCAGCTCGATGTACGG
B	ORAI1/2S Scid	pCAGGSforUW	AACBTGCTGGTTGTTGTGC
	pCAGGSM2/IRES GFP	pCAGGSrevUW	CATATAGACAAACGCACACC

Confirmed ORAI1 Scid and ORAI2S Scid-containing pcDNA3 plasmids were treated as follows:

ORAI1 Scid pcDNA3 (Fig. 5)

Plasmid vector was cut by XhoI.

DNA fragments were separated by gel electrophoresis on 0.8 % GTQ-agarose (Roth, Karlsruhe, Germany) gel.

Expected DNA band for the mORAI1 Scid fragment (915 bp) was electro-eluated, ammonium acetate precipitated and dissolved in 22.75 µl deionized H_2O.

Blunting (= sticky ends due to XhoI cut were filled up with dNTPs to blunt ends):

22.75 µl DNA template

1.25 µl dNTP mix (1.25 mM; New England BioLabs)

2 µl T4-polynucleotide kinase (New England BioLabs)

1 µl T4 DNA-polymerase (New England BioLabs)

3 µl ligase buffer (New England BioLabs)

(30 min at 37°C, 10 min at 75°C (enzyme inactivation))

Ammonium acetate precipitation

DNA template was dissolved in 20 µl deionized H_2O

Over night ligation at 16°C of the blunted ORAI1 Scid DNA template into EcoRV cut pCAGGSM2/IRES GFP vector plasmid:

1 µl ligase (New England BioLabs)

2 µl ligase buffer (New England BioLabs)

1 µl pCAGGSM2/IRES GFP, EcoRV, AA (50 ng/µl)

16 µl blunted ORAI1 Scid insert

ORAI2S Scid pcDNA3 (Fig. 5)

ORAI2S Scid fragment was amplified from the OAI2S Scid-containing pcDNA3 vector:
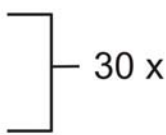
2.5 µl UW 605 (10 pmol/µl; Operon:

5´-[Phos]CCGCCGCCACCATGAGTGCAGAGCTCAATGTGC-3´)

2.5 µl UW 606 (10 pmol/µl; Operon:

5´-[Phos]TCACACCACCTGCAGGCTC-3´)

1.0 µl dNTP mix (1.25 mM; New England BioLabs)

10 µl HF-buffer (Finnzymes)

1 µl Phusion™ High-fidelity DNA polymerase (Finnzymes)

ad 50 µl H$_2$O deionized

PCR temperature cycle:

98°C 1 min
98°C 5 s
58°C 10 s   30 x
72°C 20 s
72°C 2 min
4°C oo

DNA fragments were separated by gel electrophoresis on 0.8 % GTQ-agarose gel (Roth, Karlsruhe, Germany).

Expected DNA band for the mORAI2S Scid fragment (750 bp) was electro-eluated, ammonium acetate precipitated and dissolved in 22.75 µl deionized H$_2$0.

Over night ligation at 16°C of the ORAI2S Scid DNA template into EcoRV cut pCAGGSM2/IRES GFP vector plasmid:

1 µl ligase (New England BioLabs)

2 µl ligase buffer (New England BioLabs)

1 µl pCAGGSM2/IRES GFP, EcoRV, AA (50 ng/µl)

5 µl blunted ORAI1 Scid insert

ad 20 µl H_2O deionized

ORAI1 Scid and ORAI2S Scid containing pCAGGSM2/IRES GFP vector plasmids were cut with EcoRI to confirm whether ligation was successful or whether the DNA insert was not integrated. In addition, the vector plasmids were sequenced using primer pair pCAGGSforUW and pCAGGSrevUW (Table 1) to confirm site-directed insertion.

Final plasmids:

mORAI1_Scid pCAGGSM2/IRES GFP Kl. 10 (Nov. 12, 2007)

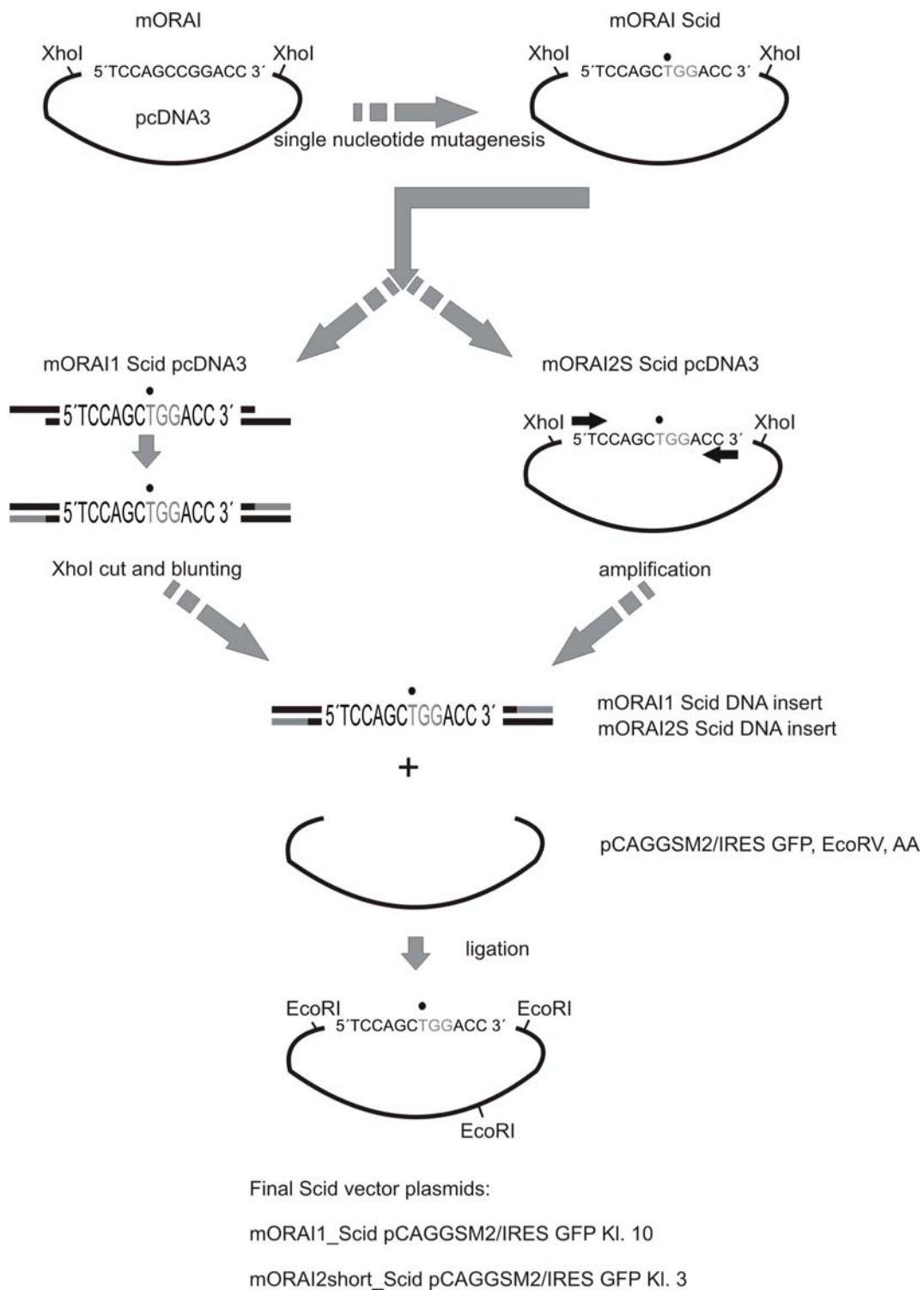mORAI2short_Scid pCAGGSM2/IRES GFP Kl. 3 (Nov. 22, 2007)

Figure 5: Schematic overview about the generation of mORAI Scid mutant pCAGGSM2/IRES GFP plasmid vectors based on mORAI1 and mORAI2S-containing pcDNA3 plasmid vectors. C to T mutation (black dot) was made using the Quick Change site-directed mutagenesis kit. XhoI cut and blunting (mORAI1 Scid) or PCR amplification (mORAI2S) was prerequisite to ligating the mutated DNA templates to pCAGGSM2/IRES GFP plasmid vectors.

3.4 Patch Clamp techniques

The patch clamp technique allows the recording of ionic currents flowing across biological membranes through pore-forming ion channels. Single as well as multiple ion channel currents can be studied using the patch clamp technique[77]. Patch clamp recordings are performed with glass micropipettes that have a tip diameter of $1 - 5$ µM. Usually, the pipettes are fire-polished in a microforge to produce a smooth surface tip improving the establishment of a so-called "gigaseal" with the cell membrane. Initially the pipette is moved towards the cell. To protect the tip of the pipette from contaminations, a positive pressure is usually applied to the pipette interior. When the pipette tip carefully touches the cell membrane, gentle suction is applied to establish a very tight contact or seal called "gigaseal". The term gigaseal describes the fact that glass pipette and cell membrane establish a very tight conjunction hindering a free ion flow between the pipette solution and the external solution and, thus, displaying resistance >1 GΩ. To obtain the so-called "tight-seal whole-cell" configuration of the patch clamp technique, a short negative pressure is applied to break the membrane patch underneath the pipette. In this configuration the membrane currents flowing through the whole membrane of the cell are recorded. With patch clamping, only one micropipette is used for both voltage clamping and current measurement in contrast to traditional voltage clamping. This means that the membrane potential is held constant, while the current flowing between intracellular and extracellular environment through ion channels is measured. A basic electrical circuitry for patch clamp measurements is shown in Fig. 6.

Table 2: Internal (A) and external (B) patch clamp solutions. Additional reagents were added to patch clamp solutions as described in the results.

A

Substance	Basic 1 Final conc. (mM)	Calcium solutions Final conc. (mM)	Basic 2 Final conc. (mM)	Provider
CsCl	120	120		Serva GmbH
NaCl	10	10	8	Merck KGaA
$MgCl_2$	3	3	3	Merck KGaA
EGTA	10	10		Sigma-Aldrich Inc.
HEPES	10	10	10	Sigma-Aldrich Inc.
Glutamic Acid			120	Sigma-Aldrich Inc.
(K^+)-BAPTA			10	Sigma-Aldrich Inc.
CsOH			pH titration	Acros
$CaCl_2$		0.01 - 10 µM free Ca^{2+}		
pH	7.2 - 7.3	7.2 - 7.3	7.2 - 7.3	

Free Ca^{2+} concentration was calculated in Webmaxc Standard;
http://www.stanford.edu/~cpatton/webmaxcS.htm

Additional reagents		
Substance	Final conc.	Provider
IP_3	20 µM	Calbiochem
4-BrA23187	200 nM	Teflabs
Ionomycin	5 µM	Calbiochem

B

Substance	Basic Final conc. (mM)	NCaF Final conc. (mM)	DVF Final conc. (mM)	Provider
NaCl	120	120	120	Merck KGaA
CsCl	10	10	10	Serva GmbH
$MgCl_2$	2	2		Merck KGaA
$CaCl_2$	5			Merck KGaA
HEPES	10	10	10	Sigma-Aldrich Inc.
Glucose	10	10	10	Merck KGaA
EGTA			1	Sigma-Aldrich Inc.
HEDTA			1	Sigma-Aldrich Inc.
pH	7.2 - 7.3	7.2 - 7.3	7.2 - 7.3	

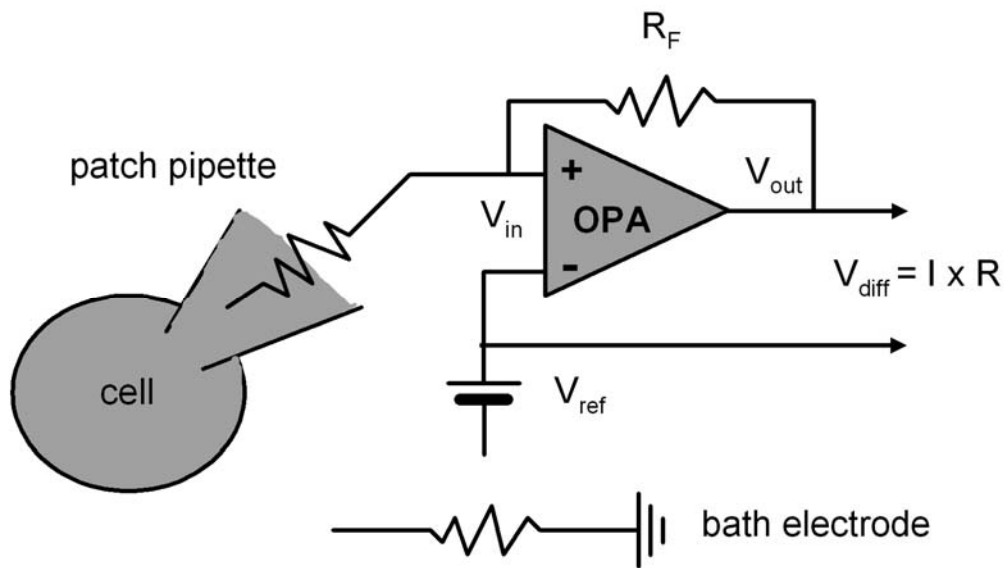| Additional reagents		
Substance	Final conc.	Provider
Carbachol	200 µM	Sigma-Aldrich Inc.
U73122	2 µM	Calbiochem
Cytochalasin D	10 µM	Calbiochem
EGF	100 ng/ml	Sigma-Aldrich Inc.
BSA	0.50%	Sigma-Aldrich Inc.

Figure 6: Conceptual diagram of the Patch clamp setup. The feedback resistor (R_F) and the operational amplifier (OPA) are the key components of this system. The amplifier induces according to a reference (Vref) of an appropriate current pulse to clamp the membrane potential at desired levels (modified from Gross, 2005[78]).

In this study, patch clamp recordings were performed in the tight-seal whole-cell patch configuration to record CRAC currents, Ca^{2+} currents through L-type Ca^{2+} channels, non-selective currents through TRPC5 channels and Na^+ currents in cortical neurons. The advantage of whole-cell recordings is that the intracellular medium is defined by the pipette solution and activating reagents can be applied to the intracellular environment.

Patch pipettes (borosilicate glass, Biomedical Instruments) were made in a two-step puller (H. Ochotzki, Homburg). The pipettes were filled with a saline solution hereafter referred to as the internal or pipette solution (Table 2, A). Cells are perfused with a solution of defined composition hereafter referred to as the external or bath solution (Table 2, B). For recording the time course of developing currents, voltage ramps from +80 mV to -100 mV (duration 50 ms; STIM1 / ORAI experiments) or from -100 mV to +100 mV (duration 50 ms; TRPC5 experiments) were applied every 2 s for at least 100 s. In the STIM1 / ORAI experiments in which the external solution was exchanged, voltage ramps were applied every 0.5 s. The holding potential was 0 mV and sampling rate was 20 kHz (STIM1 / ORAI) and 10 kHz (TRPC5). In STIM1 / ORAI1 experiments inward current development was monitored at -90 mV for each individual voltage clamp ramp whereas potentials of -80 mV and +80 mV were used

to monitor inward and outward currents, respectively, in TRPC5 experiments. Current densities were calculated as the current amplitude a) subtracted by the individual background current in STIM1 / ORAI experiments or b) non-subtracted amplitude in TRPC5 experiments and divided by the appropriate initial C_{slow}. Capacitive currents were determined and corrected in advance of each voltage ramp. Step protocols were delivered from -100 mV to +100 mV in 10 mV steps from the holding potential at 0 mV or at 60 mV (L-type channel experiments). TRPC5 / L-type channel activation was recorded by applying a two step voltage protocol every 2 s. From holding potential at -60 mV (50 ms), voltage step to 0 mV (100 ms) and voltage step to +80 mV (50 ms). Local external solution perfusion was applied with a pressure-controlled 8-valve local perfusion system (ALA Scientific Instruments, New York, USA; PR-10, ALA-VM8; 4 channel perfusion pencil[TM], Micromanifolds[®] QMM-4 and custom made pipette tips: dead volume ~ 150 µl). Pulse v8.80 (HEKA) software was used to control the EPC-9 patch clamp amplifier (HEKA, Lambrecht, Germany) and to record and visualize the currents. PulseFit v8.80 (HEKA), Igor Pro 5.0.1.0 (Wavemetrics Inc.) and SigmaPlot 9.01 (SPSS Inc.) were used for analysis.

3.5 Ca^{2+} imaging

Ca^{2+} imaging is used to study the calcium status of a tissue or individual cell. It takes advantage of Ca^{2+} indicators that respond to the binding of Ca^{2+} ions by changing their spectral properties[79]. Single wavelength Ca^{2+} indicators (Fluo-3) as well as ratiometric indicators (Indo-1, Fura-2) are commonly used for Ca^{2+} imaging. The advantage of ratiometric dyes over single wavelength indicators is that possible artefacts due to photobleaching and different dye loading are avoided. For instance, upon Ca^{2+}-binding, the fluorescence excitation maximum of FURA-2 undergoes a blue shift from 363 nm (Ca^{2+}-free) to 335 nm (Ca^{2+}-saturated), while the fluorescence emission maximum is relatively unchanged at approximately 510 nm. Therefore, the ratio of intensities of the fluorescence emitted by exciting at 340 and 380 nm is directly related to the free Ca^{2+} concentration.

Ca^{2+} imaging experiments were performed to record the intracellular Ca^{2+} transients due to store depletion in response to thapsigargin or charbachol. The advantage of

the system is that the intracellular environment is not changed and further effects due to Ca^{2+} release from the stores are detectable. Moreover, the Ca^{2+} entry through non-selective TRP5 channels can be monitored.

In the present study, intracellular Ca^{2+} transients were measured using FURA-2 in individual cells by fluorescence microscopy using the iMIC (TILL photonics, Gräfelfing, Germany) and TILLvisION (TILL photonics) software. Cells (HEK 293 and TRPC5-stably transfected HEK 293) were grown on poly-L-lysine-coated cover slips and incubated with 10 µM FURA-2AM (Molecular Probes) for 40 min at room temperature and then washed with basic external solution (HBSS; Table 2). The coverslips were placed into a circular open-bottom chamber and mounted onto the stage of the iMIC. Intracellular Ca^{2+} transients in individual cells were monitored at room temperature exciting FURA-2 alternately at 340 nm and 380 nm for 10 ms each using a Polychrome V (TILL photonics; no excitation filter) and recording the emitted fluorescence at 510 nm (Dicroic: DCLP410; Emitter filter: LP470 TILL photonics). All reagents were applied by adding the reagent containing basic solution to the cells (principle shown in Fig. 7).
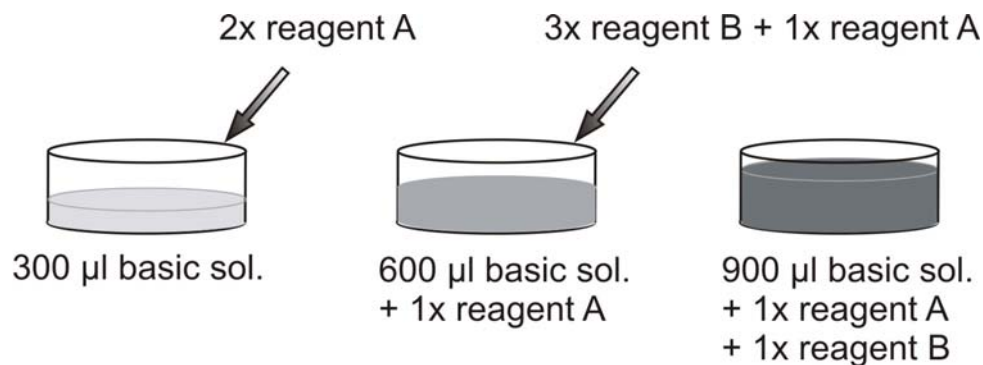

Figure 7: Simplified perfusion in Ca^{2+} and membrane potential imaging experiments. Activating reagents were dissolved 2 or 3 times higher in basic solution (basic sol.) and added in to appropriate volumes to the cell chamber to obtain the desired final concentrations.

Results are given as the background subtracted ratios of F_{340}/F_{380} calculated in TILLvisION (TILL Photonics) and Sigma Plot 9.01 (SPSS Inc.). Regions containing no cells were used as background. Solutions are listed in Table 3.

3.6 Membrane potential imaging

Membrane potential is defined as the electrical potential difference (voltage) across the plasma membrane of a cell and is determined by the ion channels present in the membrane as well as by the ionic gradients across the membrane At rest, the membrane potential is kept relatively stable and changes in membrane potential provide the basis for a fast communication between cells in a functional environment such as neuronal networks. In the case of the standard membrane potential across, potassium and sodium concentration gradients are established by the Na-K-ATPase (Na^+-K^+-exchanger). Under stable conditions, cells maintain a resting potential which can be calculated for Na^+, K^+ and Cl^- using the Goldman equation (equation (1); also referred as Goldman-Hodgkin-Katz equation)[80].

equation (1)
$$E_m = \frac{RT}{F} \ln \frac{P_K[K^+]_O + P_{Na}[Na^+]_O + P_{Cl}[Cl^-]_I}{P_K[K^+]_I + P_{Na}[Na^+]_I + P_{Cl}[Cl^-]_O}$$

E_m = The membrane potential
T = The temperature in kelvins
R = The ideal gas constant
P_{ion} = the permeability for that ion
F = The Faraday´s constant
$[ion]_O$ = the extracellular concentration of that ion
$[ion]_I$ = the intracellular concentration of that ion

As shown in equation (1), the permeability of the cell membrane (P) for specific ions is an important value for establishing the membrane potential and reflects the number of open channels, which are selective for a specific ion. If ion channels change their open probability in response to specific reagents, a shift in membrane potential will be expected.

Table 3: External solutions used for Ca^{2+} and membrane potential imaging.

	Substance	final conc. (mM)	Provider
HBSS	CaCl$_2$	1.26	Molecular Devices
	KCl	5.36	
	KH$_2$PO$_4$	0.44	
	MgSo4	0.81	
	NaHCO$_3$	4.16	
	NaCl	136.89	
	Na$_2$HPO$_4$	0.34	
	Glucose	5.5	
Ca^{2+}-free	NaCl	120	Merck KGaA
	KCl	4	Merck KGaA
	MgCl$_2$	2	Merck KGaA
	Hepes	10	Sigma-Aldrich Inc.
	Glucose	10	Merck KGaA
high K$^+$	NaCl	93	Merck KGaA
	KCl	67	Merck KGaA
	HEPES	10	Sigma-Aldrich Inc.
	Glucose	5	Merck KGaA
Additional reagents	Carbachol	0.13	Sigma-Aldrich Inc.
	Thapsigargin	0.001	Calbiochem

A fluorescence-based assay for detecting changes in voltage across the plasma membrane was used in the present experiments. The advantage of such an approach is that the internal milieu of the cell is not modified. In the present study, the activation of non-selective TRPC5 channels resulted in a membrane potential shift, as the permeability for Na$^+$ and Cs$^+$ was changed.

The FLIPR$^®$ Membrane Potential Assay Kit (Molecular Devices, California, USA) consists of the Membrane Potential Assay BLUE hereafter referred to as FLIPR$^®$ dye and Hanks´BSS (HBSS listed in table 3 with 20 mM HEPES, pH = 7.4 (Kit number: R8042). The membrane potential dye solution was prepared by dissolving the contents of one bottle FLIPR$^®$ dye in HBSS / Hepes to a volume of 10 ml. The solution was kept in the dark and was stable at room temperature. Cells (HEK 293 control cells or TRPC5-stably transfected HEK 293 cells) were grown on poly-L-lysine-coated cover slips and incubated with FLIPR$^®$ dye containing HBSS for 12 min at room temperature. Importantly, the FLIPR$^®$ dye is *not* washed out after cell loading as it is done with FURA-2AM. Therefore all solutions used during an experiment

contain the FLIPR® dye at the same concentration as the loading solution HBSS. After incubation, coverslips were placed into a circular open-bottom chamber and mounted onto the stage of the iMIC (Experimental setup and software as described for Ca^{2+} imaging). To determine background fluorescence signals, the dye was excited at 350 nm for 5 ms. During the recording, cells were excited at 530 nm for 5 ms and the emitted fluorescence was recorded at 600 nm (Dicroic: 565 DCXR; Emitter filter: ET 605/70m AF Analysetechnik, Tübingen, Germany). The changes in the FLIPR® dye fluorescence are presented as $\Delta I/I_0$ values, whereby positive values represent a depolarization of the cell membrane. In the present study, $\Delta I/I_0$ values below zero that represent hyperpolarization of the cell membrane were not observed. The $\Delta I/I_0$ values (I = intensity) were obtained as follows: First, the 3rd pulse of the 350 nm excitation protocol was subtracted from the 10th pulse of the 530 nm excitation protocol ($I_0 = 530_{p10} - 350_{p3}$), which represent the basal fluorescence before stimulation. Second, this basal fluorescence was subtracted from the fluorescence signals recorded over time ($\Delta I = 530 - 530_{p10}$). Third, the ratio between ΔI and I_0 was calculated (Microsoft Excel, Microsoft).

3.6.1 Combination of Ca^{2+} imaging and membrane potential detection

Due to defined differences in fluorescence properties (Fig. 8), FURA-2 signals and FLIPR® signals could be recorded simultaneously to achieve a high resolution chronology of Ca^{2+} signals and membrane potential changes.

Cells (HEK 293 and TRPC5-stably transfected HEK 293) were grown on poly-L-lysine-coated cover slips and incubated with 10 µM FURA-2AM (Molecular Probes) for 40 min at room temperature and then washed with basic external Hank´s Buffered Salt Solution (HBSS). Afterwards cells were incubated with FLIPR® dye containing HBSS for 12 min at room temperature. As mentioned before FLIPR® dye is not washed out. To record FURA-2 and FLIPR® signals, a macro was programmed in TILL visION to change the corresponding filtersets alternately (Fig. 8, Fig. 9). Data analysis and statistical analysis were performed as described for individual Ca^{2+} imaging experiments or membrane potential detection.
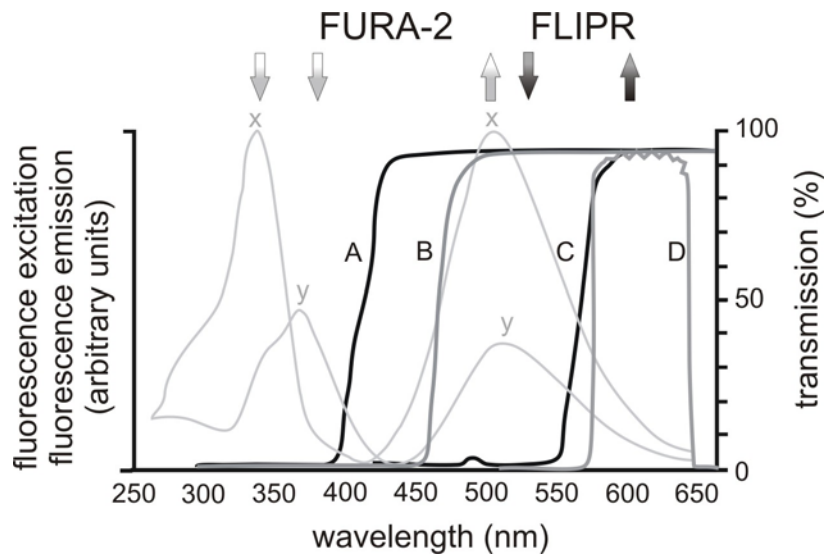
Figure 8: Excitation and emission fluorescence spectra for Fura-2 (y) and Ca^{2+}-saturated Fura-2 (x). Arrows indicate excitation wavelength (downward) and emission wavelength (upward) for FURA-2 experiments (grey gradient) or FLIPR experiments (black gradient). (A) and (B) show the optical properties for FURA-2 filterset: (A) dicroic: DCLP410; (B) emitter: LP470; (C) and (D) show FLIPR filterset: (C) dicroic: 565 DCXR; (D) emitter: ET 605/70m.
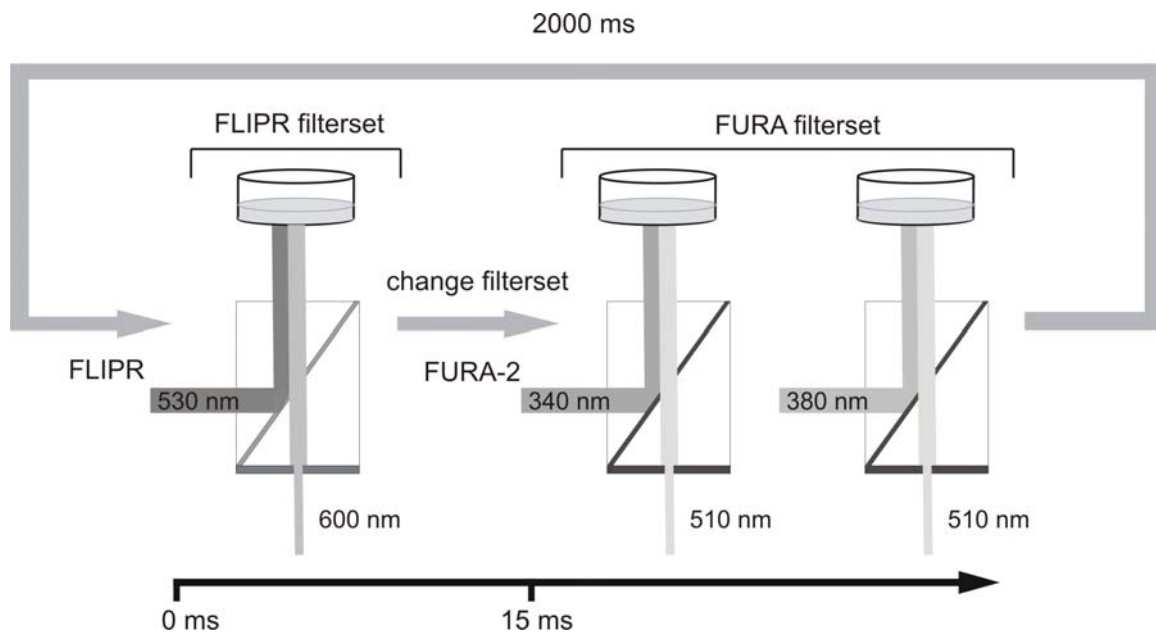

Figure 9: Simultaneous recordings of FLIPR and FURA-2 signals. In each cycle, the FLIPR signals were measured before FURA-2 signals. First, the FLIPR dye was excited at 530 nm for 5 ms and the emitted fluorescence was obtained at 600 nm using the FLIPR filterset. Second, the FURA-2 filterset was placed in position and FURA-2 was excited at 340 nm for 10 ms and the emitted light was obtained at 510 nm and then excited at 380 nm for 10 ms and the emitted fluorescence was obtained at 510 nm. Afterwards, the FLIPR filterset was placed in position and the cycle was repeated.

3.7 Statistical analysis

Statistical analysis was performed using Microsoft Excel 2003 (Microsoft Coorp., Washington, USA), Igor Pro 5.0.1.0 (Wavemetrics Inc., Oregon, USA) and SigmaPlot 9.01 (SPSS Inc., Illinois, USA). Paired or unpaired Student's t-test analyses were performed to determine differences between samples. Statistical data are given as mean ± s.e.m, where n is the number of individual experiments in electrophysiological recordings or individually recorded cells in fluorescence imaging experiments. $P < 0.05$ (asterisk), $P < 0.01$ (two asterisk) and $P < 0.001$ (three asterisk) are considered to be significant.

4 Results

4.1 Murine ORAI proteins form functional CRAC channels

The molecular components which reconstitute CRAC channels have been enigmatic for years until STIM1 and ORAI1 were reported to play a role in I_{CRAC} activation. In this thesis, murine ORAI1, ORAI2L, ORAI2S, ORAI2S (N130Y) and STIM1 were cloned as described elsewhere[36] and used to elucidate the functional properties of these proteins.

First, endogenous I_{CRAC} was recorded in both, HEK 293 and RBL 2H3 cells to define a threshold that allows the detection of CRAC currents through recombinant channels (Fig. 10, Fig. 11). Each of the cell lines provides a different background of endogenous STIM1 and ORAI protein expression[36] and endogenous CRAC current (Fig. 10, Fig. 11). I_{CRAC} was activated by adding IP_3 to the pipette solution under buffer of internal Ca^{2+} with 10 mM EGTA and the currents were measured in the presence of 5 mM external Ca^{2+}. In the whole-cell configuration of the patch-clamp technique, RBL 2H3 cells showed a clearly detectable and fast developing inward-rectifying current (Fig. 10 E, F) with an average current density of approximately -2.5 pA/pF (Fig. 11 B). In HEK 293 cells, only 4 out of 13 cells showed a small inward-rectifying I_{CRAC} with an average current density of -0.5 pA/pF (Fig. 10 A, B; Fig. 11 A). The cell lines vary in endogenous expression of STIM1 and ORAI proteins and thus the size of endogenous CRAC currents (Fig. 10, Fig. 11).

Overexpression of STIM1 resulted in an increase of CRAC currents in RBL 2H3 and HEK 293 cells. In RBL 2H3 cells, I_{CRAC} density was doubled by overexpression of the CRAC component STIM1 (-4.5 pA/pF vs. 2.5 pA/pF, Fig. 11 B). The inward-rectifying current-voltage relationship and activation kinetics exhibit the characteristics of endogenous CRAC currents. In STIM1-transfected HEK 293 cells, I_{CRAC} was barely detectable. The average current density was slightly increased to -1 pA/pF (Fig. 11 A) when compared to endogenous CRAC currents. In conclusion, HEK 293 cells represent a cell background, in which I_{CRAC} is hardly detectable even after over-expression of STIM1. In contrast CRAC currents in RBL 2H3 cells appeared to be readily modulated by the overexpression of STIM1. The individual STIM1-dependent

current densities served as threshold levels (indicated as dashed line in Fig. 11 A, B) for the detection of CRAC currents mediated by recombinant ion channels formed by ORAI proteins.
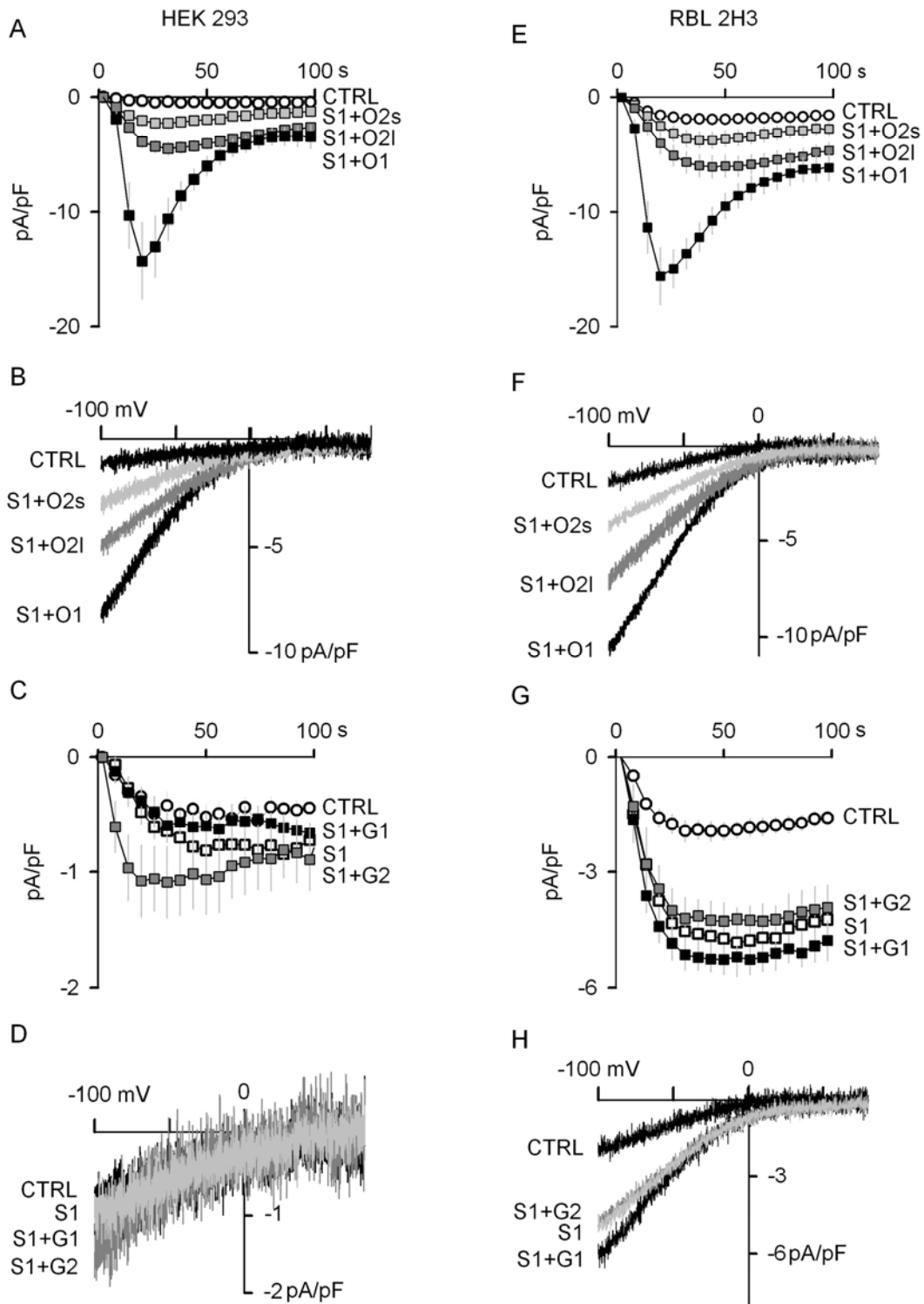

Figure 10: Overexpression of the murine ORAI1, ORAI2L, ORAI2S, GAMMA1 and GAMMA2 in two different cell backgrounds. HEK 293 (A-D) and RBL 2H3 (E-H) cells were transfected either with STIM1 alone (S1) or with STIM1 plus ORAI1 (S1+O1), ORAI2L (S1+O2L), ORAI2S (S1+O2S),

Co-expression of STIM1 and ORAI1, ORAI2L or ORAI2S induced clearly detectable CRAC currents in both, HEK 293 and RBL 2H3 cells showing the hallmark inward-rectifying current-voltage characteristic of CRAC currents (Fig. 10 B, F). Cells transfected with STIM1 plus ORAI2L or ORAI2S showed an immediate current increase after break-in followed by a plateau phase that remained stable for at least 100 s. The ionic currents measured in STIM1 + ORAI1 overexpressing cells show a spontaneous inactivation (Fig. 10 A, E). Independently of the cell background the peak current densities followed the sequence ORAI1 > ORAI2L > ORAI2S in the co-expression experiments with STIM1 (Fig. 11 A, B). In HEK 293 cells, the CRAC current densities measured after co-expression are significantly larger than those measured after individual overexpression of STIM1 (Fig. 11 A). In contrast, co-overexpression of STIM1 and ORAI2L or ORAI2S in RBL 2H3 cells showed current densities comparable to STIM1-transfected cells (Fig. 11 B). This indicates that the overexpressed ORAI2 variants might not contribute to the functional CRAC channel resource in RBL 2H3 cells which express endogenous ORAI2 proteins[36].

In addition, I co-expressed the GAMMA subunits of the voltage-dependent Ca^{2+} channels which are structurally similar to ORAI proteins[35] with STIM1 in HEK 293 and RBL 2H3 cells to elucidate whether these proteins interfere with the function of STIM1 in forming or activating CRAC channels. As for the individual overexpression of STIM1, the co-expression of STIM1 with GAMMA 1 or GAMMA 2 induced a strong inward-rectifying, fast activating current (Fig. 10 C, D, G, H). In RBL 2H3 cells, I observed a similar increase in current densities compared to individually STIM1-transfected cells (Fig. 11 B) which was also true in transfected HEK 293 cells (Fig. 11 A). Thus, despite the structural similarities between GAMMA and ORAI proteins[35], the overexpression of GAMMA 1 and GAMMA 2 did not interfere with the function of CRAC channels.
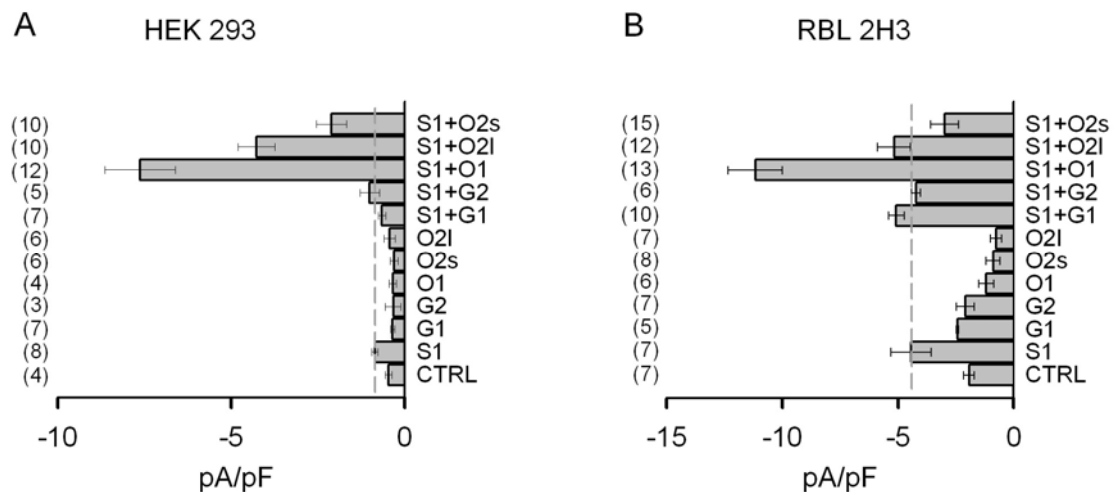
Figure 11: Comparison of inward current densities in cells over-expressing murine ORAI, GAMMA and STIM1 proteins. HEK 293 (A) and RBL 2H3 (B) cells were transfected with STIM1 (S1), ORAI1 (O1), ORAI2L (O2L), ORAI2L (O2S), GAMMA1 (G1) and GAMMA2 (G2) either individually or in combination, as indicated. Transfected cells that did not express the transfection marker GFP as well as non-transfected cells were used as controls (CTRL). Inward current densities were measured at -90 mV in experiments similar to those shown in Fig. 10 and, for statistical analysis, current densities obtained 40 s after break-in were used. The levels for detection of ionic currents through channels formed by the transfected ORAI proteins are indicated with dashed lines and correspond to the mean current densities measured after transfection of STIM1 alone in HEK 293 (A) and RBL 2H3 (B) cells. The number of cells is given in parenthesis.

In further experiments, I explored the effects of transfecting ORAI1, ORAI2L and ORAI2S individually. The endogenous I_{CRAC} was not enhanced by the individual overexpression neither in HEK 293 nor in RBL 2H3 cells (Fig. 11 A and B). Due to hardly detectable endogenous CRAC current densities in HEK 293 cells, possible inhibitory effects could not be observed (Fig. 11 A). In contrast, overexpressed ORAI1, ORAI2L or ORAI2S attenuated the endogenous I_{CRAC} in RBL 2H3 cells (Fig. 11 B), suggesting that ORAI2L and ORAI2S, as well as ORAI1 interact with endogenous CRAC channels in these cells.

4.1.1 Internal Ca^{2+} rise inactivates CRAC currents

HEK 293 cells overexpressing STIM1 and ORAI1, ORAI2L or ORAI2S showed that CRAC current densities strongly depend on the transfected ORAI isoform (Fig. 11 A). During these experiments, I additionally observed an inactivation of CRAC currents over time, which was more prominent in cells overexpressing STIM1 plus ORAI1 than in cells transfected with STIM1 plus an ORAI2 variant (Fig. 10 A). Therefore, I investigated whether the different levels of CRAC current densities reflected differences in the Ca^{2+}-dependent inactivation previously reported for endogenous I_{CRAC} [81, 82]. In this series of experiments, internal Ca^{2+} levels were buffered with BAPTA instead of EGTA. Under these conditions almost no inactivation of CRAC currents could be observed in HEK 293 overexpressing STIM1 plus ORAI1 or ORAI2 variants (Fig. 12 A, C, E), suggesting that the current decay observed under EGTA buffered conditions reflected a Ca^{2+}-dependent inactivation process. To evaluate the amount of CRAC current inactivation (ΔI_{80}) in the individual cells the recorded current densities at 80 s after break-in were subtracted from the peak current densities (I_{Peak}). By plotting I_{Peak} vs ΔI_{80}, a direct relationship between the CRAC current densities and the current inactivation over time is clearly apparent in STIM1 and ORAI1 overexpressing cells under internal EGTA conditions (Fig. 12 B), indicating that the amount of current inactivation is proportional to the Ca^{2+} influx through ORAI proteins. In the experiments with BAPTA, the ΔI_{80} to I_{Peak} relationship is shifted to higher I_{Peak} values in such a way that CRAC current inactivation was detectable starting at I_{Peak} >30 pA/pF (Fig. 12 B). In the majority of cells with I_{Peak} <30 pA/pF, inactivation of CRAC currents was almost abolished by BAPTA. A similar analysis of the CRAC currents in cells overexpressing STIM1 plus ORAI2L showed that BAPTA almost completely prevents the inactivation of CRAC currents, probably because I_{Peak} current densities higher than 30 pA/pF, were not detectable in these cells (Fig. 12 D).
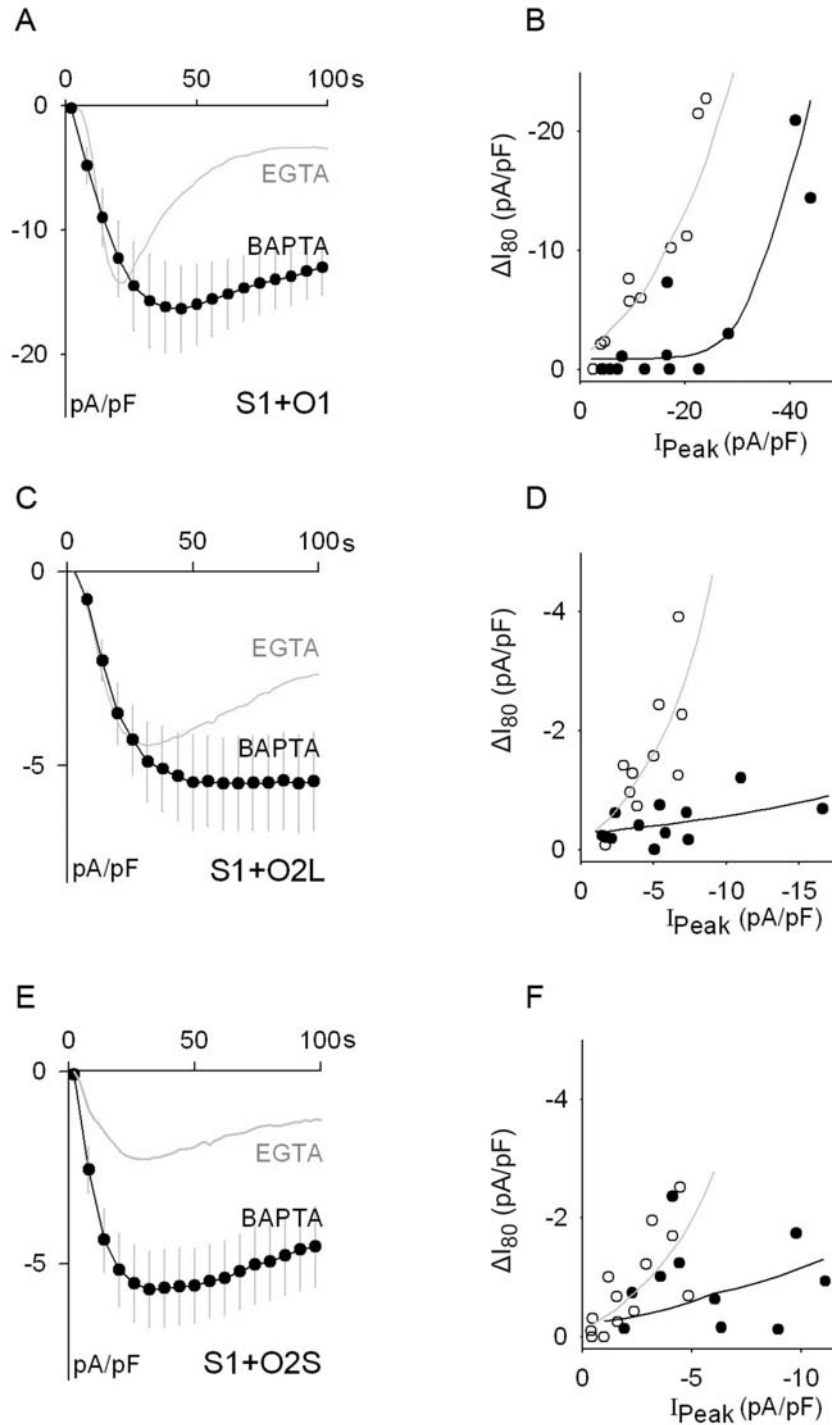
Figure 12: Ca^{2+} dependent inactivation of CRAC currents in cells over-expressing ORAI1, ORA2L and ORAI2S. HEK 293 cells were transfected with STIM1 plus ORAI1 (S1+O1), ORAI2L (S1+O2L) and ORAI2S (S1+O2S). In addition to 20 μM IP$_3$, the pipette solution contained either 10 mM EGTA or 10 mM BAPTA as indicated. The activation of CRAC currents was monitored using inward current densities at -90 mV. Average time courses of CRAC current activation in cells over-expressing STIM1 plus ORAI1 (A, n=12), ORAI2L (C, n=11) and ORAI2S (E, n=10) and dialysed with BAPTA are shown superimposed on time courses observed in cells dialysed with EGTA (same experiments as in Fig. 10 A). The external solution contained 5 mM Ca^{2+}. The amount of CRAC current inactivation (ΔI$_{80}$) was measured in individual cells as the peak current density (I$_{Peak}$) subtracted by the current density obtained 80 s after break-in. ΔI$_{80}$ is plotted vs. I$_{Peak}$ for cells transfected with STIM1 plus ORAI1 (B), ORAI2L (D) and ORAI2S (F). Symbols represent individual cells dialysed either with EGTA (open symbols) or BAPTA (closed symbols) and lines are approximated fittings to the data.

Interestingly, peak currents recorded under EGTA or BAPTA conditions did not statistically differ from each other in STIM1 plus ORAI1 or ORAI2L co-expressing HEK 293 cells (Fig. 12 A, C). In cells overexpressing STIM1 plus ORAI2S, however, the CRAC current densities measured with BAPTA were 2.6 – 3.0-fold larger than those recorded with EGTA (Fig. 12 E). Cells overexpressing STIM1 plus ORAI2L or ORAI2S showed similar current density levels under BAPTA conditions (Fig 12 C, E). Although there was a considerable scatter in the ΔI_{80} to I_{Peak} plots, the effect of BAPTA on the CRAC current inactivation were detectable in individual cells co-expressing STIM1 and ORAI2S (Fig. 12 F).

In summary, the experiments with BAPTA indicated that this Ca^{2+} chelator largely prevented CRAC current inactivation over time in cells overexpressing STIM1 plus ORAI1 or ORAI2L. More importantly, CRAC current densities in cells co-expressing STIM1 and ORAI2S were significantly increased under BAPTA conditions in comparison to EGTA buffered pipette solution.

4.1.2 Na$^+$ currents through murine ORAI isoforms

Since ORAI2L and ORAI2S failed to enhance CRAC currents in RBL 2H3 cells as shown in Fig. 11 B, I further tested whether these ORAI2 variants modify the capability of endogenous CRAC channels to conduct Na$^+$ currents (I_{Na}) in RBL 2H3 cells. Fig. 13 A illustrates that the exchange of Ca^{2+}- and Mg^{2+}-containing extracellular solution to divalent free (DVF) solution results in a strong Na$^+$ influx through CRAC channels[81, 82]. Subsequent reperfusion of the divalent containing solution showed the anomalous mole fraction effect and exposure to a nominally Ca^{2+}-free solution (NCaF) completely abolished the Ca^{2+} current flow through CRAC channels. This indicates that the main charge carrier of ionic currents recorded in Ca^{2+}-containing solution were Ca^{2+} ions (I_{Ca}). Similar responses were observed in perfusion experiments with RBL 2H3 cells co-expressing STIM1 plus ORAI1 or ORAI2 variants (Fig. 13 B, C, D). These perfusion experiments displayed the typical I-V-characteristics for Ca^{2+} and Na$^+$ currents through CRAC channels[11, 21, 83], exemplarily shown for STIM1 plus ORAI2L overexpressing cells (Fig 13 E). Furthermore, I measured the ratios I_{Na}/I_{Ca} to determine whether the proportionality

between Na$^+$ and Ca^{2+} current densities is modified by the over expression of STIM1 plus ORAI isoforms. Both, in control cells as well as in RBL 2H3 cells overexpressing STIM1 plus ORAI2 variants, the average I$_{Na}$/I$_{Ca}$ ratios were in the range of 2 - 4 (Fig. 13 F), indicating that the overexpression of ORAI2 isoforms did not modify the capability of endogenous CRAC currents to conduct Na$^+$ ions. The same is true for RBL 2H3 cells co-expressing STIM1 plus ORAI1 (Fig. 13 F).
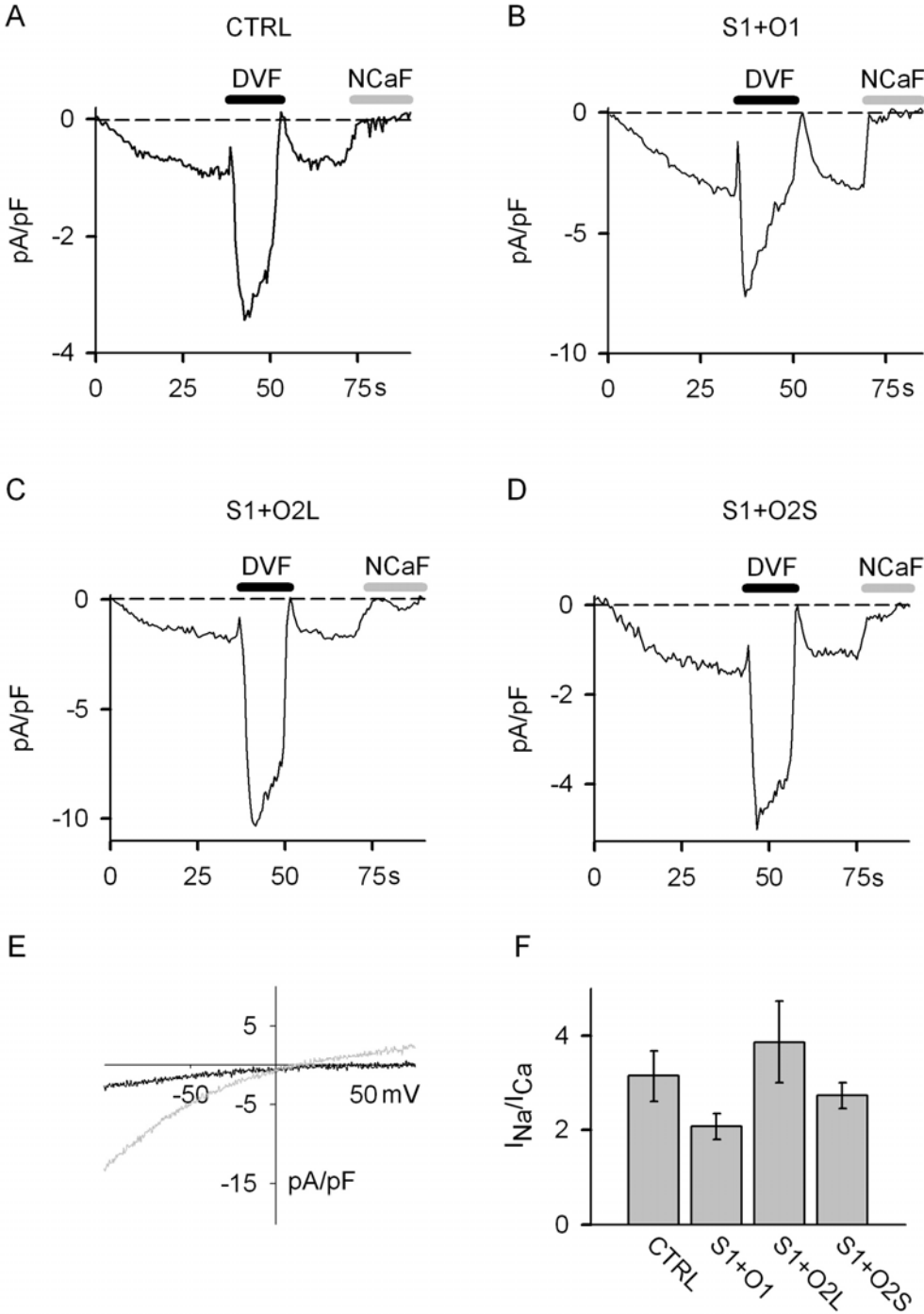

Figure 13: Na$^+$ and Ca^{2+} currents in cells over-expressing the murine ORAI1, ORA2L and ORAI2S and non-transfected RBL 2H3 cells. RBL 2H3 cells were transfected with STIM1 plus ORAI1 (S1+O1), ORAI2L (S1+O2L) and ORAI2S (S1+O2S). Controls (CTRL) were transfected

cells that did not express the transfection marker GFP. Representative examples of experiments with a control cell are shown. (A), RBL 2H3 cells over-expressing ORAI1 plus STIM1 (B), ORAI2L plus STIM1 (C) and ORAI2S plus STIM1 (D). The external solution contained 10 mM Ca^{2+} and was present in the external solution except as otherwise indicated. The nominally Ca^{2+} free solution (NCaF) containing no divalent cations and the divalent free solution (DVF) containing 10 mM EDTA were superfused as indicated above the traces. The recording pipette contained IP_3 (20 µM) and BAPTA (10 mM). Ca^{2+} (I_{Ca}) and Na^+ (I_{Na}) current amplitudes were determined at -90 mV in the presence of the 10 mM Ca^{2+} and DVF solutions, respectively. Representative I-V- characteristics are shown for Ca^{2+} current (E, black) and Na^+ current (E, grey) through CRAC channels in STIM1 plus ORAI2L overexpressing RBL 2H3 cells. The average ratios I_{Na}/I_{Ca} obtained in control and transfected cells are shown (F). The number of cells is given in parenthesis.

4.1.3 Influence of ORAI2 proteins on CRAC currents carried by ORAI1

Cells overexpressing ORAI2L and ORAI2S exhibit lower CRAC current densities than cells overexpressing ORAI1, independently of whether internal Ca^{2+} was chelated by EGTA or BAPTA (Fig. 11 and 12). Since it has been shown that ORAI proteins form heteromultimeres[84], I tested whether ORAI2 variants alter the functional expression of ORAI1 in triple transfection experiments in HEK 293 cells (Fig. 14). The plasmid ratio STIM1:ORAI1 was 1:2 (Fig. 10, A and Fig. 11, A) and low amounts of the previously mentioned ORAI2L or ORAI2S plasmids were added to obtain the triple combinations STIM1:ORAI1:ORAI2L and, respectively, STIM1:ORAI1:ORAI2S at a ratio of 1:2:1. Accordingly, cells transfected with STIM1 and ORAI1 were used as controls. The CRAC current densities of cells transfected with STIM1, ORAI1 and ORAI2S were lower than the current densities in cells co-expressing STIM1 plus ORAI1. This pointed to a possible interference of ORAI2S with the functional expression of ORAI1 (Fig. 14, A). The maximum current densities of STIM1, ORAI1 and ORAI2L transfected HEK 293 cells were in the same range as the STIM1 plus ORAI1 cells. The current voltage relationships for each set of triple transfections were indistinguishable from the I-V-characteristics for STIM1 and ORAI1 transfected cells (Fig. 10, B and Fig. 14, B) showing a strong inward rectifying current with a reversal potential in the highly positive voltage range. Additionally, ion current development over time was clearly changed under internal EGTA conditions. STIM1, ORAI1 and ORAI2L as well as STIM1, ORAI1 and ORAI2S transfected cells did not show the Ca^{2+}-dependent inactivation compared to STIM1- and ORAI1-overexpressing cells HEK 293. Interestingly, each triple transfection perfectly resembled the current development over time of its STIM1 plus ORAI2 variant counterpart (Fig. 12, C, D and Fig. 14, A).
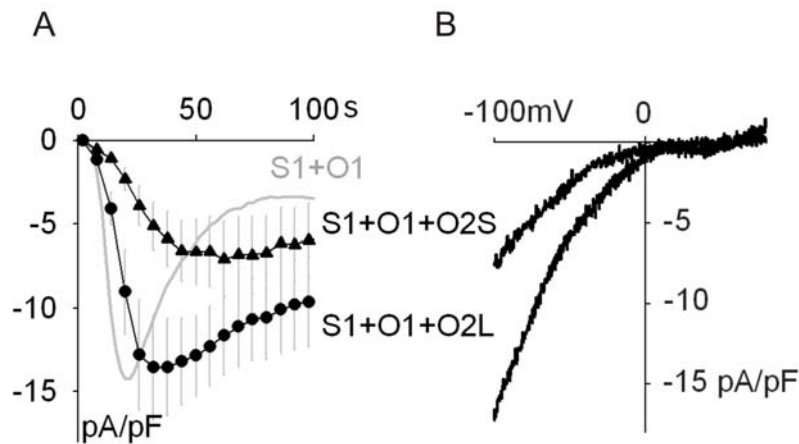
Figure 14: Co-expression of ORAI1 with ORAI2 variants. HEK293 cells were transfected with STIM1, ORAI1 and either ORAI2L (S1+O1+O2L) or ORAI2S (S1+O1+O2S) at a ratio of 1:2:1. Cells transfected with STIM1 plus ORAI1 (S1+O1) at a ratio of 1:2 (same experiments as in Fig. 10 A) served as controls. The pipette solution contained 20 μM IP_3 plus 10 mM EGTA and the external solution contained 5 mM Ca^{2+}. The activation of CRAC currents was monitored using inward current densities at -90 mV. (A) Average time courses of CRAC current activation in cells over-expressing STIM1 plus ORAI1 and ORAI2L (n=8) or ORAI2S (n=9) are shown superimposed on the time course observed in cells transfected with STIM1 plus ORAI1. (B) Representative current-voltage relationships of cells co-expressing ORAI1 and ORAI2 variants. The transfection protocols are indicated close to the traces.

4.1.4 The murine ORAI2S (N130Y) variant

As mentioned in the introduction, U. Wissenbach detected a third ORAI2 variant in mice named ORAI2S (N130Y) that corresponds to ORAI2S with the amino acid exchange N130Y[35]. HEK 293 cells transfected with STIM1 and ORAI2S (N130Y) at a ratio 1:2 showed an inward rectifying current after store depletion by internal IP_3 comparable to the currents observed in STIM1 plus ORAI2S overexpressing cells (Fig. 10 B and Fig. 15 B). Thus, both ORAI2S variants developed I_{CRAC} with a higher current density for the ORAI2S (N130Y) (~-8 pA/pF) in comparison to cell overexpressing STIM1 plus ORAI2S (~-5 pA/pF). These findings indicate that both gene transcripts generate functional channel proteins (Fig. 10 A and Fig. 15 A).
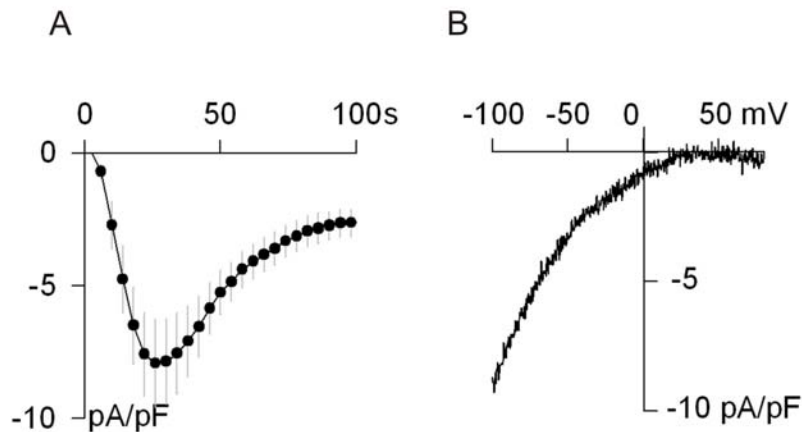
Figure 15: Over-expression of STIM1 and the ORAI2S (N130Y) sequence from the murine orai2 locus on chromosome 16. HEK 293cells were transfected with STIM1 and ORAI2S (N130Y) plasmids. The activation of ionic currents was induced with IP_3 (20 µM) in 0 Ca^{2+} (with EGTA) internal solution and in the presence of 5 mM external Ca^{2+}. The time course of inward current densities (A) shows the average development of ionic currents at -90 mV in 13 transfected cells. The current-voltage relationship (B) is a representative recording obtained 40 s after break-in.

4.1.5 Non-functional murine ORAI proteins

Feske et al. first described that a mutation in ORAI1 protein causes immune deficiency by abrogating CRAC channel function. The mutated ORAI1 protein was named ORAI1 Scid[8] (detailed information can be found on page 23ff). I generated the amino acid substitution from arginine to tryptophan at position 91 in murine ORAI1 and the arginine to tryptophan substitution at position 78 in murine ORAI2S proteins according to the human ORAI1 Scid mutation and investigated the resultant functional properties. Whole-cell recordings revealed prominent CRAC currents in STIM1 plus ORAI1 or ORAI2S co-expressing HEK 293 cells induced by the dialysis of 20 µM IP_3, but hardly any current development was observed in cells transfected with STIM1 plus ORAI1 Scid or STIM1 plus ORAI2S Scid, respectively (Fig. 16 A). Notably, the ORAI1 Scid and ORAI2S Scid proteins appeared to have a dominant-negative effect on endogenous CRAC currents in HEK 293 cells, supporting the concept of a multimeric ORAI protein assembly to form a functional ion channel[33, 35] (Fig. 16 B).

In summary, the average current densities in cells overexpressing STIM1 plus ORAI1 Scid or ORAI2S Scid were close to the resolution limit of whole-cell recordings and smaller than endogenous I_{CRAC} in HEK 293 cells or CRAC current density in HEK 293

cells overexpressing STIM1 (Fig. 16 C). Murine ORAI1 and ORAI2S Scid mutations represent the non-functional counterpart to previously described human ORAI1 Scid[8].
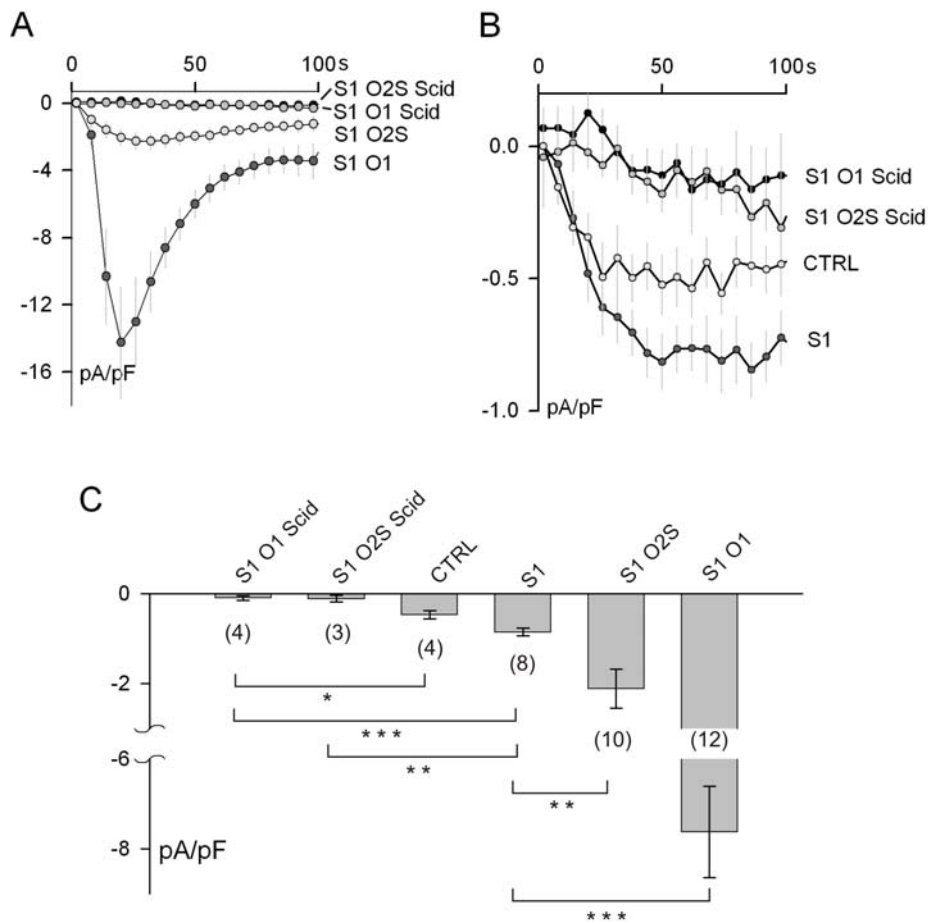

Figure 16: Non-functional murine ORAI1 Scid (S1 O1 Scid) and ORAI2S Scid (S1 O2S Scid) proteins co-transfected in HEK 293 cells with STIM1 in comparison to transfections of STIM1 plus ORAI1 (S1 O1) or ORAI2S (S1 O2S), STIM1 (S1) and non-transfected control HEK 293 cells (CTRL). (A) and (B) Average current development over time induced by 20 μM internal IP$_3$ in 5 mM Ca^{2+} containing external solution. Current densities were recorded at -90 mV in whole-cell patch clamp configuration. (C) Current densities 80 s after break-in. The number of cells is given in parenthesis.

4.1.6 Neuronal expression of ORAI proteins

CRAC currents have been studied extensively in hematopoietic cells, but there are at present no detailed studies in non-hematopoietic cells due to the fact that endogenous CRAC currents are hard to detect[81] in these cells. In contrast, STIM1 and ORAI transcripts and proteins, respectively, were detected in virtually every cell type including cortical neurons[35]. To demonstrate that neurons express ORAI proteins, single cells isolated from murine cortex were identified as neurons by

whole-cell recordings of voltage-gated Na$^+$-currents (Fig. 17 A) and subsequently each cell was collected in an individual PCR tube and immediately stored in liquid nitrogen. The mRNA served as a template for reverse transcription and PCR. This approach resulted in the detection of 5 out of 13 single neurons expressing ORAI2L transcripts (Fig. 17 C by S.A. Gross and U. Wissenbach). In contrast, no CRAC current in cortical neurons was observed in whole-cell patch clamp experiments (Fig. 17 A). As illustrated in Fig. 17, common store-depleting reagents were used to induce CRAC currents in murine cortical neurons. Neither dialysis with IP$_3$ nor ionophores such as 4-BrA23187 or Ionomycin could activate I$_{CRAC}$ resulting in extremely small, rather linear currents showing inward current densities smaller than -0.5 pA/pF 80 s after break-in (Fig. 17, A, B).
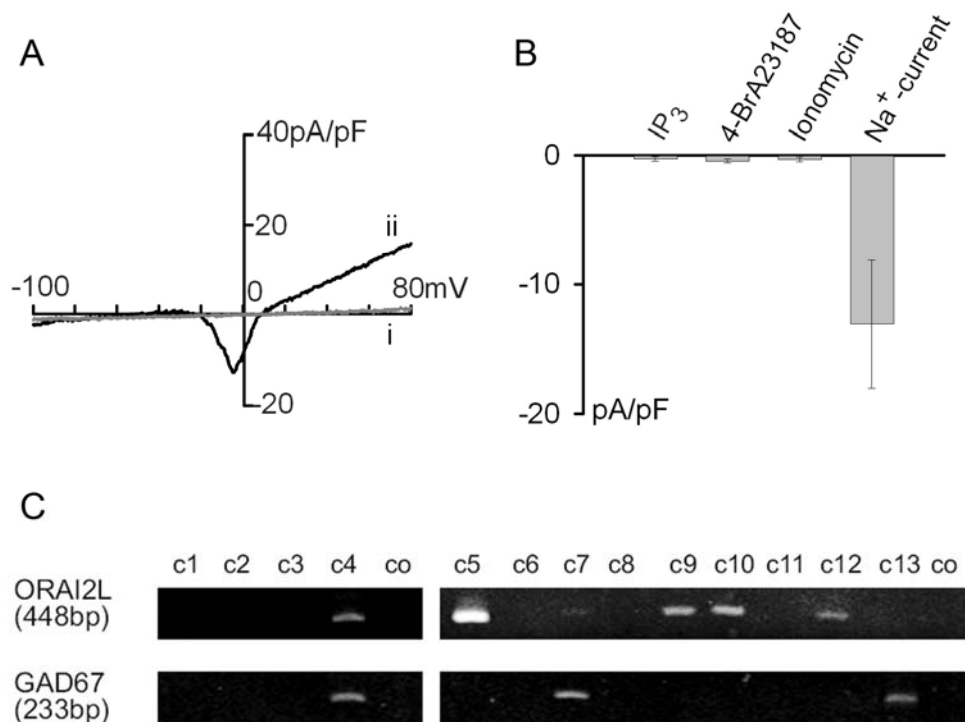

Figure 17: Expression of ORAI2L and functional tests for CRAC currents in cortical neurons. (A) Representative current-voltage relations obtained with experimental protocols designed to detect CRAC currents (i) and voltage-dependent sodium currents (ii). (B) Average current densities measured at -90 mV 80 s after establishing the whole-cell configuration in neurons (c1 – c13) were dialysed with 20 µM IP$_3$ (n=7), 200 nM 4-BrA23187 (n=3) and 5 µM ionomycin (n=5). The densities of voltage-dependent sodium currents (Na$^+$ current) were determined at -10 mV (n=7). (C) by S. A. Gross and U. Wissenbach[35]. Thirteen independent isolated murine cortical neurons identified by whole-cell recordings of voltage-gated Na$^+$-currents. The cytoplasm of each individual cell was sucked into the patch pipette and transferred to single PCR tubes and analysed for the expression of ORAI2L. For positive controls, primers were used to amplify the cDNA of glutamic acid decarboxylase (GAD67). Co, no template control.

4.2 Functional interactions between STIM1, ORAI and TRPC proteins

CRAC currents are a subpopulation of inward Ca^{2+} currents of the so called SOCE (store-operated Ca^{2+} entry) or ROCE (receptor-operated Ca^{2+} entry) type[5, 85-90]. Besides the strong evidence that ORAI proteins form CRAC channels[8, 9, 33, 34, 91] activated by STIM1 translocation[11, 12] (see also section 4.1), the canonical transient receptor potential (TRPC) ion channel subfamily are believed to be involved in both SOCE and ROCE[38, 92, 93]. In the present study, I investigated whether there is a functional interaction between TRPC, STIM1 and ORAI proteins. For this purpose, HEK 293 cells were transiently transfected with TRPC3 or TRPC5 plus STIM1 and ORAI1. Under these conditions, it was tested whether the depletion of internal Ca^{2+} stores activates TRPC3 and TRPC5 currents in addition to CRAC currents (Fig. 18). HEK 293 cells transfected with STIM1 plus ORAI1 and also HEK 293 cells transfected with STIM1, ORAI1 plus TRPC5 or TRPC3 were dialysed with 20 µM IP_3 to activate I_{CRAC}. Since I_{CRAC} in STIM1 plus ORAI1 overexpressing cells did not show any significant outward current at +80 mV (Fig. 10), the additional outward current development at +80 mV was used to monitor the possible activation of TRPC3 and TRPC5 channels (Fig. 18 A, B). In contrast to HEK 293 cells transfected with STIM1 plus ORAI1, triple-transfected cells showed clearly detectable outward currents with average peak current densities of about 5 pA/pF (STIM1 + ORAI1 + TRPC3) and about 16 pA/pF (STIM1 + ORAI1 + TRPC5) in comparison to about 0.5 pA/pF for STIM1 plus ORAI1 overexpressing HEK 293 cells (Fig. 18 A). As illustrated in Fig. 18, outward currents and inward currents at +80 mV and -80 mV, respectively, activated in parallel to each other in STIM1, ORAI1 plus TRPC3 overexpressing cells whereas in STIM1, ORAI1 and TRPC5 transfected HEK 293 cells, a delay in outward current development compared to inward current activation was observed. Furthermore, average inward current densities were larger in triple-transfected HEK 293 cells (Fig. 18 A), indicating the additivity of CRAC and TRPC5 currents at negative potentials.
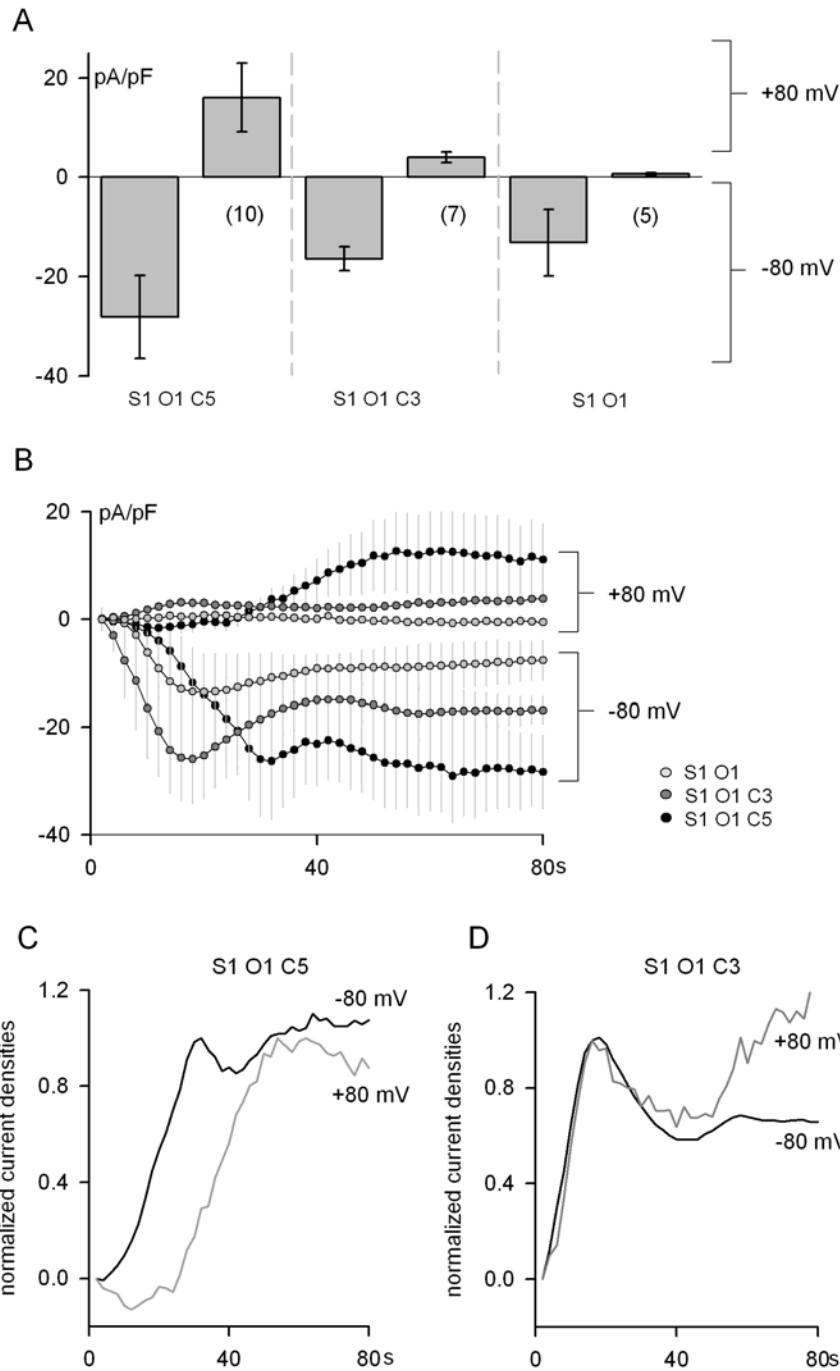
Figure 18: Co-activation of TRPC3, TRPC5 and CRAC currents by depletion of internal Ca^{2+} stores. HEK 293 cells were transiently transfected with STIM1 + ORAI1 (S1 O1), STIM1 + ORAI1 + TRPC3 (S1 O1 C3) and STIM1 + ORAI1 + TRPC5 (S1 O1 C5). Voltage clamp ramps from -100 mV to +100 mV were applied every 2 seconds. (A) Average peak current densities for outward currents (at +80 mV) and inward currents (at -80 mV) measured 80 s after establishing the whole-cell configuration. The numbers of cells is given in parenthesis. (B) Inward and outward current development after dialysis with 20 µM IP$_3$ under Ca^{2+}-bufferd conditions (10 mM EGTA) in whole-cell patch clamp configuration. (C) Comparison of the inward (at -80 mV) and outward (at +80 mV) current development in S1 O1 C5 transfected HEK 293 cells. Current densities were normalized. (D) Comparison of the inward (at -80 mV) and outward (at +80 mV) current development in S1 O1 C3 transfected HEK 293 cells. Current densities were normalized.

Since TRPC3 and TRPC5 currents were activated by intracellular IP$_3$ infusion in HEK 293 cells co-transfected with STIM1 plus ORAI1 (Fig. 18) but did not show activation by IP$_3$ when individually overexpressed (Fig. 19), it was tested whether the interplay of STIM1 and ORAI1 is essential for TRPC channel activation or whether either ORAI1 or STIM1 are sufficient. HEK 293 cells transfected with TRPC5 plus ORAI1 or STIM1 did not display clear I$_{CRAC}$ after dialysis with IP$_3$ and TRPC5 outward currents failed to activate as well (Fig. 19 A, B). Similarly TRPC3 specific outward currents did not develop after the depletion of Ca^{2+} stores in co-transfection experiments with ORAI1 (Fig. 19 C, D). In HEK 293 cells overexpressing STIM1, ORAI2S and TRPC3, strong CRAC currents were observed but TRPC3 specific outward currents did not develop (Fig. 19 C, D). Unsurprisingly, HEK 293 cells transfected with ORAI2S plus TRPC3 showed neither I$_{CRAC}$ nor TRPC3 currents (Fig. 19 C, D). In summary, TRPC3 and TRPC5 currents were activated by internal dialysis with IP$_3$ in HEK 293 cells overexpressing STIM1 and ORAI1 plus TRPC3 or TRPC5. Although significant outward currents were observed in STIM1, ORAI1 and TRPC3 transfected HEK 293 cells, TRPC5 current development in STIM1, ORAI1 and TRPC5 overexpressing cells was much more prominent (Fig. 18, 19). Therefore, from here on, my experiments focused on the functional interaction between STIM1, ORAI1 and TRPC5.
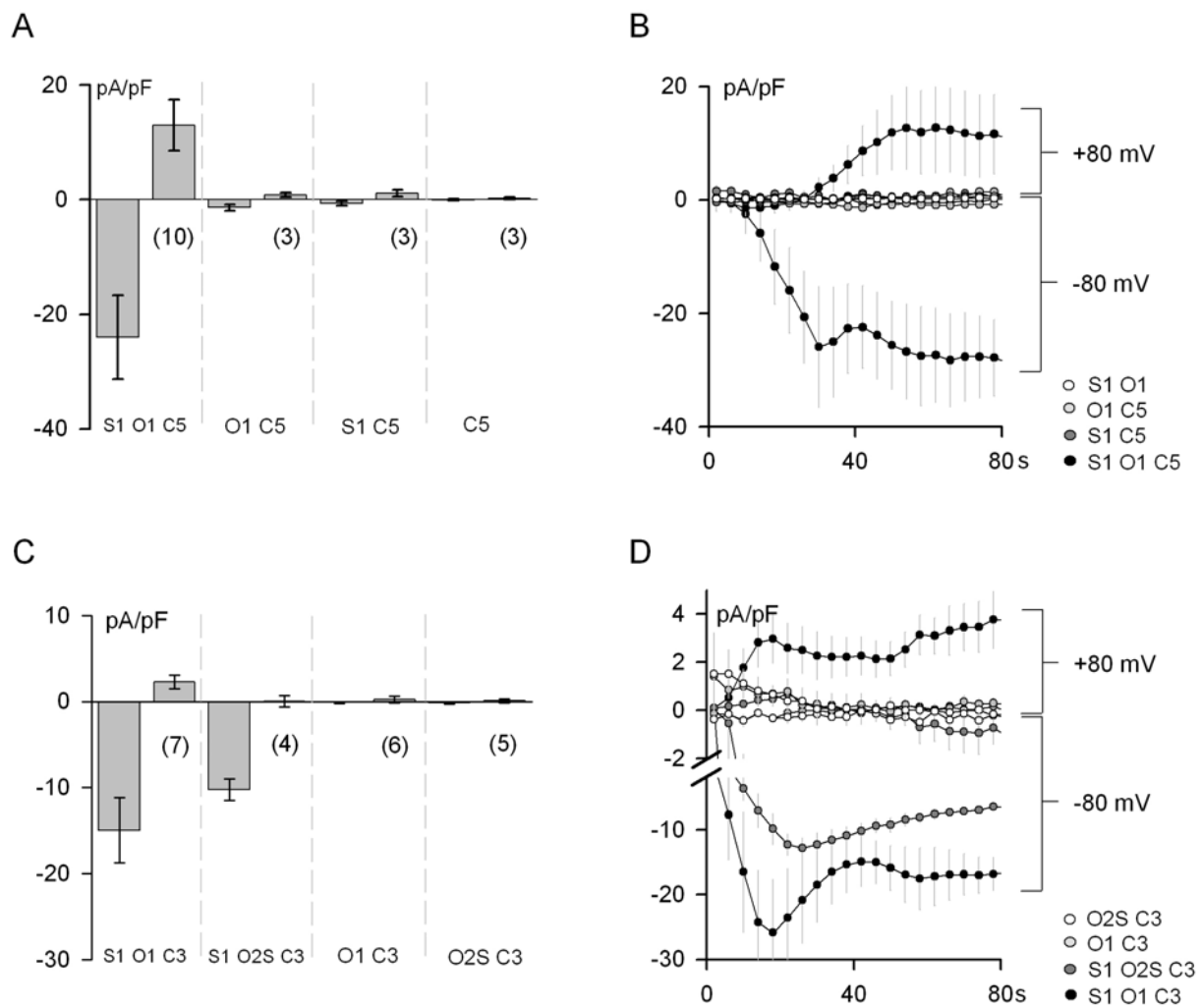
Figure 19: Functional interactions between STIM1, ORAI1, ORAI2S, TRPC3 and TRPC5 proteins. HEK 293 cells were transfected with TRPC5 (C5), STIM1 + TRPC5 (S1 C5), ORAI1 + TRPC5 (O1 TRPC5), STIM1 + ORAI1 + TRPC5 (S1 O1 C5), ORAI1 + TRPC3 (O1 C3), ORAI2S + TRPC3 (O2S C3), STIM1 + ORAI1 + TRPC3 (S1 O1 C3) and STIM1 + ORAI2S + TRPC3 (S1 O2S C3). In whole-cell patch clamp experiments voltage clamp ramps from -100 mV to +100 mV were delivered every 2 seconds. (A, C) Statistical analysis of peak current densities for inward (-80 mV) and outward currents (+80 mV) measured 40 s after establishing the whole-cell configuration. Numbers of cells are given in parenthesis. (B, D) Inward and outward current development over time in experimental conditions as described in Fig. 18.

The experiment shown in Fig. 20 illustrates the basic features observed in experiments with cells transfected with TRPC5, ORAI1 plus STIM1. Immediately after starting dialysis with IP_3 and buffering internal Ca^{2+}, I_{CRAC} developed and revealed the hallmark inward-rectifying I-V-characteristic (Fig. 20 A, B i). After some seconds delay, TRPC5 outward currents were activated and I-V-characteristics changed from an I_{CRAC} type to a typical TRPC5 current-voltage relationship (Fig. 20 A, B i) including a reversal potential shift from about +50 mV to approximately +5 mV (Fig. B ii), as it was expected, because TRPC5 forms non-selective cation channels[94], while CRAC

channels are essentially Ca^{2+}-selective channels[21]. Thus, the double-rectifying I-V-shape of non-selective TRPC5 channels[13, 55, 95] was clearly detected in HEK 293 overexpressing STIM1, ORAI1 plus TRPC5.
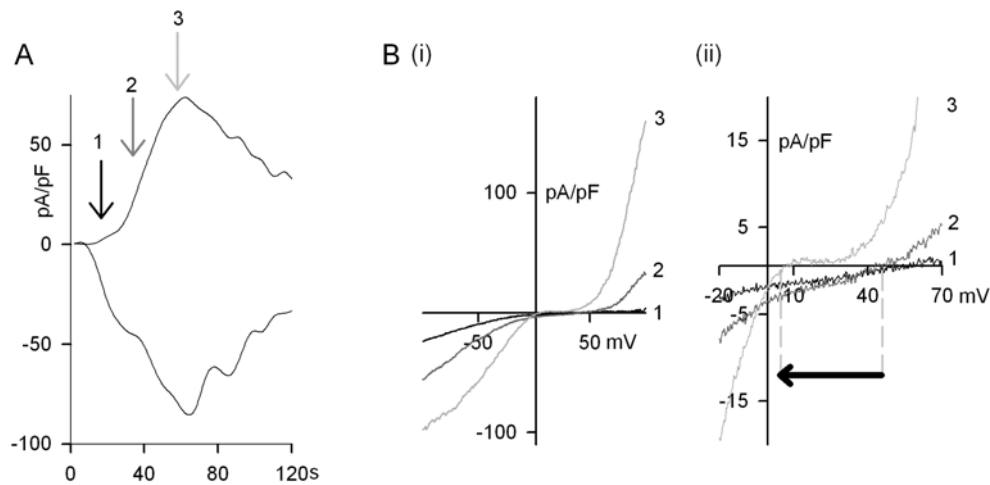

Figure 20: TRPC5 channel activation by internal IP$_3$ in STIM1, ORAI1 and TRPC5 overexpressing HEK 293 cells. (A) Representative current development over time. Displayed are inward current densities (-80 mV) and outward current densities (+80 mV) measured in whole-cell recordings by applying voltage clamp ramps from +100 mV to -100 mV every 2 seconds. (B i) Current-voltage characteristics at different time points as indicated by arrows in (A). (B ii) Enlarged version of the I-Vs of (B i) showing the reversal potential shift as indicated by the black arrow. Experimental conditions as in Fig. 18.

4.3 Functional coupling of TRPC5 to calcium-selective ion channels

4.3.1 Local [Ca^{2+}]$_i$ rise induced by CRAC currents activates TRPC5 channels

Two hypotheses provided a basis for the experiments designed to study the functional interaction between STIM1, ORAI1 and TRPC5. First, STIM1, ORAI1 and TRPC5 might interact directly with each other. Such protein-protein interactions have been reported[66, 96-98] but the role of internal Ca^{2+} in the activation of TRPC5 channels has not studied in detail. Second, I considered the possibility that Ca^{2+} influx through ORAI1 induced the TRPC5 channel activation. TRPC5-stably transfected HEK 293 cells, hereafter referred to as TRPC5 stable cells or the TRPC5 cell line, were used in

the following experiments, which were designed to study the role of internal Ca^{2+} in the activation of TRPC5 channels.

First, the role of Ca^{2+} influx through CRAC channels in the activation of TRPC5 channels was explored by removing external Ca^{2+} and using the non-functional ORAI Scid proteins (see section 4.1.5). The TRPC5 cell line co-expressing STIM1 and ORAI1 showed a clear inward-rectifying CRAC current upon activation by IP_3 dialysis under intracellular Ca^{2+}-buffered conditions (10 mM EGTA) (Fig. 21 B, D). The external solution contained 5 mM $CaCl_2$. In immediate response to I_{CRAC} activation, outward and additional inward currents developed (Fig. 21 A) showing the typical TRPC5 I-V-characteristic (Fig. 21 B). In contrast, TRPC5 stable cells transfected with STIM1 plus the non-functional ORAI1 Scid showed neither CRAC current nor TRPC5 current development (Fig. 21 A). In order to test whether intact ORAI1 and TRPC5 protein interaction is responsible for additional TRPC5 currents upon IP_3 dialysis or whether the Ca^{2+} signal mediated by functional ORAI1 is the key component in TRPC5 activation, I performed comparable experiments under nominally Ca^{2+}-free conditions (NCaF). As illustrated in Fig. 21 C i, STIM1 plus ORAI1-overexpressing TRPC5 stable cells showed neither I_{CRAC} nor TRPC5 currents. As soon as a 5 mM Ca^{2+} containing external solution was perfused, I_{CRAC} and TRPC5 currents developed (Fig. 21 C ii) showing typical I-V-characteristics (Fig. 21 D). As shown in Fig. 18, the activation of TRPC5 currents was clearly delayed compared to the rapid increase of I_{CRAC}. Since TRPC5 currents disappeared due to NCaF reperfusion (Fig. 21 C ii), local $[Ca^{2+}]_i$ rise was the likely to be the ultimate signal in the activation of TRPC5 channels. To test this hypothesis, 10 mM BAPTA was added to the standard pipette solution to obtain a mix of 10 mM EGTA and 10 mM BAPTA. In previous studies of exocytosis in chromaffin cells, this mix of Ca^{2+} chelators efficiently buffer the fast Ca^{2+} transients[99]. In the presence of 5 mM external Ca^{2+}, internal IP_3 induced strong CRAC currents in STIM1 plus ORAI1 transfected TRPC5 cells but no TRPC5 currents were observed (Fig. 22 A, B). Thus, the Ca^{2+} influx supported by CRAC channels likely induced a rise of local $[Ca^{2+}]_i$, which in turn activated TRPC5 channels in the experiments shown in Fig. 21.
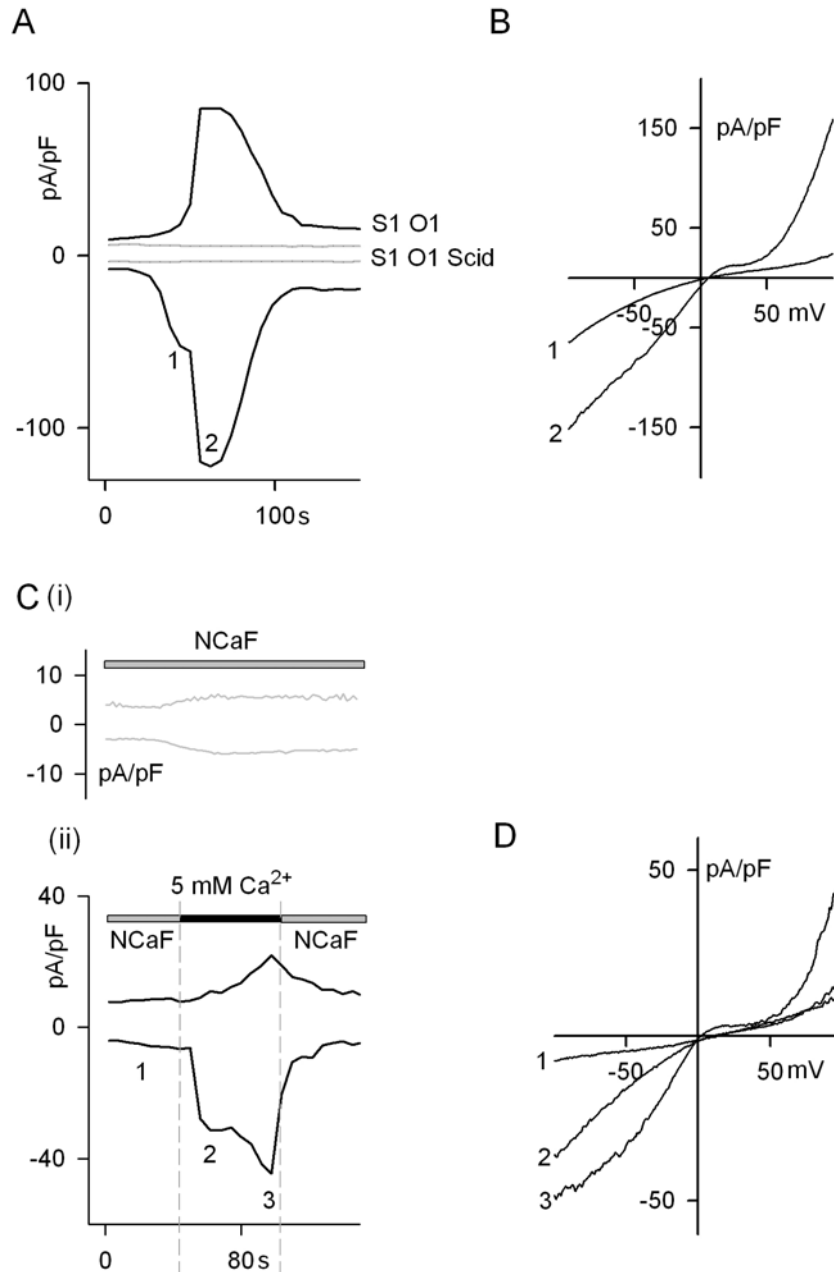
Figure 21: Involvement of the Ca^{2+} influx through CRAC channels in the activation of TRPC5 channels. TRPC5-stably transfected HEK 293 cells were transiently transfected with STIM1 + ORAI 1 (S1 O1) or STIM1 + ORAI1 Scid (S1 O1 Scid). Voltage ramps from -100 mV to +100 mV were applied every 2 s in the whole-cell patch clamp configuration. Inward and outward currents were measured at -80 mV and +80 mV, respectively. **(A)** Inward and outward current development was recorded over time in the presence of 5 mM external Ca^{2+}. Currents were activated by 20 µM internal IP$_3$ in 10 mM EGTA buffered conditions. TRPC5 stable cells transfected with STIM1 + ORAI1 Scid did not activate under these conditions. **(B)** I-V-characteristics for STIM1 + ORAI1 transfected TRPC5 cells at different time points of current development as indicated by numbers in (A). **(C i)** STIM1 + ORAI1-transfected TRPC5 cell line was activated as described. Perfusion of nominally Ca^{2+}-free solution (NCaF) prevented current activation. **(C ii)** Reperfusion of Ca^{2+}-containing solution reversibly activated I$_{CRAC}$ and TRPC5 currents. **(D)** I-V-characteristics for current development at different time points indicated by numbers in (C ii).
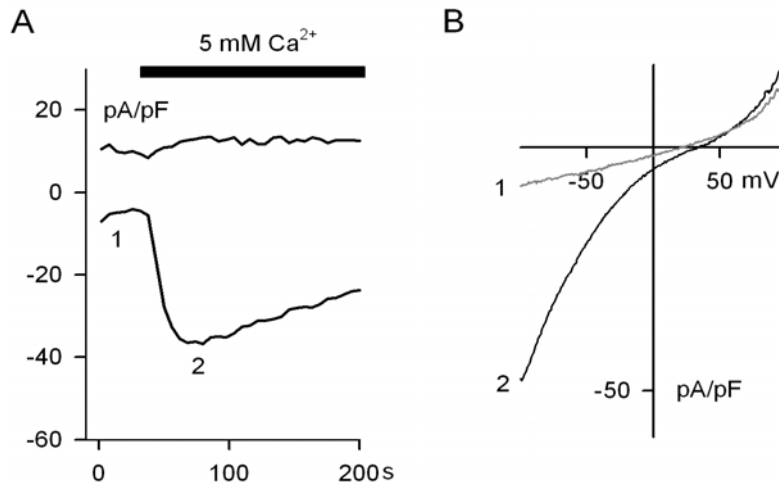
Figure 22: The rise of local [Ca^{2+}]$_i$ induced by CRAC currents activates TRPC5 channels. A representative ion current development over time for STIM1 and ORAI1 overexpressing TRPC5 stable cells in voltage clamp eperiments. Experimental conditions as described in Fig. 21 with the exception that 10 mM BAPTA were added to achieve maximal buffering of internal Ca^{2+}. (A) Current densities showing inward (-80 mV; black line) and outward currents (+80 mV; grey line). (B) Representative I-V-characteristic as indicated by numbers in (A).

According to the triple transfection experiments with TRPC5, ORAI1 plus STIM1 (Fig. 18, 19), the TRPC5 cell line was transfected individually with STIM1 or ORAI1 to test whether TRPC5 currents develop under these conditions in response to IP$_3$ dialysis (Fig. 23 A). The pipette solution contained 10 mM EGTA and cells were perfused with a 5 mM Ca^{2+}-containing solution. The non-transfected TRPC5 cell line and the TRPC5 cells individually transfected with STIM1 or ORAI1 showed neither inward-rectifying CRAC currents nor TRPC5 development (Fig. 23 A). The detectable currents, seen under these conditions, represent linear background currents in TRPC5 stable cells. In contrast, average current densities for STIM1 plus ORAI1-transfected TRPC5 stable cells showed initial high levels of inward current densities, indicating the activation of CRAC channels, followed by the activation of TRPC5 channels as indicated by the increase high levels of late outward current densities (Fig. 23 A). Thus, as in the transiently transfected HEK 293 cells (Fig. 18, Fig. 19), the activation of TRPC5 channels in the TRPC5 cell line required the presence of both ORAI1 and STIM1.
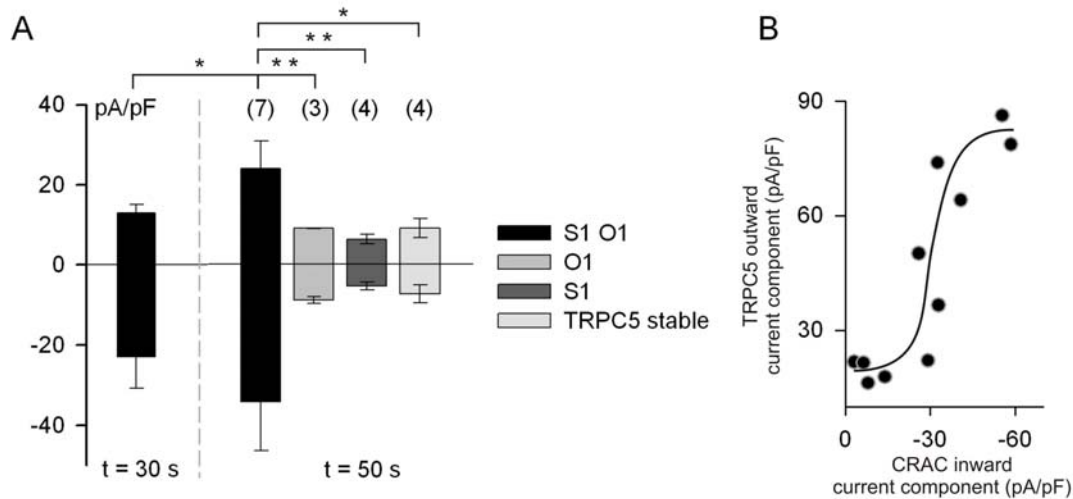
Figure 23: Activation of CRAC and TRPC5 channels and correlation between CRAC and TRPC5 currents in the TRPC5 cell line. STIM1 + ORAI1 (S1 O1), ORAI1 (O1) or STIM1 (S1) were transfected in the TRPC5 cell line. Ton-transfected cells (TRPC5 stable) were used as controls. Cells were dialysed with IP_3 under buffering of internal Ca^{2+} with 10 mM EGTA and ion currents were measured in the presence of 5 mM external Ca^{2+} as described in Fig. 21 A. (A) Average inward (-80 mV) and outward (+80 mV) currents recorded 30 s and 50 s after establishing whole-cell patch configuration. The inward currents recorded at 30 s represent likely pure CRAC currents while the outward currents measured at 50 s correspond to TRPC5 currents. Cell numbers are given in parenthesis. Error bars indicate s.e.m. (B) CRAC current (-80 mV, 30 s) plotted versus TRPC5 outward currents (+80 mV, 50 s) for the TRPC5 cell line transfected with STIM1 plus ORAI1.

Finally, the relationship between Ca^{2+} influx mediated by ORAI1 and TRPC5 outward currents was analyzed in more detail. I tested whether the TRPC5 current densities are related to CRAC current densities, which likely represent a measure for the amount of Ca^{2+} influx into the cells. In Fig. 23 B, CRAC TRPC5 outward current densities monitored at +80 mV were plotted versus inward current densities monitored at -80 mV recorded in TRPC5 cells transfected with STIM1 plus ORAI1. Inward currents were recorded 30 s after break-in when I_{CRAC} was clearly detectable but TRPC5 was still inactive (Fig. 23 A) and TRPC5 outward current densities represent peak TRPC5 currents ~50 s after establishing whole-cell configuration (Fig. 23 A). As expected from the experiments shown in Fig. 18 and 21, in which CRAC current activation preceded the activation of TRPC5 currents, a correlation between TRPC5 outward current development and the CRAC current densities was found in individual cells (Fig. 23 B). This clearly supports the hypothesis for a direct and dose-dependent effect of intracellular Ca^{2+} on TRPC5 channel activation.

4.3.2 Intracellular Ca^{2+} activates TRPC5 currents

The activation of TRPC5 currents was dependent on the $[Ca^{2+}]_i$ rise induced by Ca^{2+} influx through CRAC channels in the TRPC5 cell line transfected with STIM1 plus ORAI1 (Fig. 23 B). Accordingly, it was tested whether TRPC5 currents are also activated by dialysing the cells with various $[Ca^{2+}]_i$. In these experiments, pipette solutions containing EGTA-buffered Ca^{2+} concentrations of 0, 10, 30, 50, 100, 300, 500, 1000, 3000 and 10000 nM were used to establish appropriate dose-response relationships for inward (-80 mV) and outward current densities (+ 80mV) (Fig. 24 C, D). Ca^{2+} was not added to the external solution. Immediately after establishing the whole-cell configuration and, accordingly, the dialysis with Ca^{2+}, a rapid increase of both outward and inward currents was observed depending on the $[Ca^{2+}]_i$ (Fig. 24 A). Current-voltage characteristics clearly showed the typical TRPC5 shape (Fig. 24 B) indicating that TRPC5 is exclusively activated in the TRPC5 cell line. In order to determine the dose-response relations, peak inward and outward currents from the experiments shown in Fig. 24 A were plotted versus $[Ca^{2+}]_i$ (Fig. 24 C, D). The data was subsequently fitted with Hill equations (Table 4). Both inward and outward currents were not affected by $[Ca^{2+}]_i$ below 100 nM and maximal current densities were attained with $[Ca^{2+}]_i$ above 1000 nM. The EC_{50} values (Table 4) indicated that outward currents were more sensitive to changes of $[Ca^{2+}]_i$. In order to test whether the recorded currents were mediated by TRPC5 channels expressed in the TRPC5 cell line, dialysis of various $[Ca^{2+}]_i$ was performed in control HEK 293 cells. At $[Ca^{2+}]_i$ as high as 10000 nM, only linear leak currents were observed (not shown). The analysis of the experiments with HEK 293 cells indicated that inward and outward leak currents were not Ca^{2+} dependent (Fig. 24 C, D). Furthermore, it was tested whether STIM1 modifies the Ca^{2+}-dependence of TRPC5 channels. In these experiments, STIM1 was transiently transfected into the TRPC5 cell line. As shown in Fig. 24 C and D, a slight increase of inward and outward currents at $[Ca^{2+}]_i$ higher than 100 nM was observed. Accordingly, there was a shift of Ca^{2+} dose-response relations to lower $[Ca^{2+}]_i$ in STIM1 expressing cells when compared to the TRPC5 stable cell line and the EC_{50} values decreased (Table 4).
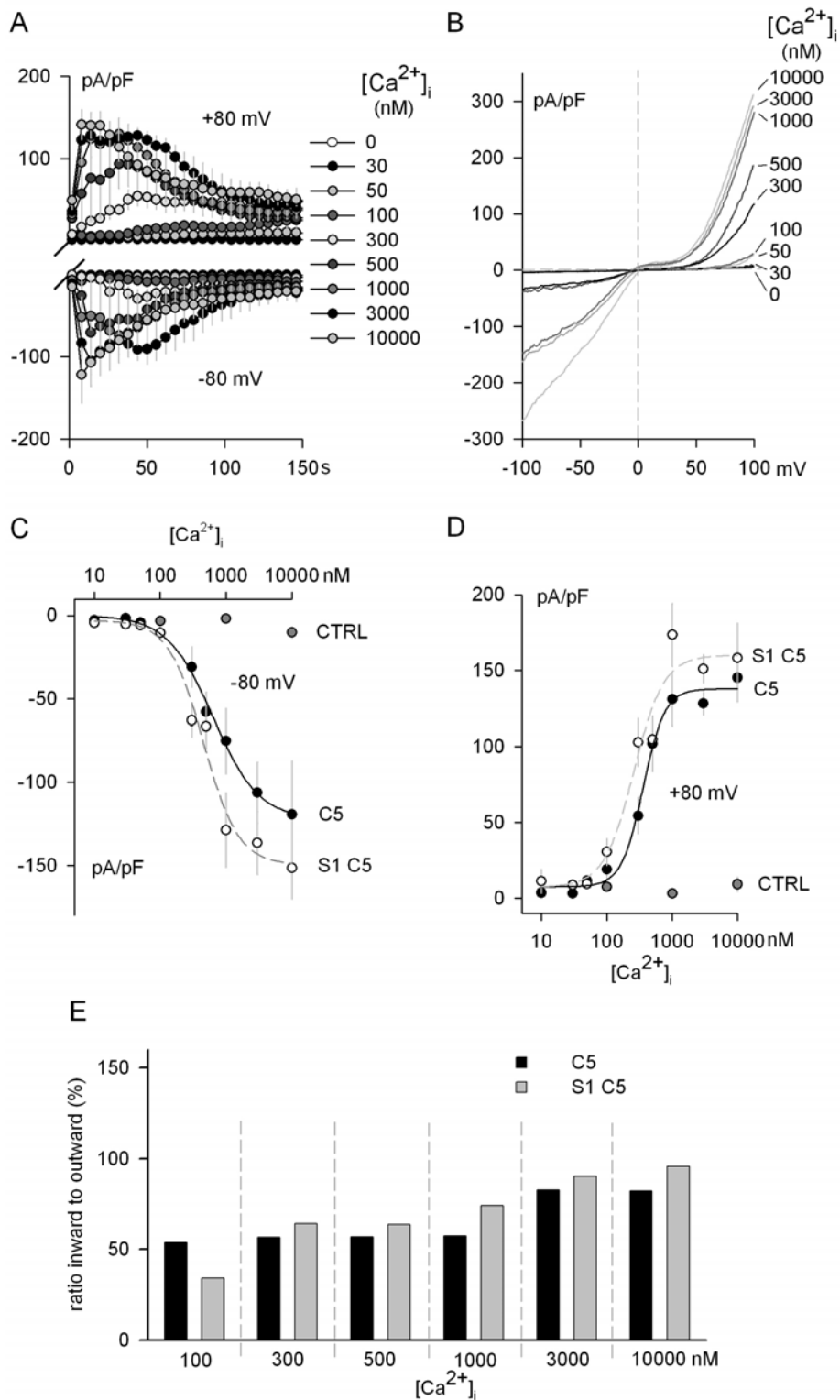
Figure 24: Dose-response relationship for the activation of TRPC5 currents by internal Ca^{2+} in the TRPC5 cell line. (A) TRPC5 current development in cells dialysed with [Ca^{2+}]$_i$ between 0 nM and 10000 nM as indicated. Voltage clamp ramps were delivered every 2 s from -100 mV to +100 mV. Current densities were measured at +80 mV (outward currents) and -80 mV (inward currents). **(B)** I-V-relations for representative experiments at the indicated [Ca^{2+}]$_i$. **(C, D)** Dose-response relationships for inward and outward current increase induced by various [Ca^{2+}]$_i$, respectively. Data were obtained using HEK 293 cells (CTRL), TRPC5 stable cells (C5) and TRPC5 cell line transiently transfected with STIM1 (S1 C5). The fittings were performed with the Hill equation with the parameters given in Table 4. **(E)** Inward to outward current ratios for various [Ca^{2+}]$_i$. n: 4 – 10.

Table 4: The dose-response relations for the Ca^{2+} dependent activation of TRPC5 currents (Fig. 24 A, B) were fitted with Hill equations. The parameters are given below for the TRPC5 cell line (TRPC5) and for TRPC5 cell line transfected with STIM1 (TRPC5 + STIM1.

	Parameters	TRPC5	TRPC5 + STIM1
inward current densities (-80 mV)	min (pA/pF)	-0.183 ± 2.68	-2.818 ± 6.85
	max (pA/pF)	-122.27 ± 4.64	-149.67 ± 9.31
	Hill coefficient	1.248 ± 0.158	1.638 ± 0.457
	EC$_{50}$ (nM)	635.11 ± 60.8	456.33 ± 72.4
outward current densities (+80 mV)	min (pA/pF)	7.676 ± 3.95	7.574 ± 10.2
	max (pA/pF)	137.9 ± 4.93	160 ± 0
	Hill coefficient	2.614 ± 0.601	1.898 ± 0.589
	EC$_{50}$ (nM)	358. 2 ± 28.8	260.06 ± 51.6

Furthermore, I determined the ratio between inward and outward currents activated by internal Ca^{2+} in the TRPC5 cell line and the transiently STIM1-transfected TRPC5 cell line, in order to see whether the rectification properties of TRPC5 channels is modulated by [Ca^{2+}]$_i$ and STIM1. Inward to outward current ratios of both the non-transfected and STIM1-transfected TRPC5 stable cells were dependent on internal Ca^{2+} levels, increasing from 50 % to ~90 % upon raising internal Ca^{2+} from 100 nM to 10 µM (Fig. 24 E). This suggests, that the outward currents are more sensitive to changes in [Ca^{2+}]$_i$ when compared to inward currents (Table 4).

In Fig. 24 A, TRPC5 activation was accelerated by increasing internal Ca^{2+} levels in both non-transfected and STIM1-transfected TRPC5 stable cells. Additionally, TRPC5 currents were observed to inactivate in a Ca^{2+}-dependent manner (Fig. 24 A). Interestingly, the inactivation of both inward and outward TRPC5 currents was modified by the expression of STIM1 in the TRPC5 cell line. The higher the internal Ca^{2+} concentration the larger is the STIM1 effect on TRPC5 run down (Fig. 25 A). For instance, in the presence of 1 µM [Ca^{2+}]$_i$ outward and inward currents inactivated with a time constant ($t_{1/2}$) of 36 s in the TRPC5 cell line and the expression of STIM1 significantly slowed down the inactivation of TRPC5 currents in a way that the time constant of inactivation almost doubled to 64 s (Fig. 25 B). In summary, inward and outward TRPC5 currents were activated by [Ca^{2+}]$_i$ in a dose-dependent manner.

STIM1 slightly enhanced the sensitivity of TRPC5 currents to internal Ca^{2+} and, additionally, slowed down the inactivation that was also Ca^{2+}-dependent.
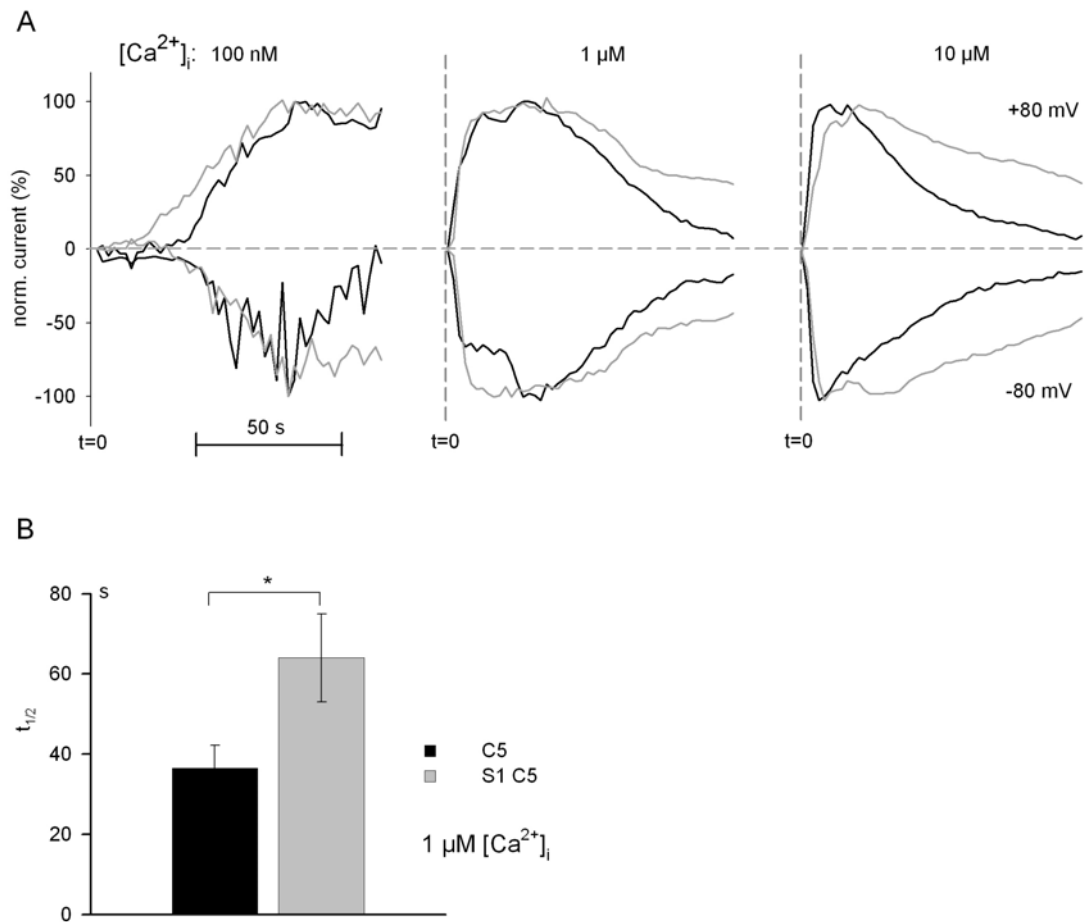

Figure 25: Normalized TRPC5 current development over time in non-transfected (black) and STIM1-transfected TRPC5 stable cells (grey) in response to various internal Ca^{2+} concentrations. (A) Same experiments as in Fig. 24 A. At $[Ca^{2+}]_i$ higher than 300 nM, both outward and inward currents showed a prominent inactivation. (B) The time for half maximal inactivation ($t_{1/2}$) is given for 1 μM $[Ca^{2+}]_i$. n: 5 - 6.

4.3.3 The role of internal Ca^{2+} in the activation of TRPC5 currents via membrane receptors

Since previous reports suggested that TRPC5 currents activate upon application of receptor-stimulating agonists such as carbachol (CCH)[100, 101], I investigated the interplay between the effects of receptor-stimulation and dialysis of defined $[Ca^{2+}]_i$ on TRPC5 currents. Upon application of 200 µM CCH, TRPC5 currents increased rapidly when $[Ca^{2+}]_i$ was 100 nM (Fig. 26 A, B). Clearly, these CCH-stimulated TRPC5 currents were larger and developed faster than those that were activated by 100 nM $[Ca^{2+}]_i$ (Fig. 24 A and Fig. 26 A). CCH-activated TRPC5 currents were completely inhibited by buffering intracellular calcium to 0 nM (Fig. 26 A). Further experiments showed that Ca^{2+}-activated TRPC5 currents were reversibly boosted by carbachol perfusion (Fig. 26 C, D). In these experiments, 1000 nM $[Ca^{2+}]_i$ was used to attain maximal activation of TRPC5 currents. Carbachol induced an additional TRPC5 current increase which was reversed by reperfusing the cells with a carbachol-free external solution. The effects of CCH on TRPC5 currents, even though smaller, were reproduced by a second carbachol reperfusion (Fig. 26 C). Notably, average inward current boost was significantly larger than average outward current boost, as shown in Fig. 26 E. With 1 µM $[Ca^{2+}]_i$, inward current densities increased at ~150 % in size upon charbachol perfusion, whereas outward current densities showed a clear 50 % increase (Fig. 26 E). In HEK 293 control cells, neither CCH nor the increase of $[Ca^{2+}]_i$ activated ion currents (Fig. 26 C). As illustrated in Fig. 28 B, carbachol-induced increase of TRPC5 currents was dependent on intracellular Ca^{2+} concentrations with the strongest CCH-effect at physiological $[Ca^{2+}]_i$ levels. Since the CCH-effects were absent in the presence of 10 mM EGTA, the present results suggest that the rise of $[Ca^{2+}]_i$ might be a central event in the activation of TRPC5 channels via stimulation of membrane receptors.
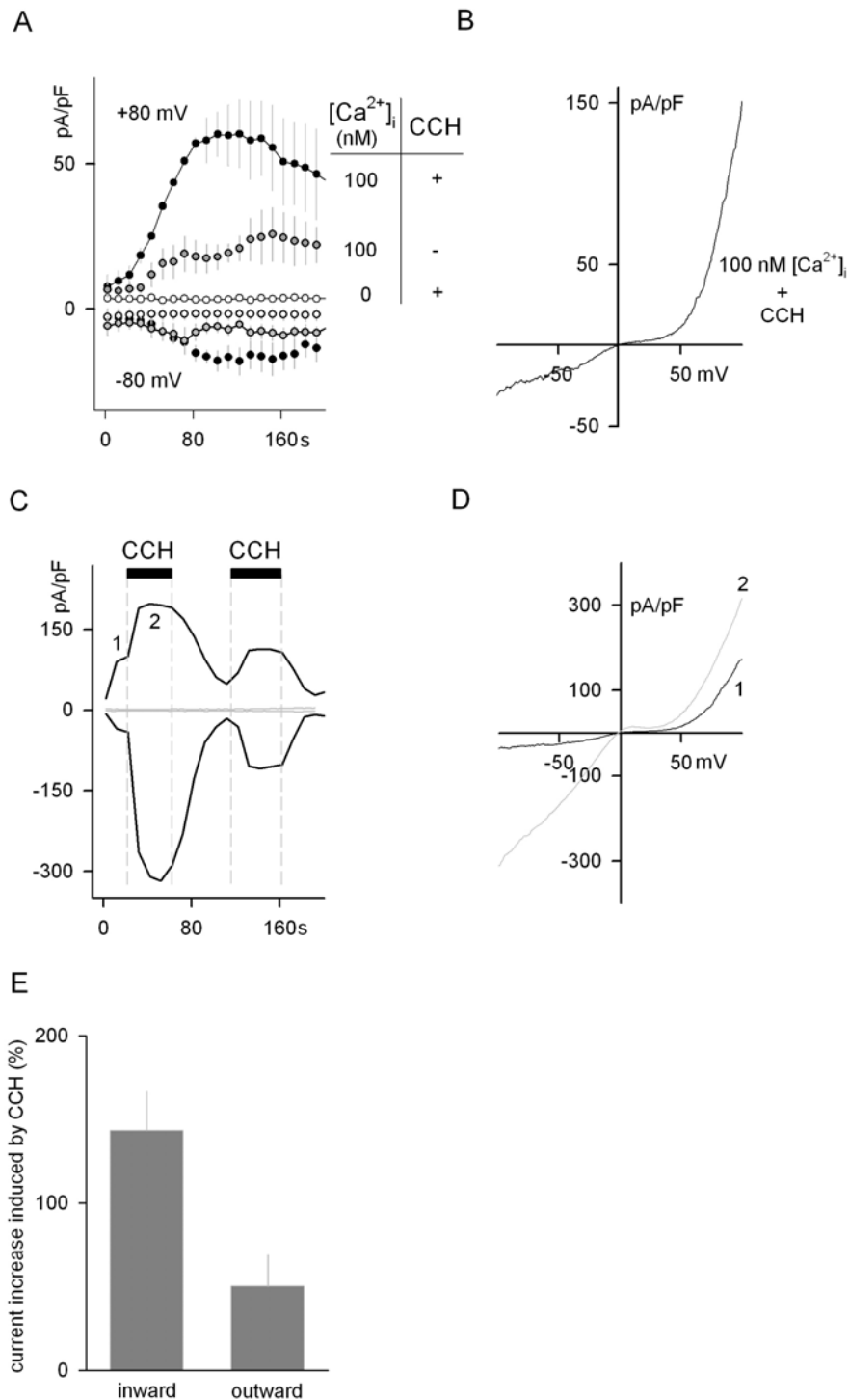
Figure 26: Activation of TRPC5 currents by stimulation of muscarinic receptors under defined [Ca^{2+}]$_i$. Whole cell voltage clamp recordings as previously described in Fig. 25. Inward currents were measured at -80 mV, outward currents at +80 mV. Carbachol (CCH, 200 µM) was applied as indicated above the graph. **(A)** Average inward and outward current densities in the TRPC5 cell line stimulated with CCH at the indicated [Ca^{2+}]$_i$. For comparison, the time courses of inward and outward currents activated with 100 nM [Ca^{2+}]$_i$ are shown (same experiments from Fig. 24 A). **(B)** Representative I-V-characteristic for CCH activated TRPC5 currents in the presence of 100 nM intracellular Ca^{2+}. **(C)** Representative inward and outward TRPC5 current development over time induced by 1 µM [Ca^{2+}]$_i$ and, additional stimulation with CCH: TRPC5 stable cells (TRPC5 stable; black line) and HEK 293 control cells (HEK 293; grey line). **(D)** Representative I-V-characteristics recorded at indicated time points in (C). **(E)** Average increase of TRPC5 currents induced by CCH with respect to the current densities attained by the activation with 1 µM [Ca^{2+}]$_i$. n = 3.

It has been reported that TRPC5 currents increased dramatically by a phenomenon called 'rapid vesicular insertion of TRP' channels (RiVIT), which means that vesicular TRPC5 channel proteins translocate and insert into the cell membrane upon epidermal growth factor (EGF) stimulation[60]. In addition, exocytotic processes, such as vesicular translocation, are also triggered by increased internal Ca^{2+} levels[102]. Since TRPC5 currents were activated by internal Ca^{2+} in a dose-dependent manner (Fig. 24 A, C, D), I tested the effects of EGF and various $[Ca^{2+}]_i$ in the TRPC5 cell line. In these experiments, the cells were incubated with 100 ng/ml EGF for 4 min to produce exocytotic events[60] and, afterwards, the effects of rising $[Ca^{2+}]_i$ were tested. As for cells dialysed with various $[Ca^{2+}]_i$ (Fig. 24), the EGF-treated cells developed outward and inward currents with time courses that were dependent on dialysed $[Ca^{2+}]_i$ (Fig. 27 A, B). Additionally, EGF-treated TRPC5 stable cells revealed an increase in inward (at -80 mV) and outward current densities (at +80 mV) for intracellular Ca^{2+} concentrations from 100 nM to 3000 nM (Fig. 27 A, B). Under sub-physiological intracellular $[Ca^{2+}]_i$, EGF incubation did not induce a detectable TRPC5 current (Fig. 27 A, B). Accordingly, a decrease of the EC_{50} value for the Ca^{2+}-dependence of TRPC5 outward currents to lower $[Ca^{2+}]_i$ was detected in EGF-treated cells (Table 5). In conclusion, EGF-induced TRPC5 currents were slightly more sensitive to intracellular Ca^{2+} rise in EGF-treated cells but current densities were not significantly different over the $[Ca^{2+}]_i$ range of 10 – 10000 nM (Table 5, Fig. 27 C).
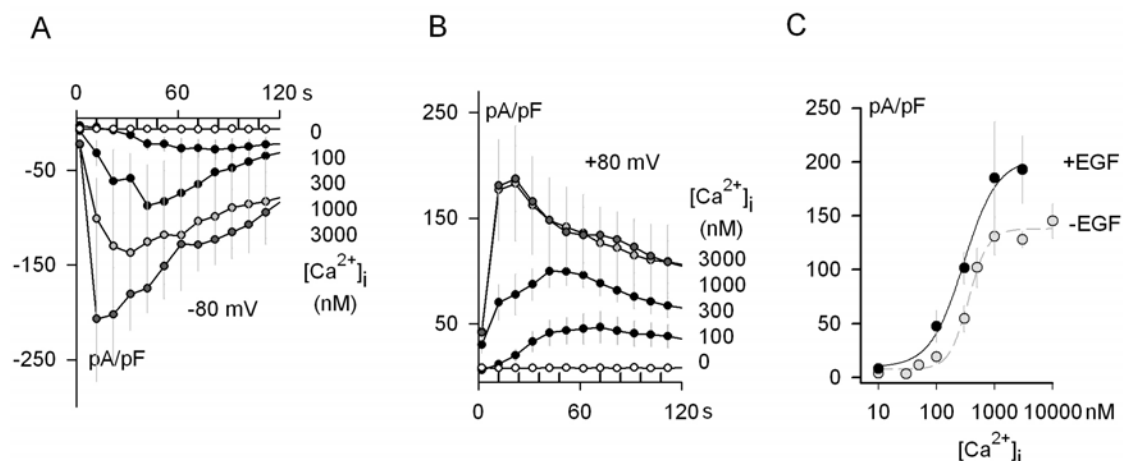

Figure 27: Effects of various $[Ca^{2+}]_i$ on TRPC5 currents in cells stimulated with EGF and non-stimulated cells. Cells stably transfected with TRPC5 were incubated with EGF (100 ng/ml) for 4 min at 37°C before establishing the whole-cell configuration to record outward and inward TRPC5 currents using $[Ca^{2+}]_i$ as described in Fig. 24. Outward currents were measured at +80 mV and inward currents were measured at -80 mV. (A, B) Average inward and outward TRPC5 current development, respectively. The $[Ca^{2+}]_i$ used in the pipette solutions are indicated. (C) Dose-response relationship for the effects of internal Ca^{2+} in EGF-treated cells (black) and non-treated (grey) TRPC5 cells. Lines represent dose response fits with the Hill equation with the parameters given in Table 5. n: 4 – 8.

Table 5: The dose-response relationship for the Ca^{2+} dependent activation of TRPC5 outward currents in the EGF-treated TRPC5 cell line (Fig. 27 B) was determined by a Hill equation fit. The parameters are given below for the TRPC5 cell line (TRPC5) and for the EGF-treated TRPC5 cell (EGF-treated STIM1).

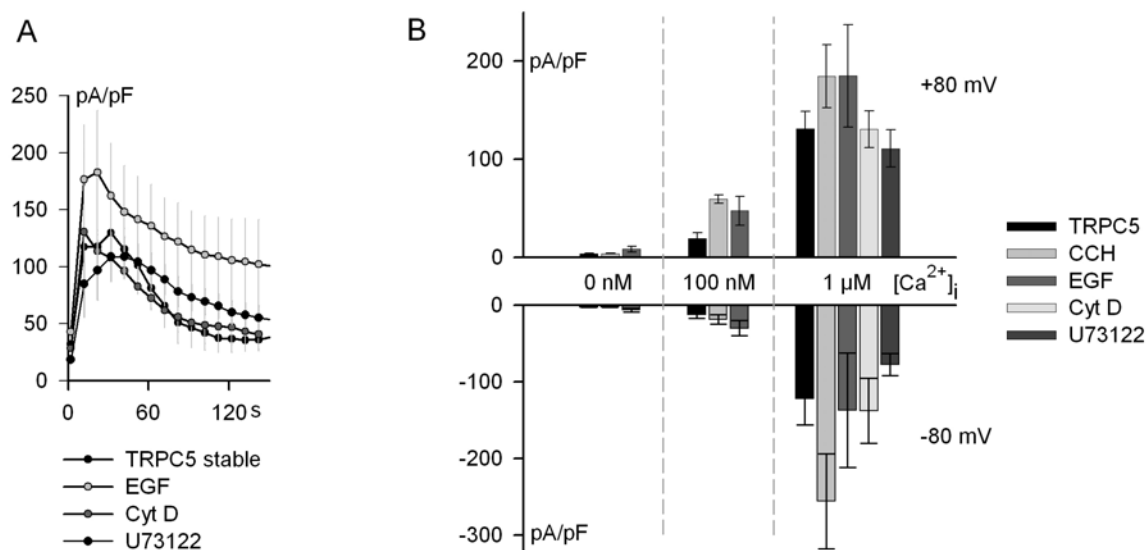|	Parameters	TRPC5	EGF-treated TRPC5
outward current densities (+80 mV)	min (pA/pF)	7.676 ± 3.95	9.518 ± 14
	max (pA/pF)	137.9 ± 4.93	203.41 ± 18
	Hill coefficient	2.614 ± 0.601	1.503 ± 0.515
	EC$_{50}$ (nM)	358. 2 ± 28.8	293.73 ± 70.1

Figure 28: (A) Mean outward current densities over time in intracellular 1 µM Ca^{2+} TRPC5-stably transfected HEK 293 cells. Cells were non-treated (TRPC5 stable) or incubated in 100 ng/ml epidermal growth factor for 4 min at 37°C (EGF), incubated in 10 µM Cytochalasin D for 10 min at 37°C (Cyt D) and in 2 µM U73122 for 5 min at 37°C (U 73122), followed by perfusion with 200 µM carbachol (CCH). (B) Average peak current densities for TRPC5 currents activated by different intracellular Ca^{2+} concentrations in TRPC5 stable cells treated as described in (A) or perfused with 200 µM carbachol (CCH). Same experiments as in Fig. 26.

Finally, I tested whether rearrangements of the cytoskeleton or activation of PLC are involved in the activation of TRPC5 currents by internal Ca^{2+}. As shown in Fig. 28 A, TRPC5 cells treated with 10 µM cytochalasin D showed a fast outward current development in the presence of 1 µM internal Ca^{2+} that was comparable to the response of non-treated TRPC5 cells. Similarly, in whole cell recordings, TRPC5 cells pre-incubated in 2 µM U73122 developed TRPC5 currents following exogenous application of 1 µM Ca^{2+} through the patch pipette (Fig. 28 A). Thus, the presented

results (Fig. 28 A) indicated that neither PLC nor the cytoskeleton appeared to be involved in the activation of TRPC5 channels by internal Ca^{2+}.

In summary, additive effects of EGF and CCH were seen at concentrations of 100 nM Ca^{2+} (Fig. 28 B). Furthermore, EGF and CCH were not effective in inducing TRPC5 currents at zero $[Ca^{2+}]_i$ suggesting that a rise of internal $[Ca^{2+}]_i$ is the ultimate signal for activation of TRPC5 channels under stimulation of membrane receptors.

4.3.4 Role of calmodulin-binding site in the Ca^{2+}-dependent activation of TRPC5 channels

Two calmodulin (CaM)-binding sites named CaM / IP3R-binding (CIRB) domain and calmodulin-binding domain II (CBII) were identified at the C-terminus of TRPC5 proteins[61, 62]. Therefore, it was tested whether these calmodulin-binding sites were involved in the activation of TRPC5 channels by internal Ca^{2+}. HEK 293 cells transiently transfected with a TRPC5 mutant that contains a triple amino acid substitution in the CIRB domain (J1305) did not show a detectable TRPC5 current in response to increased intracellular Ca^{2+} levels (Fig. 29 A, B). In contrast, 1 µM intracellular Ca^{2+} activated TRPC5 currents in HEK 293 cells transfected with a mutated form of the TRPC5 protein lacking the CBII (J1307) (Fig. 29 A, B). Activated TRPC5 currents in J1307 transfected cells showed the TRPC5 typical I-V-characteristic, whereas in HEK 293 cells transfected with J1305 only linear leak currents were detectable (Fig. 29 C). Thus, these results indicated that CBII is not required for the action of internal Ca^{2+} on TRPC5 channels. Conversely, CIRB might be responsible for the activation of TRPC5 channels by internal Ca^{2+}.
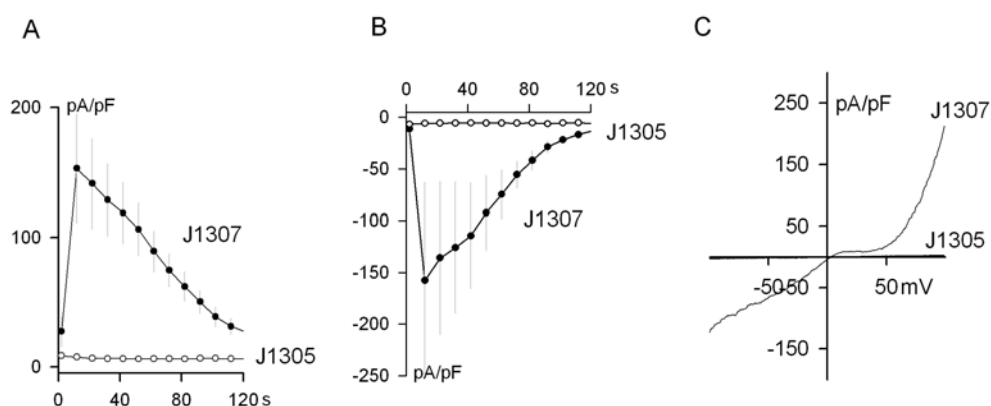

Figure 29: Intracellular Ca^{2+} (1 µM) activated TRPC5 currents in HEK 293 cells overexpressing CIRB mutated TRPC5 (J1305; white circles; n = 5) or CBII deleted TRPC5 (J1307; black circles;

4.3.5 Intracellular Ca^{2+} release results in TRPC5 dependent membrane depolarization

In the experiments shown in Fig. 18 – 29, the whole-cell configuration of the patch-clamp technique was used to record TRPC5 channel currents under tight control of the ion composition of the cytosol. In the next series of experiments, the activation of TRPC5 channels is explored in intact cells. For this purpose, it was tested whether the increase of [Ca^{2+}]$_i$ by Ca^{2+}-store depletion activates TRPC5 channels in the TRPC5 cell line. Since the activation of the non-selective TRPC5 ion channels might result in membrane depolarization, fluorometric measurements of the membrane potential and Ca^{2+} signalling were performed in the TRPC5 cell line and also in HEK 293 control cells (Fig. 30). The change in the membrane potential in response to 1 µM thapsigargin and 130 µM carbachol was tracked. Thapsigargin perfusion induced membrane depolarization in TRPC5 stable cells whereas HEK 293 cells remained at basal membrane potential levels (Fig. 30 A). The Ca^{2+} signals measured in TRPC5 cells were inistinguishable from Ca^{2+} signals in HEK 293 control cells (Fig. 30 C). Notably, carbachol perfusion induced a strong and fast membrane potential depolarization in both TRPC5 stable and HEK 293 cells with a 50 % stronger signal in TRPC5 stable cells (Fig. 30 B). In contrast to the indistinguishable [Ca^{2+}]$_i$ rise in thapsigargin-treated cells, the Ca^{2+} signals recorded in carbachol-treated cells were stronger in TRPC5 cells than in HEK 293 control cells (Fig. 30 C, D). Carbachol was always effective independently from the experimental design, whereas membrane depolarization and Ca^{2+} signals induced by thapsigargin could hardly be monitored when applied after carbachol perfusion (Fig. 30).

In conclusion, Charbachol-induced membrane depolarization was detectable in TRPC5 cells and also HEK 293 control cells. By contrast, TRPC5 dependent membrane depolarization was recorded exclusively in the TRPC5 cell line triggered by thapsigargin. Under non-buffered intracellular conditions   the [Ca^{2+}]$_i$ rise induced by the thapsigargin via Ca^{2+}-store depletion activated TRPC5 channels.
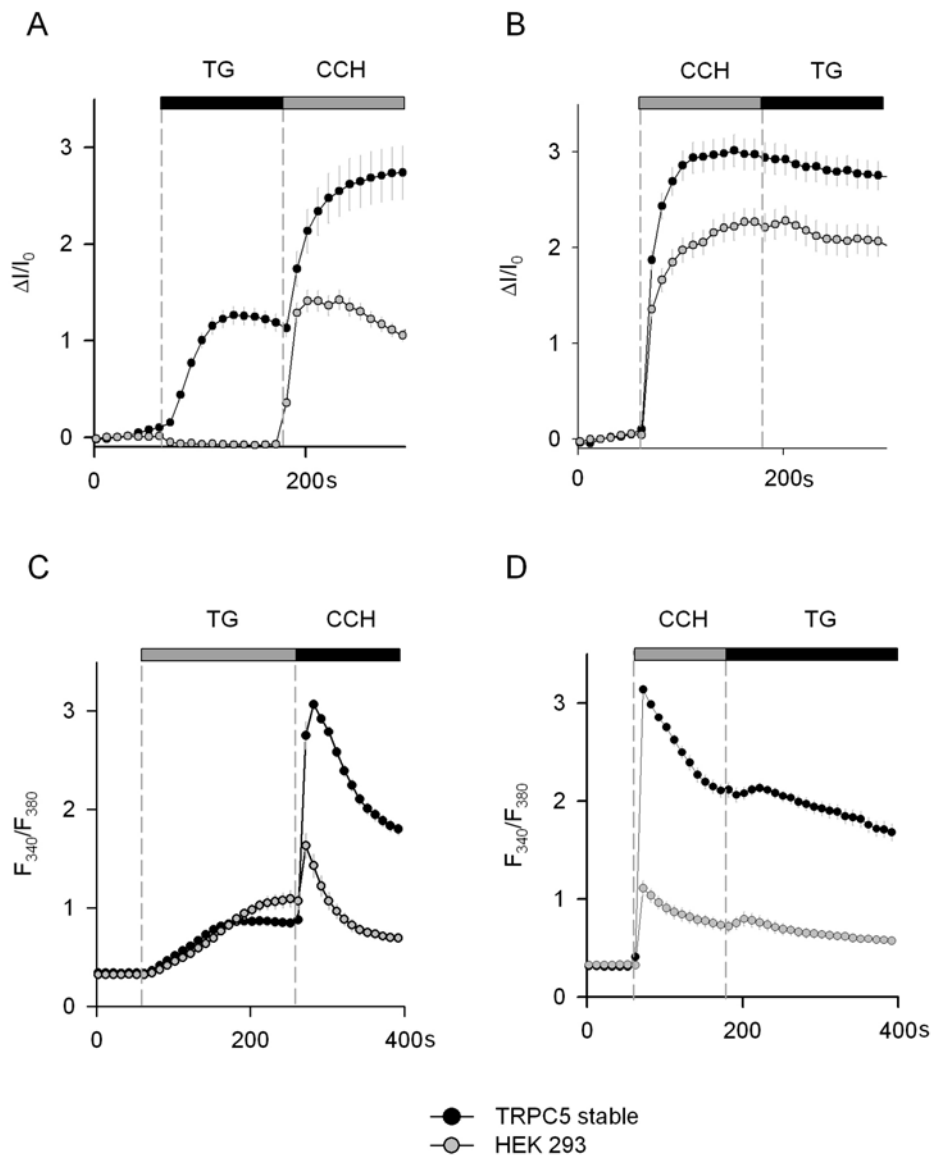
Figure 30: Fluorometric measurements of membrane potential and Ca^{2+} imaging in the TRPC5 cell line (TRPC5 stable; black) and HEK 293 control cells (HEK 293: grey). Store-depleting reagent thapsigargin (TG; 1 µM) and 130 µM muscarinic-receptor agonist carbachol (CCH) were applied as indicated above graph. (A, B) Cells were incubated with standard external solution (HBSS) containing the FLIPR® dye for 15 min at room temperature (RT). Cells were monitored by exciting FLIPR® dye at 530 nm and the emitted fluorescence was recorded at 600 nm. The bath solution (HBSS) contained (in mM): 1.26 Ca^{2+}, 5.36 K^{+}, 136.89 Na^{+} (see Materials and Methods). Before and after each experiment, unspecific background fluorescence was measured by exciting at 350 nm. (C, D) Cells were loaded with FURA-2AM (10 µM) for 40 min at RT and then washed twice with HBSS. Individual cells were monitored exciting FURA-2 at 340 nm and 380 nm and recording emitted fluorescence at 510 nm. Non-specific background fluorescence was subtracted from displayed ratio F$_{340}$/F$_{380}$. At least two independent experiments were performed. For each experimental setting, the signals of individual cells (n: 46 – 83) were pooled to obtain average FLIPR® and FURA-2 signals.

To further test whether the thapsigargin-induced [Ca^{2+}]$_i$ rise is inducing the membrane depolarization in the TRPC5 cell line, membrane potential changes and Ca^{2+} signals were recorded simultaneously. TRPC5 cells were loaded with FURA-

2AM and the membrane potential dye FLIPR$^{®}$. In the presence of extracellular Ca^{2+} (1.26 mM) the membrane potential depolarized in response to thapsigargin and Ca^{2+} signals increased as well (Fig. 31, A). As a control for a proper function of the membrane potential dye and visualization of the actual cell condition, I perfused the cells with a high K^{+} solution (25 mM) at the end of each experiment. These experiments were designed to investigate whether the Ca^{2+} signals precede the membrane potential depolarization. As illustrated in Fig. 31, Ca^{2+} signals in TRPC5 cells revealed a fast increasing Ca^{2+} signal, followed by a depolarization of the membrane potential carried by TRPC5 channels. The Ca^{2+} increase reached the half maximum signal strength ($t_{1/2}$) after 33.8 ± 0.98 s and the membrane potential at 55.9 ± 4.57 s after thapsigargin perfusion (Fig. 31, B). In order to prove that the delay in depolarization in comparison to Ca^{2+} increase was not due to the inertia of the membrane potential dye, the depolarization signal in response to high extracellular K^{+} was measured. Half maximal signal strength was reached rapidly, only 4.55 ± 0.28 s after perfusion (Fig. 31 B). Comparable results were obtained under extracellular Ca^{2+}-free conditions (Fig. 31 C). Ca^{2+} signals increased to half maximum within 53.0 ± 2.38 s in response to thapsigargin perfusion followed by membrane depolarization due to TRPC5 activation ($t_{1/2}$ = 75.08 ± 0.98 s) (Fig. 31 D).

Thus, Ca^{2+} signals preceded membrane depolarization in the TRPC5 cell line, indicating, that the [Ca^{2+}]$_i$ rise induced by thapsigargin activated TRPC5 channels, which in turn induced a membrane depolarization.
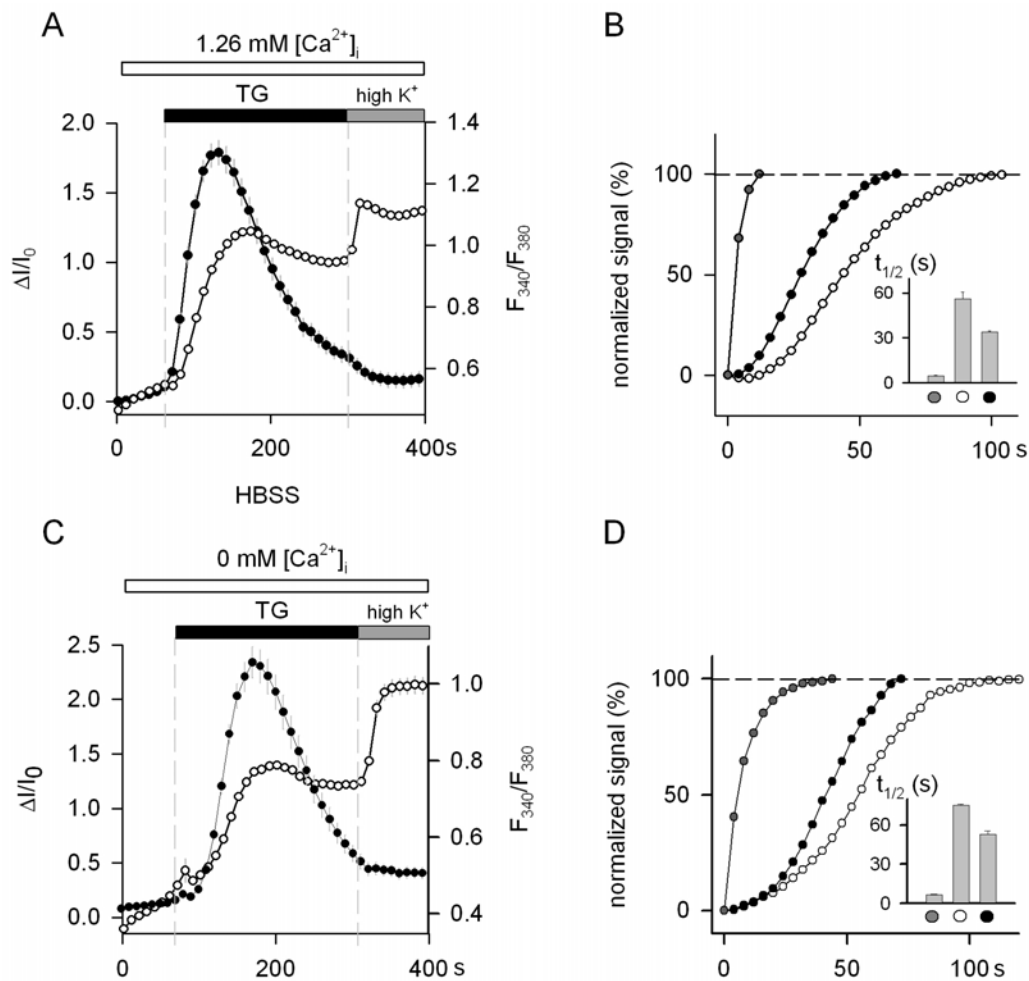
Figure 31: Comparison of the time course of membrane potential and $[Ca^{2+}]_i$ changes. Fluorescence videomicroscopy was used to track membrane potential changes and Ca^{2+} signals simultaniously. TRPC5 cells were incubated for 40 min at RT in FURA-2AM (10 µM), washed and incubated for 15 min in FLIPR® dye. Same experimental procedure as previously described in Fig. 30. Corresponding filtersets and excitation wavelengths were controlled by macros (see Materials and Methods). FURA-2 signals are given as black circles, FLIPR® tracking is indicated as white circles. Numbers of cells: n: 43-72. (A, C) Time courses of membrane potential and $[Ca^{2+}]_i$ changes in cells bathed in HBSS containing 1.26 mM Ca^{2+} and in a Ca^{2+}-free solution, respectively. As indicated, 1 µM thapsigargin (TG) and high K^+ solution (high K^+) are perfused. (B, D) Normalized FURA-2 (black circles) and FLIPR® signals in response to 1 µM TG (white circles) or high K^+ (25 mM; grey circles) in TRPC5-stably transfected HEK 293 cells. Embedded bar graphs display the time to half maximum signal strength.

4.3.6 L-type Ca^{2+} channels act as Ca^{2+} donors for TRPC5 activation

Voltage-gated Ca^{2+} channels represent an important source for cellular Ca^{2+} influx in excitable cells, similar to the function of ORAI and STIM1 dependent CRAC currents in non-excitable cells. Voltage-gated Ca^{2+} channels are formed as a complex of different subunits: α_1, $\alpha_2\delta$, β_{1-4} and γ[103]. The subunit α_1 forms the ion conducting pore while the associated subunits have several functions including the modulation of

gating. In TRPC5-stably transfected HEK 293 cells overexpressing the α_1C subunit of the L-type Ca^{2+} channel plus the β_2 subunit, inward (at -60 mV) and outward TRPC5 current development (at +80 mV) was clearly detectable when Ca^{2+} influx (at 0 mV) was activated by depolarizing the cell membrane of TRPC5 cells (Fig. 32 A).
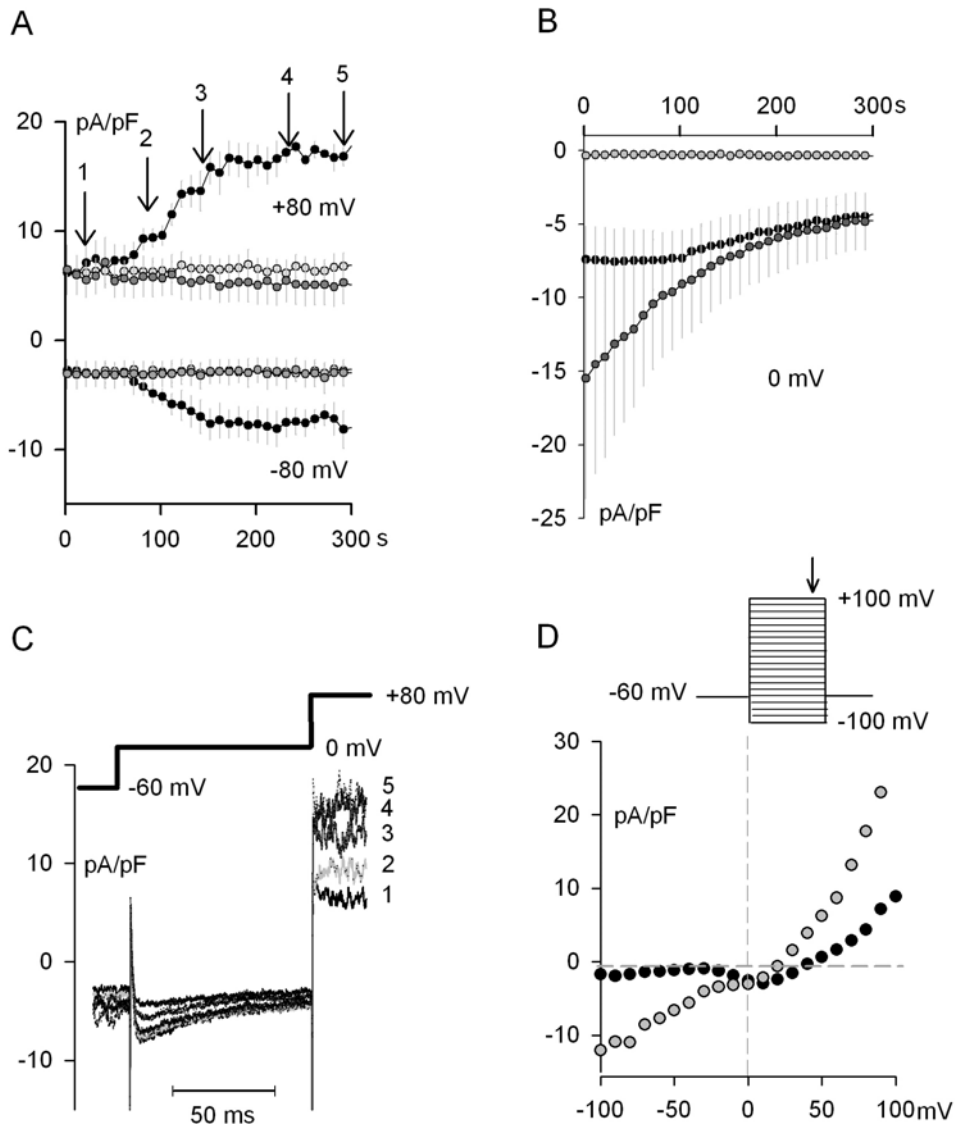

Figure 32: (A, B) Whole cell recordings reveal TRPC5 ion current development (at -60 and +80 mV) and L-Type channel-dependent Ca^{2+} currents (at 0 mV) in TRPC5 stable cell line overexpressing α_1C- and β_2-subunits of L-Type Ca^{2+} channels. Time courses for outward (+80 mV) and inward currents (-60 mV) are shown for the TRPC5 cell line (grey circles; n = 6) and for transient transfections of α_1C- and β_2-channel proteins in the TRPC5 cell line (black circles; n = 5) and in non-transfected HEK 293 cells (white circles; n= 4). Current densities were monitored by applying a voltage step protocol shown in (C). (C) Representative I-V-ion current traces taken at indicated time points during experiment (black arrows in (A)). Applied voltage step protocol is displayed. (D) Representative I-V-characteristics for L-type-overexpressing TRPC5 stable cells recorded before (black circles) and after (grey circles) TRPC5 channel activation recordings from (A). Step protocols were applied as indicated.

In these experiments, it was tested whether L-type Ca^{2+} channels can provide sufficient Ca^{2+} influx to activate TRPC5 channels as it was previously shown for CRAC channels (Fig. 21). In the presence of 5 mM extracellular Ca^{2+}, inward and outward currents activated in TRPC5 cells transiently transfected with the $\alpha_1 C$ plus β_2 subunits approximately 100 s after establishing the whole-cell configuration under intracellular buffered Ca^{2+} conditions (10 mM EGTA). A voltage-step protocol was applied every 2 s, to activate the voltage-gated L-type channels resulting in Ca^{2+} influx (recorded at 0 mV) (Fig. 32 B). These VGCC dependent Ca^{2+} currents showed an inactivation over time in TRPC5 cells overexpressing the VGCC subunits as well as in HEK 293 control cells transfected with the $\alpha_1 C$ plus β_2 subunits. Ca^{2+} currents were not detectable in non-transfected TRPC5 stable cells (Fig. 32 B). The inward and outward current development at -60 mV and +80 mV, respectively, were exclusively observed in TRPC5 stable cells which show a clear Ca^{2+} influx through L-type channels. Neither HEK 293 control cells revealing Ca^{2+} influx currents through L-type channels nor non-transfected TRPC5 stable cells lacking Ca^{2+} signals showed detectable inward and outward current activation (Fig. 32 A, B). As illustrated in Fig. 32, TRPC5 stable cells overexpressing the $\alpha_1 C$ subunit of L-type Ca^{2+} channels plus the β_2 subunit showed clear Ca^{2+} influx at 0 mV which is inactivating over time. Notably, inward (at -60 mV) and outward currents (at +80 mV) which developed over time revealed the expected TRPC5 current-voltage characteristics (Fig. 32 D). Thus, non-selective TRPC5 currents were activated by a local $[Ca^{2+}]_i$ rise which is generated by Ca^{2+}-influx through L-type Ca^{2+} channels. Thus, the present experiments suggest that L-type Ca^{2+} channels represent a signaling pathway for TRPC5 activation in excitable cells.

5   Discussion

5.1   Murine ORAI variants form functional CRAC channels

Recent experiments have put forward that ORAI and STIM represent the molecular components of CRAC currents[11, 83]. The ER membrane-located proteins STIM1 and STIM2 appear to act as Ca^{2+} sensors with a C-terminal EF-hand motif reaching into the ER lumen. Latest reports revealed that STIM2 activates Ca^{2+} influx upon smaller decreases in ER Ca^{2+} levels [29] and also mediates store-independent Ca^{2+} influx[104]. However, STIM1 seems to play the major role in CRAC current activation. Upon store depletion, STIM1 relocalizes into punctae and STIM1 / STIM1 multimerization occurs followed by STIM1/ORAI interaction activating the Ca^{2+} entry through ORAI protein complexes[105].

ORAI proteins, however, are believed to be located in the plasma membrane of a cell and exhibit the CRAC channel itself by forming multimeric assemblies[33]. The replacement of conserved glutamate residues in the first and third transmembrane segments as well as aspartate to arginine substitution in the first extracellular loop of ORAI change the ion selectivity characteristics of CRAC currents. This change in ion selectivity provides good evidence that ORAI proteins forming the CRAC channel pore[33]. So far, most investigations have been performed either with human or *Drosophila* isoforms[106].

Here, I determined the functional properties of CRAC currents activated by intracellular dialysis of IP_3 in either HEK 293 or RBL 2H3 cells transiently transfected with murine STIM1 and murine ORAI1, ORAI2L or ORAI2S (Section 4.1). Murine ORAI1 in combination with STIM1 induced large, strongly inward rectifying currents in HEK 293 and RBL 2H3 cells, independent of endogenously expressed ORAI proteins, respectively. Similar findings were reported for human and *Drosophila* STIM1/ORAI conducted currents[106]. Since HEK 293 and RBL 2H3 cells differ in their endogenous STIM and ORAI expression, the recorded CRAC currents triggered by intracellular IP_3 differ in current density as well. Low STIM and ORAI expression in HEK 293 cells resulted in a hardly detectable CRAC current, whereas clearly inward

rectifying currents were recorded in RBL 2H3 cells displaying detectable endogenous ORAI1, ORAI2 and STIM1 expression (Section 4.1[36]).

Overexpression of ORAI2 variants induced CRAC current densities which were smaller than those induced by ORAI1 in HEK 293 cells under identical experimental conditions (Fig. 11, A). Since STIM1 was co-overexpressed in each experiment, the difference in current density might result from the ability of ORAI to interact with STIM1. Since the main difference between the ORAI variants, especially ORAI1 and ORAI2S, resides in the length of the N-terminus, these results suggest an important role for the N-terminus of ORAI proteins. However, Muik et al.[105] recently reported that the dynamic coupling of STIM1 and ORAI1 occurs at the C-terminus of ORAI proteins but the CRAC current development highly depends on an intact N-terminus, which was originally shown for human Scid patients and is also true for ORAI1 and ORAI2S proteins with a arginine to tryptophan substitution at position 91 or 78, respectively (Fig. 16). These findings lead to the conclusion that the ORAI N-terminus is responsible for proper channel gating. Furthermore, CRAC current densities of RBL 2H3 cells overexpressing STIM1 and ORAI2 variants did not exceed current densities recorded in RBL 2H3 cells transiently transfected with STIM1 alone (Fig. 11, B). Thus, the capability of ORAI2L and ORAI2S to form recombinant CRAC channels depends on the cell background in which these proteins are expressed. In conclusion, ORAI2 isoforms, including the endogenously non-expressed ORAI2S (N130Y) variant, substitute ORAI1-dependent CRAC currents only partly (Fig. 15).

Additionally, STIM1 and the GAMMA1 or GAMMA2 subunit of voltage-gated Ca^{2+} channels were co-overexpressed in HEK 293 as well as in RBL 2H3 cells. Similarities in the tertiary structure[35] inspired these comparative experiments but neither cells co-transfected with STIM1 and GAMMA1 or GAMMA2 nor GAMMA1 or GAMMA2 alone transfected cells exhibited altered current densities in comparison to STIM1 expressing cells or endogenous CRAC currents. Thus, GAMMA subunits cannot substitute ORAI proteins for proper SOCE.

IP_3-induced CRAC currents in non-transfected RBL 2H3 cells display several hallmarks which are also exhibited in STIM1 plus ORAI variants-expressing RBL 2H3 cells. As seen in Fig. 13, CRAC channels are highly Ca^{2+} selective and conduct inward rectifying currents. Under extracellular Ca^{2+} and Mg^{2+}-free conditions, endogenous CRAC channels and recombinant CRAC channels, formed by murine

ORAI1, ORAI2L or ORAI2S, conduct Na^+ ions and do not show a detectable current by removing extracellular Ca^{2+}. These features, originally described for CRAC currents in 1993[21], give another evidence for STIM1 and ORAI as functional CRAC channel-forming proteins.

In addition, the influence of intracellular Ca^{2+} on the CRAC currents in STIM1 plus ORAI transfected cells was investigated. Comparison of CRAC inactivation in dependence on the Ca^{2+} chelators EGTA and BAPTA on the inactivation of CRAC currents in HEK 293 cells overexpressing STIM1 plus ORAI1 or ORAI2 variants, led to the conclusion that CRAC channels formed by ORAI proteins undergo an intracellular Ca^{2+}-dependent inactivation. This inactivation is proportional to the level of CRAC current density and, thus, to the levels of recombinant CRAC channels expressed in HEK 293 cells (Fig. 12). Accordingly, the degree of CRAC current inactivation and its inhibition by BAPTA was also dependent on the cells individual levels of recombinant CRAC channel expression. However, the inhibition of CRAC current inactivation by BAPTA had no influence on the maximum current densities recorded in HEK 293 cells cotransfected with STIM1 and ORAI1 or ORAI2L. HEK cells overexpressing STIM1 plus ORAI2S showed enhanced maximum current densities under intracellular BAPTA conditions. Thus, it appears that ORAI2S is more sensitive to inactivation by intracellular Ca^{2+} than ORAI2L or ORAI1, respectively.

In triple transfection experiments overexpressing STIM1, ORAI1 and ORAI2S, smaller current densities were recorded than in cells overexpressing STIM1 plus ORAI1 (Fig. 14). A similar observation was not made in cells transfected with STIM1, ORAI1 plus ORAI2L. Thus, it appears that ORAI2S plays a dominant-negative role in the formation of functional CRAC channels by ORAI1 proteins giving rise to the assertion that heteromultimeric CRAC channels exist, consisting of both ORAI1 and ORAI2 proteins. In addition, ORAI2L or ORAI2S transfected RBL 2H3 cells had smaller current densities in comparison to endogenous I_{CRAC} (Fig. 11) leading to the conclusion that endogenous I_{CRAC} is mainly carried by ORAI1 homomultimers. When recombinant ORAI2 variants are expressed, heteromultimeric assemblies occur and current density decreases. The possibility to form heteromultimeric channels seems to be a good mechanism to control and specify Ca^{2+} entry. Vig et al.[33] reported multimeric assemblies of ORAI proteins suggesting homomultimeric as well as heteromultimeric protein complexes.

In addition to reports from several groups working on SOCE and CRAC, my investigations suggest that STIM1 and ORAI1, ORAI2L and ORAI2S reconstitute CRAC currents in cell systems overexpressing STIM1 plus an ORAI variant. STIM1 appears to play a role as an ER membrane-located Ca^{2+} sensor that is translocated and rearranged into punctae in close proximity to the plasma membrane in response to store depletion[31]. A dynamic coupling[105] activates the multimeric ORAI channel complex and CRAC currents develop. In conclusion, proteins form heteromultimeric CRAC channels and the resultant current densities appear to be dependent on the N-terminus of ORAI proteins.

The importance of the ORAI N-terminus was described first in 2006 when Feske et al.[8] discovered a single amino acid mutation at position 91 of ORAI1 leading to an abrogated Ca^{2+} entry in T cells derived from SCID patients. In HEK 293 cells overexpressing STIM1 plus murine ORAI1 or ORAI2S proteins possessing a single point mutation (ORAI1 Scid, ORAI2S Scid) that was introduced according to the human SCID mutation, CRAC currents were not detectable (Fig. 16). Moreover, single HEK 293 cells either transfected with ORAI1 Scid or ORAI2S Scid showed reduced I_{CRAC} compared to endogenous CRAC, providing additional evidence for a functional interaction or heteromultimeric assembly between ORAI protein variants.

Here, my investigations provide strong evidence that murine STIM1 and ORAI variants represent the molecular components of the CRAC current showing all the hallmark features of I_{CRAC} originally discovered in mast cells[21]. Upon store-depletion STIM1 is responsible for the signal transduction to the ion channel forming ORAI proteins. Channel gating is controlled by the N-terminus of ORAI proteins.

Although the presented data is very compelling with respect to the molecular components of CRAC currents, investigations are still limited to hematopoietic cells due to the fact that CRAC currents are hardly detectable in non-hematopoietic cells. As extensively documented in Wissenbach et al., 2007, STIM and ORAI proteins are expressed in a vast array of different cell types. In both, lymphocytes and mast cells CRAC currents were first described and characterized, and STIM1 and ORAI protein expression was reported[21, 22]. As previously shown in Fig. 10 and 11, the molecular components for CRAC currents seem to be revealed by the fact that STIM1 plus ORAI-transfected cells exhibit inwardly rectifying currents in response to store

depletion independent of the cell background. Fig. 33 illustrates the I_{CRAC} activation in response to store-depletion with the store Ca^{2+} sensor STIM1 and the multimeric, pore-forming ORAI proteins as molecular components of CRAC channels.
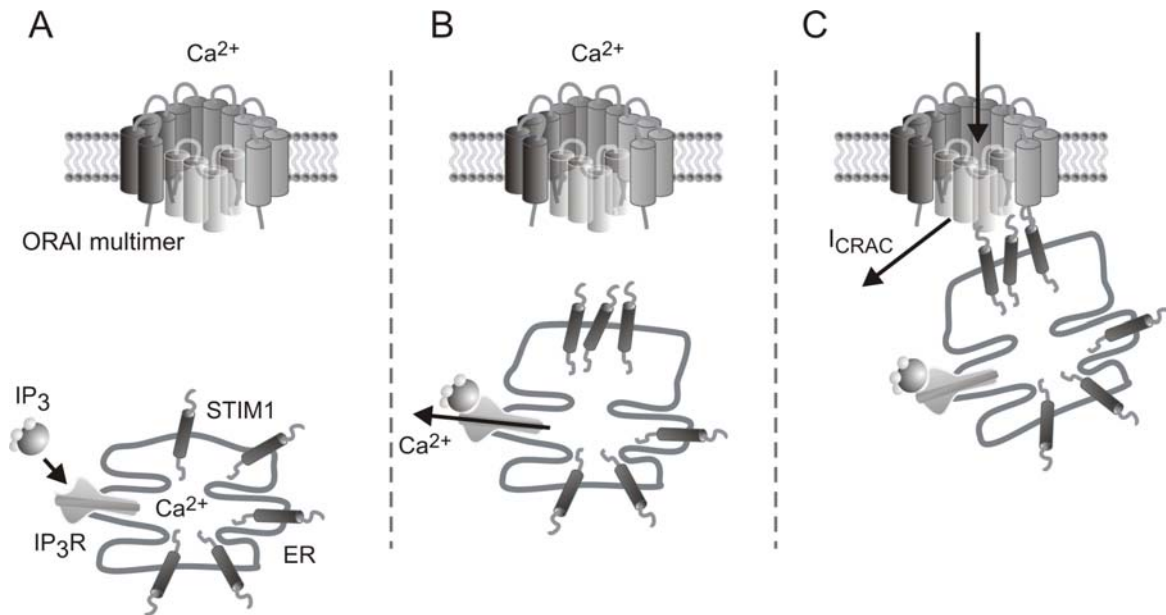

Figure 33: Activation mechanism of CRAC currents. The pore-forming ORAI protein complex (ORAI multimer) is located in the plasma membrane. The Ca^{2+}-sensor stromal-interacting molecule 1 (STIM1) is randomly distributed in the membrane of the endoplasmic reticulum (ER), the major intracellular Ca^{2+}-store. (A) IP_3 is binding to the IP_3-receptor (IP_3R). (B) Upon IP_3R stimulation, Ca^{2+} is depleted and STIM1 proteins assemble to multimers. (C) Multimeric STIM1 complexes interact with the multimeric ORAI complex and I_{CRAC} activates. Illustration modified from Muik et al., 2008[105].

In clear contrast to the present findings that STIM1 and ORAI proteins reconstitute I_{CRAC}, cortical neurons displaying a clearly detectable ORAI expression did not show any Ca^{2+} inward current in response to store-depleting reagents such as IP_3, ionomycin or 4-BrA23187. Whole cell recordings could only display voltage-gated Na^+ currents which were used as identification critera for cortical neurons besides GAD67 amplification (Fig. 17). These results leave room for different interpretations. First, cortical neurons may express non-functional ORAI proteins for instance proteins containing critical mutations at the N-terminus or at the C-terminus changing the coiled-coil region being essential for STIM1 and ORAI interaction[105]. Another very simplistic interpretation might be that neither STIM1 nor ORAI nor even both proteins are sufficiently expressed, so that current densities are just below detectable levels. A third and most provocative interpretation implicates a third molecular component required to generate SOCE, at least in non-hematopoietic cells. The second part of my thesis addresses this highly discussed model elucidating the wide field of SOCE, CRAC and TRPC ion channels.

5.2 Functional coupling of TRPC5 and Ca^{2+}-selective ion channels

TRPC ion channels are believed to participate in store-operated Ca^{2+} entry. As described in this study, STIM1 and ORAI proteins have been proposed to form functional SOCE channels. Consequently, I investigated whether TRPC channels participate in SOCE that is dependent on or regulated by STIM1 and / or ORAI proteins.

In triple transfection experiments, HEK 293 cells overexpressing STIM1, ORAI1 and TRPC3 or TRPC5 ion channels showed additional outward current development which was not detectable in HEK 293 cells co-transfected with STIM1 and ORAI1 alone. Outward current activation was accompanied by increasing inward currents leading to the conclusion that another current component adds to the CRAC current in response to intracellular dialysis of IP$_3$ (Fig. 18). Interestingly, the TRPC-dependent current activation via store-depletion was dependent on STIM1 and ORAI1 proteins. TRPC5-transfected HEK 293 cells did not exhibit any IP$_3$-evoked currents and neither did STIM1 plus TRPC5-transfected cells nor ORAI1 plus TRPC5-transfected cells. The same is true for TRPC3. In contrast to recent reports[96, 97], SOCE was neither detectable nor increased in TRPC3-overexpressing HEK 293 cells co-transfected with ORAI1.

Thus, STIM1, ORAI1 and TRPC proteins appear to functionally interact with each other since TRPC channels show a response to store-depletion that is exclusively detectable in triple-transfected cells. Based on the hypothesis that either the CRAC current-dependent Ca^{2+} signal or a direct protein-protein interaction between STIM1, ORAI1 and TRPC channels are responsible for the initial results, I focused on TRPC5 ion channels and their activation mechanism.

TRPC5 was originally reported as a SOCE[13] channel whereas receptor activation via the PLC pathway is the common activation mechanism reported so far[55]. As mentioned above, IP$_3$-evoked TRPC5 currents were only detectable in cells overexpressing STIM1 and ORAI1 leading to CRAC currents in response to store-depletion under extracellular 5 mM Ca^{2+} containing conditions. As seen in Fig. 20, whole-cell current recordings over time resolved an initial inward rectifying current followed by additional outward and inward current activation. Moreover, the reversal potential shifts from a typical CRAC current of +50 mV to +5 mV, which is

characteristic of TRPC5 currents. Additionally, the TRPC5 Mg^{2+} block[95] between +5 mV and approximately +30 mV gives a further evidence for TRPC5 activation under described conditions. In contrast, TRPC5 currents did not develop in response to intracellular IP_3 when Ca^{2+} was removed from the external solution. However, TRPC5 currents were activated when cells were reperfused with a 5 mM Ca^{2+}-containing external solution. Similar results were observed in TRPC5 cells overexpressing STIM1 and non-functional ORAI1 Scid proteins lacking the Ca^{2+} influx into the cytosol (Fig. 21).

Therefore, the functional interaction of CRAC currents and TRPC5 appears to depend on the Ca^{2+} influx carried by functional and STIM1 activated ORAI1 channel complexes. Fig. 22 shows, that TRPC5 currents did not activate when intracellular Ca^{2+} levels were controlled by the fast Ca^{2+} chelator BAPTA, instantaneously chelating Ca^{2+} influx in close proximity to the plasma membrane. The fact that larger CRAC currents result in stronger TRPC5 activation leads to the conclusion that TRPC5 activation depends on local Ca^{2+} influx (Fig. 23).

Subsequently experiments were performed under extracellular Ca^{2+}-free conditions and I provided defined amounts of free intracellular Ca^{2+} concentrations buffered by 10 mM EGTA in TRPC5-stably transfected HEK 293 cells. These experiments revealed that TRPC5 is activated in a dose-dependent manner by cytosolic Ca^{2+} levels. I determined EC_{50} = 358 nM free Ca^{2+} for outward current development and EC_{50} = 635 nM for inward currents carried by TRPC5 proteins. The phenomenon that TRPC5 channels show distinct gating properties called `phases´ was described in TRPC5-transfected HEK 293 cells receptor-activated by histamine[107]. Accordingly, the properties of TRPC5 channels change from outward-rectifying to double-rectifying I-V-shapes during current development over time[107]. Here, I observed similar biophysical properties dependent on intracellular Ca^{2+} concentrations. As mentioned above, EC_{50} of the outward currents is 45 % lower than EC_{50} for inward currents mediated by TRPC5 meaning that outward rectifying currents develop in response to lower intracellular Ca^{2+} levels followed by inward current development (Fig. 24). The ratio between inward currents and outward currents increase in proportion to the provided intracellular Ca^{2+} concentration (Fig. 24).

Even in TRPC5 stable HEK 293 cells transfected with murine STIM1, outward current development precedes inward current development showing similar `phases´ as non-transfected TRPC5 cells do. But more interestingly, the overall current activation is

shifted to 30 % lower intracellular Ca^{2+} levels for both outward and inward currents in the presence of recombinant STIM1. Several publications have reported an interaction of TRPC ion channels and STIM1[54, 66, 97] and my observations at least reveal a modulatory effect by STIM1 on TRPC5 activation (Fig. 24) in addition to a significant delay in current desensitization in STIM1-overexpressing TRPC5 stable cells compared to non-transfected TRPC5 stable cells (Fig. 25).

The present experiments suggest that TRPC5 currents develop in response to increasing cytosolic Ca^{2+} levels with STIM1 shifting the current activation to lower intracellular Ca^{2+} concentrations showing a modulatory effect on TRPC5 channels. The importance of intracellular Ca^{2+} levels for TRPC5 activation has been eagerly discussed for years, but so far a simple and direct Ca^{2+} dependence has not been shown.

As shown in Fig. 26, carbachol activation strongly depends on intracellular Ca^{2+} levels. No current development was detectable in response to CCH perfusion when internal Ca^{2+} levels were buffered to 0 nM (Fig. 26). Physiological concentrations (100 nM) of intracellular Ca^{2+} were prerequisite for CCH-induced TRPC5 activation. Additionally, CCH perfusion could enhance TRPC5 currents activated by increased intracellular Ca^{2+} levels. In particular, inward currents did more than double in size whereas outward currents showed a decent 50 % current boost (Fig. 26) in response to CCH perfusion. In contrast, Ca^{2+}-activated TRPC5 currents did not show any reduction in size when treated with U73122, a PLC inhibitor, leading to the conclusion that receptor stimulation can increase current densities but the PLC pathway activation does not play an essential role in TRPC5 development.

Similar results were obtained when TRPC5 stable cells were incubated with EGF to stimulate the fusion of TRPC5-containing secretory vesicles with the plasma membrane[60]. Since more TRPC5 channels are incorporated into the plasma membrane following EGF stimulation and, moreover, EGF may support current activation, TRPC5 stable transfected cells showed a small shift to lower Ca^{2+} concentrations and bigger current densities. Cytochalsin D incubation, which prevents secretion by inhibiting the rearrangement of the cytoskeleton, did not change TRPC5 activation by intracellular Ca^{2+} at all.

These results provide additional evidence that TRPC5 is activated by increased Ca^{2+} levels. Most Ca^{2+} signals are prevalently mediated to acceptor proteins via Ca^{2+}-calmodulin complexes. Ca^{2+} binds to the EF hand motif of calmodulin

priming specific calmodulin binding sites which can then mediate the Ca^{2+} signaling to other proteins. For instance, TRPC5 with a mutation in its calmodulin binding sites were activated by 1 μM intracellular Ca^{2+}. CBII mutants (J1307) showed unaltered current developments in comparison to current development recorded in WT TRPC5 HEK 293 cells. The CIRB site mutants (J1305), however, did not exhibit TRPC5 currents in response to 1 μM intracellular Ca^{2+}. These results agree with the absence of TRPC5 currents in receptor-activated CIRB site mutants[62]. A reduction in Ca^{2+} entry as reported for CBII mutants[62] could not be confirmed since Ca^{2+}-activated CBII mutants did not show a reduction in the recorded current density (Fig. 29).

In conclusion, the CBII binding site of TRPC5 does not play a role in Ca^{2+}-dependent TRPC5 activation whereas the CIRB site mutations abolished TRPC5 current activation. The question remains whether CIRB site mutants represent functional ion channels at all, since they showed neither CCH-induced nor intracellular Ca^{2+}-activated TRPC5 currents. At present, it is not clear whether CCH activation of TRPC5 is due to Ca^{2+} release from intracellular stores and, thus, increasing Ca^{2+} levels or whether an alternative pathway (for instance via IP_3 or DAG interaction) is involved. Final conclusions about a Ca^{2+}-calmodulin activation and the described current boost mediated by CCH perfusion remain fragmentary and will be subject of further investigations.

Originally described as a store-operated ion channel, my investigations show that TRPC5 is activated by increasing cytosolic Ca^{2+} levels. Since store-operated Ca^{2+} entry channels are strictly defined as ion channels activated by store depletion in buffered intracellular conditions[17], TRPC5 does not belong to the group of SOCE channels in contrast to ORAI proteins. However, TRPC5 is activated in response to thapsigargin (TG) perfusion in fluorescence-imaging experiments recording membrane potential changes (Fig. 30). TG-induced membrane changes are due to TRPC5 activation, whereas CCH induces Ca^{2+} signals in addition to membrane depolarization in both TRPC5 stable HEK 293 and WT HEK 293 cells (Fig. 30). Under non-buffered intracellular conditions, store-depletion activated TRPC5 channels as a result of increasing intracellular Ca^{2+} levels. The Ca^{2+} rise clearly precedes membrane depolarization (Fig. 31) providing further evidence that TRPC5 is another Ca^{2+}-activated member of the TRP family.

As mentioned before, a local Ca^{2+} rise conducted by CRAC currents can induce TRPC5 current development. Na^+ and Ca^{2+} influx through TRPC5 channels depolarize the membrane potential reducing the driving force for Ca^{2+} influx through CRAC channels. Thus, Ca^{2+}-activated TRPC5 currents may play a role in negative feedback for SOCE in mast cells which express STIM and ORAI proteins in addition to TRPC5.

Moreover, voltage-gated Ca^{2+} channels (VGCCs), here L-type Ca^{2+} channels, can also act as a Ca^{2+} donor. Illustrated in Fig. 32, TRPC5 current development occurs in response to Ca^{2+} influx mediated by voltage-gated channels. Thus, in excitable cells frequent action potentials (APs) may generate high local Ca^{2+} accumulation that activates TRPC5 currents resulting in sustained depolarization. Further conclusions are very speculative, but however, strong expression of TRPC5 proteins in hippocampus neurons could play a major role for intracellular Ca^{2+} signaling being essential for neurotransmitter release.

In conclusion, TRPC5 proteins may play a modulating role in cellular Ca^{2+} signalling. As a Ca^{2+}-activated non-selective ion channel, it is sensitive to local Ca^{2+} changes due to Ca^{2+} influx or Ca^{2+} store depletion. TRPC5 activation leads to membrane depolarization, thus, resulting in a very sensitive and precise way of feedback mechanism to establish specific Ca^{2+} signals (Fig. 34).
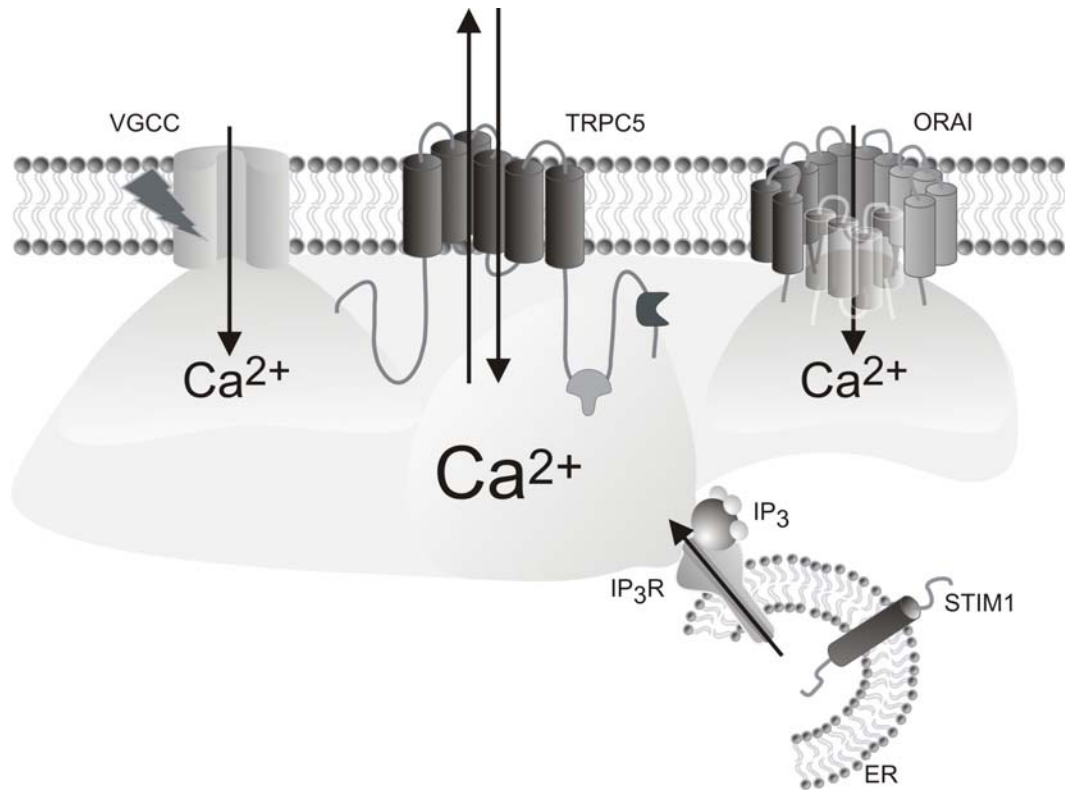
Figure 34: Ca^{2+} activated TRPC5 channels play a central role in cellular Ca^{2+} signaling. `Donor´channels such as ORAI or voltage-gated Ca^{2+} channels (VGCC) may provide the required local Ca^{2+} rise to activate non-selective TRPC5 channels. STIM1 may modulate channel activity but TRPC5 does not act as a typical SOCE channel. The response to store-depleting reagents is a secondary effect based on local Ca^{2+} increase due to CRAC currents or release from intracellular stores.

6 References

1.   Berridge, M. J., Bootman, M. D. & Lipp, P. Calcium--a life and death signal. Nature 395, 645-8 (1998).

2.   Lipp, P. & Niggli, E. A hierarchical concept of cellular and subcellular Ca(2+)-signalling. Prog Biophys Mol Biol 65, 265-96 (1996).

3.   Dolmetsch, R. E., Xu, K. & Lewis, R. S. Calcium oscillations increase the efficiency and specificity of gene expression. Nature 392, 933-6 (1998).

4.   Dolmetsch, R. E., Lewis, R. S., Goodnow, C. C. & Healy, J. I. Differential activation of transcription factors induced by Ca2+ response amplitude and duration. Nature 386, 855-8 (1997).

5.   Hoth, M. & Penner, R. Depletion of intracellular calcium stores activates a calcium current in mast cells. Nature 355, 353-6 (1992).

6.   Williams, R. T. et al. Identification and characterization of the STIM (stromal interaction molecule) gene family: coding for a novel class of transmembrane proteins. Biochem J 357, 673-85 (2001).

7.   Zhang, S. L. et al. STIM1 is a Ca2+ sensor that activates CRAC channels and migrates from the Ca2+ store to the plasma membrane. Nature 437, 902-5 (2005).

8.   Feske, S. et al. A mutation in Orai1 causes immune deficiency by abrogating CRAC channel function. Nature 441, 179-85 (2006).

9.   Vig, M. et al. CRACM1 is a plasma membrane protein essential for store-operated Ca2+ entry. Science 312, 1220-3 (2006).

10.   Yeromin, A. V. et al. Molecular identification of the CRAC channel by altered ion selectivity in a mutant of Orai. Nature 443, 226-9 (2006).

11.   Peinelt, C. et al. Amplification of CRAC current by STIM1 and CRACM1 (Orai1). Nat Cell Biol 8, 771-3 (2006).

12.   Soboloff, J. et al. Orai1 and STIM reconstitute store-operated calcium channel function. J Biol Chem 281, 20661-5 (2006).

13.   Philipp, S. et al. A novel capacitative calcium entry channel expressed in excitable cells. Embo J 17, 4274-82 (1998).

14.	Zagranichnaya, T. K., Wu, X. & Villereal, M. L. Endogenous TRPC1, TRPC3, and TRPC7 proteins combine to form native store-operated channels in HEK-293 cells. J Biol Chem 280, 29559-69 (2005).

15.	Freichel, M. et al. Lack of an endothelial store-operated Ca2+ current impairs agonist-dependent vasorelaxation in TRP4-/- mice. Nat Cell Biol 3, 121-7 (2001).

16.	Cancela, J. M., Van Coppenolle, F., Galione, A., Tepikin, A. V. & Petersen, O. H. Transformation of local Ca2+ spikes to global Ca2+ transients: the combinatorial roles of multiple Ca2+ releasing messengers. Embo J 21, 909-19 (2002).

17.	Clapham, D. E. Calcium signaling. Cell 131, 1047-58 (2007).

18.	Feske, S., Giltnane, J., Dolmetsch, R., Staudt, L. M. & Rao, A. Gene regulation mediated by calcium signals in T lymphocytes. Nat Immunol 2, 316-24 (2001).

19.	Raraty, M. et al. Calcium-dependent enzyme activation and vacuole formation in the apical granular region of pancreatic acinar cells. Proc Natl Acad Sci U S A 97, 13126-31 (2000).

20.	Mattson, M. P. & Chan, S. L. Neuronal and glial calcium signaling in Alzheimer's disease. Cell Calcium 34, 385-97 (2003).

21.	Hoth, M. & Penner, R. Calcium release-activated calcium current in rat mast cells. J Physiol 465, 359-86 (1993).

22.	Zweifach, A. & Lewis, R. S. Rapid inactivation of depletion-activated calcium current (ICRAC) due to local calcium feedback. J Gen Physiol 105, 209-26 (1995).

23.	Parekh, A. B. & Penner, R. Activation of store-operated calcium influx at resting InsP3 levels by sensitization of the InsP3 receptor in rat basophilic leukaemia cells. J Physiol 489 (Pt 2), 377-82 (1995).

24.	van Rossum, D. B., Patterson, R. L., Ma, H. T. & Gill, D. L. Ca2+ entry mediated by store depletion, S-nitrosylation, and TRP3 channels. Comparison of coupling and function. J Biol Chem 275, 28562-8 (2000).

25.	Hermosura, M. C., Monteilh-Zoller, M. K., Scharenberg, A. M., Penner, R. & Fleig, A. Dissociation of the store-operated calcium current I(CRAC) and the Mg-nucleotide-regulated metal ion current MagNuM. J Physiol 539, 445-58 (2002).

26. Roos, J. et al. STIM1, an essential and conserved component of store-operated Ca2+ channel function. J Cell Biol 169, 435-45 (2005).

27. Manji, S. S. et al. STIM1: a novel phosphoprotein located at the cell surface. Biochim Biophys Acta 1481, 147-55 (2000).

28. Liou, J. et al. STIM is a Ca2+ sensor essential for Ca2+-store-depletion-triggered Ca2+ influx. Curr Biol 15, 1235-41 (2005).

29. Brandman, O., Liou, J., Park, W. S. & Meyer, T. STIM2 is a feedback regulator that stabilizes basal cytosolic and endoplasmic reticulum Ca2+ levels. Cell 131, 1327-39 (2007).

30. Oh-Hora, M. et al. Dual functions for the endoplasmic reticulum calcium sensors STIM1 and STIM2 in T cell activation and tolerance. Nat Immunol 9, 432-43 (2008).

31. Wu, M. M., Buchanan, J., Luik, R. M. & Lewis, R. S. Ca2+ store depletion causes STIM1 to accumulate in ER regions closely associated with the plasma membrane. J Cell Biol 174, 803-13 (2006).

32. Zhang, S. L. et al. Genome-wide RNAi screen of Ca(2+) influx identifies genes that regulate Ca(2+) release-activated Ca(2+) channel activity. Proc Natl Acad Sci U S A 103, 9357-62 (2006).

33. Vig, M. et al. CRACM1 multimers form the ion-selective pore of the CRAC channel. Curr Biol 16, 2073-9 (2006).

34. Lis, A. et al. CRACM1, CRACM2, and CRACM3 are store-operated Ca2+ channels with distinct functional properties. Curr Biol 17, 794-800 (2007).

35. Wissenbach, U., Philipp, S. E., Gross, S. A., Cavalie, A. & Flockerzi, V. Primary structure, chromosomal localization and expression in immune cells of the murine ORAI and STIM genes. Cell Calcium 42, 439-46 (2007).

36. Gross, S. A. et al. Murine ORAI2 splice variants form functional Ca2+ release-activated Ca2+ (CRAC) channels. J Biol Chem 282, 19375-84 (2007).

37. Montell, C., Birnbaumer, L. & Flockerzi, V. The TRP channels, a remarkably functional family. Cell 108, 595-8 (2002).

38. Hardie, R. C. & Minke, B. Novel Ca2+ channels underlying transduction in Drosophila photoreceptors: implications for phosphoinositide-mediated Ca2+ mobilization. Trends Neurosci 16, 371-6 (1993).

39. Montell, C. & Rubin, G. M. Molecular characterization of the Drosophila trp locus: a putative integral membrane protein required for phototransduction. Neuron 2, 1313-23 (1989).

40. Hoenderop, J. G. et al. Homo- and heterotetrameric architecture of the epithelial Ca2+ channels TRPV5 and TRPV6. Embo J 22, 776-85 (2003).

41. Ramsey, I. S., Delling, M. & Clapham, D. E. An introduction to TRP channels. Annu Rev Physiol 68, 619-47 (2006).

42. Chuang, H. H. et al. Bradykinin and nerve growth factor release the capsaicin receptor from PtdIns(4,5)P2-mediated inhibition. Nature 411, 957-62 (2001).

43. Peier, A. M. et al. A TRP channel that senses cold stimuli and menthol. Cell 108, 705-15 (2002).

44. Caterina, M. J. et al. Impaired nociception and pain sensation in mice lacking the capsaicin receptor. Science 288, 306-13 (2000).

45. Mizuno, A., Matsumoto, N., Imai, M. & Suzuki, M. Impaired osmotic sensation in mice lacking TRPV4. Am J Physiol Cell Physiol 285, C96-101 (2003).

46. Zhang, Y. et al. Coding of sweet, bitter, and umami tastes: different receptor cells sharing similar signaling pathways. Cell 112, 293-301 (2003).

47. Suzuki, M., Mizuno, A., Kodaira, K. & Imai, M. Impaired pressure sensation in mice lacking TRPV4. J Biol Chem 278, 22664-8 (2003).

48. Buess, M., Engler, O., Hirsch, H. H. & Moroni, C. Search for oncogenic regulators in an autocrine tumor model using differential display PCR: identification of novel candidate genes including the calcium channel mtrp6. Oncogene 18, 1487-94 (1999).

49. Wissenbach, U. et al. Expression of CaT-like, a novel calcium-selective channel, correlates with the malignancy of prostate cancer. J Biol Chem 276, 19461-8 (2001).

50. Pedersen, S. F., Owsianik, G. & Nilius, B. TRP channels: an overview. Cell Calcium 38, 233-52 (2005).

51. Greka, A., Navarro, B., Oancea, E., Duggan, A. & Clapham, D. E. TRPC5 is a regulator of hippocampal neurite length and growth cone morphology. Nat Neurosci 6, 837-45 (2003).

52. Sutton, K. A. et al. Enkurin is a novel calmodulin and TRPC channel binding protein in sperm. Dev Biol 274, 426-35 (2004).

53. Beech, D. J., Muraki, K. & Flemming, R. Non-selective cationic channels of smooth muscle and the mammalian homologues of Drosophila TRP. J Physiol 559, 685-706 (2004).

54. Ma, H. T. et al. Canonical transient receptor potential 5 channel in conjunction with Orai1 and STIM1 allows Sr2+ entry, optimal influx of Ca2+, and degranulation in a rat mast cell line. J Immunol 180, 2233-9 (2008).

55. Schaefer, M. et al. Receptor-mediated regulation of the nonselective cation channels TRPC4 and TRPC5. J Biol Chem 275, 17517-26 (2000).

56. Kanki, H. et al. Activation of inositol 1,4,5-trisphosphate receptor is essential for the opening of mouse TRP5 channels. Mol Pharmacol 60, 989-98 (2001).

57. Jung, S. et al. Lanthanides potentiate TRPC5 currents by an action at extracellular sites close to the pore mouth. J Biol Chem 278, 3562-71 (2003).

58. Kinoshita-Kawada, M. et al. Inhibition of TRPC5 channels by Ca2+-binding protein 1 in Xenopus oocytes. Pflugers Arch 450, 345-54 (2005).

59. Zhu, M. H. et al. Desensitization of canonical transient receptor potential channel 5 by protein kinase C. Am J Physiol Cell Physiol 289, C591-600 (2005).

60. Bezzerides, V. J., Ramsey, I. S., Kotecha, S., Greka, A. & Clapham, D. E. Rapid vesicular translocation and insertion of TRP channels. Nat Cell Biol 6, 709-20 (2004).

61. Tang, J. et al. Identification of common binding sites for calmodulin and inositol 1,4,5-trisphosphate receptors on the carboxyl termini of trp channels. J Biol Chem 276, 21303-10 (2001).

62. Ordaz, B. et al. Calmodulin and calcium interplay in the modulation of TRPC5 channel activity. Identification of a novel C-terminal domain for calcium/calmodulin-mediated facilitation. J Biol Chem 280, 30788-96 (2005).

63. Xu, S. Z. et al. Block of TRPC5 channels by 2-aminoethoxydiphenyl borate: a differential, extracellular and voltage-dependent effect. Br J Pharmacol 145, 405-14 (2005).

64. Shimizu, S. et al. Ca2+-calmodulin-dependent myosin light chain kinase is essential for activation of TRPC5 channels expressed in HEK293 cells. J Physiol 570, 219-35 (2006).

65.	Okada, T. et al. Molecular cloning and functional characterization of a novel receptor-activated TRP Ca2+ channel from mouse brain. J Biol Chem 273, 10279-87 (1998).

66.	Yuan, J. P., Zeng, W., Huang, G. N., Worley, P. F. & Muallem, S. STIM1 heteromultimerizes TRPC channels to determine their function as store-operated channels. Nat Cell Biol 9, 636-45 (2007).

67.	Djouder, N., Aneiros, E., Cavalie, A. & Aktories, K. Effects of large clostridial cytotoxins on activation of RBL 2H3-hm1 mast cells indicate common and different roles of Rac in FcepsilonRI and M1-receptor signaling. J Pharmacol Exp Ther 304, 1243-50 (2003).

68.	Tseng, P. H. et al. The canonical transient receptor potential 6 channel as a putative phosphatidylinositol 3,4,5-trisphosphate-sensitive calcium entry system. Biochemistry 43, 11701-8 (2004).

69.	Warnat, J., Philipp, S., Zimmer, S., Flockerzi, V. & Cavalie, A. Phenotype of a recombinant store-operated channel: highly selective permeation of Ca2+. J Physiol 518 (Pt 3), 631-8 (1999).

70.	Neumann, H., Cavalie, A., Jenne, D. E. & Wekerle, H. Induction of MHC class I genes in neurons. Science 269, 549-52 (1995).

71.	Muallem, S., Kwiatkowska, K., Xu, X. & Yin, H. L. Actin filament disassembly is a sufficient final trigger for exocytosis in nonexcitable cells. J Cell Biol 128, 589-98 (1995).

72.	Valentijn, K., Valentijn, J. A. & Jamieson, J. D. Role of actin in regulated exocytosis and compensatory membrane retrieval: insights from an old acquaintance. Biochem Biophys Res Commun 266, 652-61 (1999).

73.	Rosado, J. A. & Sage, S. O. The actin cytoskeleton in store-mediated calcium entry. J Physiol 526 Pt 2, 221-9 (2000).

74.	Stam, J. C., Michiels, F., van der Kammen, R. A., Moolenaar, W. H. & Collard, J. G. Invasion of T-lymphoma cells: cooperation between Rho family GTPases and lysophospholipid receptor signaling. Embo J 17, 4066-74 (1998).

75.	Fallon, J. H. et al. Epidermal growth factor immunoreactive material in the central nervous system: location and development. Science 224, 1107-9 (1984).

76. Odell, A. F., Scott, J. L. & Van Helden, D. F. Epidermal growth factor induces tyrosine phosphorylation, membrane insertion, and activation of transient receptor potential channel 4. J Biol Chem 280, 37974-87 (2005).

77. Hamill, O. P., Marty, A., Neher, E., Sakmann, B. & Sigworth, F. J. Improved patch-clamp techniques for high-resolution current recording from cells and cell-free membrane patches. Pflugers Arch 391, 85-100 (1981).

78. Gross, S. A. in Laboratory of Cell and Molecular Signaling (LCMS), (John A. Burns School of Medicine, University of Hawaii, Honolulu, 2005).

79. Yuste, R., Lanni, F., Konnerth, A. Imaging Neurons, a laboratory manual (2000).

80. Hille, B. Ion Channels of Excitable Membranes (2001).

81. Parekh, A. B. & Penner, R. Store depletion and calcium influx. Physiol Rev 77, 901-30 (1997).

82. Moreau, B., Straube, S., Fisher, R. J., Putney, J. W., Jr. & Parekh, A. B. Ca2+-calmodulin-dependent facilitation and Ca2+ inactivation of Ca2+ release-activated Ca2+ channels. J Biol Chem 280, 8776-83 (2005).

83. Mercer, J. C. et al. Large store-operated calcium selective currents due to co-expression of Orai1 or Orai2 with the intracellular calcium sensor, Stim1. J Biol Chem 281, 24979-90 (2006).

84. Gwack, Y. et al. Biochemical and functional characterization of Orai proteins. J Biol Chem 282, 16232-43 (2007).

85. Takemura, H., Hughes, A. R., Thastrup, O. & Putney, J. W., Jr. Activation of calcium entry by the tumor promoter thapsigargin in parotid acinar cells. Evidence that an intracellular calcium pool and not an inositol phosphate regulates calcium fluxes at the plasma membrane. J Biol Chem 264, 12266-71 (1989).

86. Putney, J. W., Jr. A model for receptor-regulated calcium entry. Cell Calcium 7, 1-12 (1986).

87. Putney, J. W., Jr. Capacitative calcium entry revisited. Cell Calcium 11, 611-24 (1990).

88. Fasolato, C., Hoth, M., Matthews, G. & Penner, R. Ca2+ and Mn2+ influx through receptor-mediated activation of nonspecific cation channels in mast cells. Proc Natl Acad Sci U S A 90, 3068-72 (1993).

89.   Franzius, D., Hoth, M. & Penner, R. Non-specific effects of calcium entry antagonists in mast cells. Pflugers Arch 428, 433-8 (1994).

90.   Thastrup, O. et al. Thapsigargin, a novel molecular probe for studying intracellular calcium release and storage. Agents Actions 27, 17-23 (1989).

91.   Prakriya, M. et al. Orai1 is an essential pore subunit of the CRAC channel. Nature 443, 230-3 (2006).

92.   Selinger, Z., Doza, Y. N. & Minke, B. Mechanisms and genetics of photoreceptors desensitization in Drosophila flies. Biochim Biophys Acta 1179, 283-99 (1993).

93.   Birnbaumer, L. et al. On the molecular basis and regulation of cellular capacitative calcium entry: roles for Trp proteins. Proc Natl Acad Sci U S A 93, 15195-202 (1996).

94.   Plant, T. D. & Schaefer, M. TRPC4 and TRPC5: receptor-operated Ca2+-permeable nonselective cation channels. Cell Calcium 33, 441-50 (2003).

95.   Obukhov, A. G. & Nowycky, M. C. A cytosolic residue mediates Mg2+ block and regulates inward current amplitude of a transient receptor potential channel. J Neurosci 25, 1234-9 (2005).

96.   Liao, Y. et al. Orai proteins interact with TRPC channels and confer responsiveness to store depletion. Proc Natl Acad Sci U S A 104, 4682-7 (2007).

97.   Liao, Y. et al. Functional interactions among Orai1, TRPCs, and STIM1 suggest a STIM-regulated heteromeric Orai/TRPC model for SOCE/Icrac channels. Proc Natl Acad Sci U S A 105, 2895-900 (2008).

98.   Worley, P. F. et al. TRPC channels as STIM1-regulated store-operated channels. Cell Calcium 42, 205-11 (2007).

99.   Neher, E. Vesicle pools and Ca2+ microdomains: new tools for understanding their roles in neurotransmitter release. Neuron 20, 389-99 (1998).

100.   Hofmann, T., Schaefer, M., Schultz, G. & Gudermann, T. Transient receptor potential channels as molecular substrates of receptor-mediated cation entry. J Mol Med 78, 14-25 (2000).

101.   Zeng, F. et al. Human TRPC5 channel activated by a multiplicity of signals in a single cell. J Physiol 559, 739-50 (2004).

102. Hay, J. C. & Martin, T. F. Resolution of regulated secretion into sequential MgATP-dependent and calcium-dependent stages mediated by distinct cytosolic proteins. J Cell Biol 119, 139-51 (1992).

103. Catterall, W. A. Structure and regulation of voltage-gated Ca2+ channels. Annu Rev Cell Dev Biol 16, 521-55 (2000).

104. Parvez, S. et al. STIM2 protein mediates distinct store-dependent and store-independent modes of CRAC channel activation. Faseb J 22, 752-61 (2008).

105. Muik, M. et al. Dynamic coupling of the putative coiled-coil domain of ORAI1 with STIM1 mediates ORAI1 channel activation. J Biol Chem 283, 8014-22 (2008).

106. Cahalan, M. D. et al. Molecular basis of the CRAC channel. Cell Calcium 42, 133-44 (2007).

107. Obukhov, A. G. & Nowycky, M. C. TRPC5 channels undergo changes in gating properties during the activation-deactivation cycle. J Cell Physiol 216, 162-71 (2008).

7 Publications

Gross SA (2005), **Multifunktionelle Rolle des TRPM4-Ionenkanals in der ß-pankreatischen Insulinsekretion**, Diplomarbeit zur Erlangung des akademischen Grades eines Diplom-Biologen, Universität des Saarlandes, Saarbrücken

Cheng H, Beck A, Launay P, **Gross SA**, Stokes AJ, Kinet JP, Fleig A, Penner R (2007), **TRPM4 controls insulin secretion in pancreatic beta-cells**, Cell Calcium, 41(1): 51 – 61

Gross SA, Wissenbach U, Philipp SE, Freichel M, Cavalié A, Flockerzi V (2007), **Murine ORAI2 splice variants form functional Ca^{2+} release-activated Ca^{2+} (CRAC) channels**, Journal of Biological Chemistry, 282(27): 19375 – 84

Wissenbach U, Philipp SE, **Gross SA**, Cavalié A, Flockerzi V (2007), **Primary structure, chromosomal localization and expression in immune cells of the murine ORAI and STIM genes**, Cell Calcium, 42(4 – 5): 439 – 46

Gross SA, Wissenbach U, Zhu MX, Flockerzi V, Cavalié A (2008), **Functional coupling of TRPC5 to calcium-selective ion channels**, *in preparation*

Conference abstracts

Gross SA, Beck A, Penner R, **Multifunctional role of the TRPM4 ion channel in β-pancreatic insulin secretion**, Joint Meeting of the German Society of Physiology and the Federation of European Physiological Societies, Munich, March 2006

Gross SA, Wissenbach U, Cavalié A, **Spleißvarianten der Maus-Orai2-Proteine bilden CRAC-Kanäle**, 48. Frühjahrstagung der DGPT, Mainz, März 2007

Gross SA, Wissenbach U, Cavalié A, **Murine Orai2 splice variants form functional CRAC channels**, 86th Annual Meeting of the German Society of Physiology, Hannover, March 2007

Gross SA and Cavalié A, **Fast MIC activation in cells expressing Stim1 and Orai1**, 87th Annual Meeting of the German Society of Physiology, Cologne, March 2008

Gross SA, Wissenbach U, Zhu MX, Flockerzi V, Cavalié A, **Functional coupling of TRPC5 to calcium-selective ion channels**, Joint PhD-Student Symposium of the Doctoral College Molecular Cell Biology and Oncology (MCBO), Innsbruck, Austria and Graduate College Calcium Signaling and Cellular Nanodomains (GK1326), Homburg, Germany, Obergurgl, Austria, April 2008

8 Aknowledgements

9 Curriculum Vitae

Personal Data:

Name: Stefan Alfred Groß

Date of Birth: March 26th, 1980 in Püttlingen, Germany

Nationality: German

Scientific education:

10/2000 – 09/2005   Basic and main study period of Human and Molecular
                           Biology at the Saarland University, Saarbrücken and
                           Homburg, Germany

02/2005 – 09/2005   Diploma-thesis with Prof. Dr. Adolfo Cavalié and Reinhold
                           Penner, Ph.D., MD at the Laboratory of Cell and Molecular
                           Signaling at Queen´s Medical Center, John A Burns
                           School of Medicine, University of Hawaii, Honolulu, HI,
                           USA

11/2005 – 06/2008   Ph.D.-thesis with Prof. Dr. Adolfo Cavalié,
                           Department of Pharmacology and Toxicology,
                           Saarland University, Germany

Other education:

11/1999 – 08/2008   Military Service, Luftlandebrigade 26, Zweibrücken
                           and Saarlouis, Germany

01/2007 – 10/2007   Further academic education in Economics for
                           Entrepreneurship and General Management,
                           KWT, Saarbrücken

Stipends and honors:

07/2006 – 02/2007   DAAD STIBET

06/2007   DFG travel scholarship

07/2007   Selected young scientist to participate in the Meeting
                       of Nobel Laureates in Lindau (Medicine and Physiology)

08/2007 – 12/2007   DAAD STIBET